UNCLASSIFIED

SECURITY CLASSIFICATION OF THIS PAGE *(When Data Entered)*

REPORT DOCUMENTATION PAGE

READ INSTRUCTIONS BEFORE COMPLETING FORM

1. REPORT NUMBER: NAVENVPREDRSCHFAC Technical Report TR 78-01	2. GOVT ACCESSION NO.
3. RECIPIENT'S CATALOG NUMBER	
4. TITLE *(and Subtitle)*: New Results of Tropical Cyclone Research from Observational Analysis	5. TYPE OF REPORT & PERIOD COVERED
	6. PERFORMING ORG. REPORT NUMBER
7. AUTHOR(s): William M. Gray and William M. Frank	8. CONTRACT OR GRANT NUMBER(s): N00228-76-C-2129
9. PERFORMING ORGANIZATION NAME AND ADDRESS: Colorado State University, Fort Collins, CO 80523	10. PROGRAM ELEMENT, PROJECT, TASK AREA & WORK UNIT NUMBERS: PE 62759N PN ZF52-551-001; TA 7W0513-CC00; NEPRF WU 6.2-14
11. CONTROLLING OFFICE NAME AND ADDRESS: Commander, Naval Air Systems Command, Department of the Navy, Washington, DC 20361	12. REPORT DATE: June 1978
	13. NUMBER OF PAGES: 108
14. MONITORING AGENCY NAME & ADDRESS *(if different from Controlling Office)*: Naval Environmental Prediction Research Facility, Monterey, CA 93940	15. SECURITY CLASS. *(of this report)*: UNCLASSIFIED
	15a. DECLASSIFICATION/DOWNGRADING SCHEDULE

16. DISTRIBUTION STATEMENT *(of this Report)*

Approved for public release; distribution unlimited.

17. DISTRIBUTION STATEMENT *(of the abstract entered in Block 20, if different from Report)*

18. SUPPLEMENTARY NOTES

Additional funding for the research reported herein was supplied by the National Science Foundation and the National Oceanographic and Atmospheric Administration.

19. KEY WORDS *(Continue on reverse side if necessary and identify by block number)*

Tropical cyclones
Typhoons
Data compositing
Tropical cyclone forecasting
Tropical cyclone modeling
Tropical cyclone observational studies

20. ABSTRACT *(Continue on reverse side if necessary and identify by block number)*

Up-to-date results of recent tropical cyclone research at Colorado State University are presented. Particular attention is paid to new findings which impact on tropical cyclone forecasting and modeling efforts. Observational studies using large amounts of composited rawinsonde, satellite and aircraft flight data have been performed to analyze tropical cyclone genesis, structure, energetics, intensity, intensity change, and motion.

DD FORM 1 JAN 73 1473 EDITION OF 1 NOV 65 IS OBSOLETE
S/N 0102-014-6601 |

UNCLASSIFIED

SECURITY CLASSIFICATION OF THIS PAGE *(When Data Entered)*

DEPARTMENT OF THE NAVY
DIRECTOR NAVAL OCEANOGRAPHY AND METEOROLOGY
NSTL STATION, MISSISSIPPI 39529

Code 32:jc
3140
Ser 782
22 JUN 1978

From: Director, Naval Oceanography and Meteorology

Subj: NAVENVPREDRSCHFAC Technical Report; forwarding of

Encl: (1) New Results of Tropical Cyclone Research from Observational Analysis, NAVENVPREDRSCHFAC TR 78-01

1. Enclosure (1) presents the results of recent research on tropical cyclones in both the Atlantic and Pacific at Colorado State University. Although the findings are not conclusive, they should be helpful to forecasters, including shipboard meteorologists. Accordingly, this research publication is being distributed to selected operational units.

2. All Naval meteorologists should review enclosure (1). The conclusions are interesting and, in some cases, surprising. Subjects addressed include the genesis, structure, energetics, intensity, intensity change, and motion of tropical cyclones.

G. L. Rice
Acting

Distribution: (see page 2)

Distribution List

SNDL Part 1

SNDL	Activity
21A1	CINCLANTFLT
21A2	CINCPACFLT
22A	Fleet Commanders
24D1	COMNAVSURFLANT
24D2	COMNAVSURFPAC
26A1	COMPHIBGRULANT
26A2	COMPHIBGRUPAC {Group 1 only}
28C2	Surface Group PAC {WESTPAC only}
29B	Aircraft Carrier {CV, CVN}
31A	Amphibious Command Ship {LCC}
31F	Amphibious Assault Ship {LHA}, {LPH}
3EA	Destroyer Tender LANT {AD} {Puget Sound only}
3EL	Deep Submergence Support Ship {AGDS}
3EKK	Misc. Command Ship {AGF}
3ETT	Training Aircraft Carrier {CVT}
50A	Unified Commands {CINCPAC only}

SNDL Part 2

A1	Special Asst. to the Asst. SECNAV {R&D}
A2A	Chief of Naval Research {Code 734}
A3	Chief of Naval Operations {OP-952}
A4A	Chief of Naval Material {MAT-034}
B2	Special Agencies, Staffs, Boards & Committees {NSA, Ft. Meade only}
C4F7	Weather Service Environmental Detachments {Agana, Asheville, Atsugi, Bermuda, Cecil Field, Charleston, Corpus Christi, Cubi Pt., Guantanamo Bay, Key West, Kingsville, Mayport, Whiting Field, Midway, Misawa, New Orleans, Offutt AFB, Roosevelt Roads, Oceana, Diego Garcia, Kadena}
E3A	Laboratory, Office of Naval Research {Code 2620}
E3B	Office of Naval Research Branch Offices
E3C	Ocean Research & Development Activity
FD1	Oceanographer of the Navy
FD2	Naval Oceanographic Office
FD3	Naval Oceanography & Meteorology
FD4	Fleet Numerical Weather Central
FD5	Fleet Weather Central
FD6	Fleet Weather Facility
FD7	Naval Weather Service Facilities
FF38	Naval Academy
FKA1A	Air Systems Command Headquarters{Air 370, Air 55}
FKA6A12	Ocean Systems Center
FT1	Chief of Naval Education and Training
FT2	Chief of Naval Air Training
FT35	Amphibious School
FT73	Naval Postgraduate School
FT75	Naval War College
FT78	Education and Training Program Develop. Center
V5	Marine Corps Air Station

SNDL Part 2 (Continued)

Officer in Charge
Service School Command Great Lakes
Detachment Chanute Stop 71
Chanute AFB, IL 61868

Commandant of the Marine Corps
*ATTN -ASL-44
Navy Department
Washington, DC 20380

Headquarters, Air Weather Service
Scott AFB, IL 62225

National Weather Service
Room 307
World Weather Bldg.
5200 Auth Rd.
Camp Springs, MD 20023

U.S. Department of Commerce
National Oceanic and Atmospheric Administration
Rockville, MD 20852

National Hurricane Center
P.O. Box 248286
Coral Gables, FL 32124

Commander
Pacific Missile Range
Point Mugu, CA 93042

AN (1) AD-A060 077
FG (2) 040200
CI (3) (U)
CA (5) COLORADO STATE UNIV FORT COLLINS
TI (6) New Results of Tropical Cyclone Research from Observational Analysis.
TC (8) (U)
DN (9) Technical rept.,
AU (10) Gray,William M.
AU (10) Frank,William M.
RD (11) Jun 1978
PG (12) 108
CT (15) N00228-76-C-2129
PJ (16) F52551
TN (17) ZF52551001
RN (18) NEPRF-TR-78-01
RC (20) Unclassified report
DE (23) *CYCLONES, *TYPHOONS, *METEOROLOGICAL DATA, WEATHER FORECASTING, DATA ACQUISITION, METEOROLOGICAL SATELLITES, WEATHER RECONNAISSANCE AIRCRAFT, STORMS, WIND DIRECTION, CLOUDS, GLOBAL, MARINE METEOROLOGY
DC (24) (U)
ID (25) *Cyclone genesis, LPN-W0513C-C00, WU6214, PE62759N
IC (26) (U)
AB (27) Up-to-date results of recent tropical cyclone research at Colorado State University are presented. Particular attention is paid to new findings which impact on tropical cyclone forecasting and modeling efforts. Observational studies using large amounts of composited rawinsonde, satellite and aircraft flight data have been performed to analyze tropical cyclone genesis, structure, energetics, intensity, intensity change, and motion. (Author)
AC (28) (U)
DL (33) 01
CC (35) 088300

NAVENVPREDRSCHFAC
TECHNICAL REPORT TR-78 - 01

NEW RESULTS OF TROPICAL CYCLONE RESEARCH FROM OBSERVATIONAL ANALYSIS

W. M. GRAY and W. M. FRANK
COLORADO STATE UNIVERSITY

JUNE 1978

APPROVED FOR PUBLIC RELEASE
DISTRIBUTION UNLIMITED

NAVAL ENVIRONMENTAL PREDICTION
RESEARCH FACILITY
MONTEREY, CALIFORNIA 93940

TABLE OF CONTENTS

I. INTRODUCTION

The authors have undertaken a comprehensive study of the origins and characteristics of tropical cyclones. Many of these results are believed to be relevant to the U.S. Navy for forecasting and numerical simulations of these storms, and this report is issued to disseminate this information. This is the second report on this subject. Last year's report by Gray and Frank (1977) gives additional information. The research project includes composite studies of large amounts of rawinsonde and DMSP satellite data.

Section II discusses our current research on cyclone genesis and suggests a parameter which might be used to operationally forecast this phenomena. Section III gives new information on the structure of typhoons and hurricanes. Section IV discusses satellite observed cloudiness as this is related to cyclone intensity. Section V briefly discusses our new information on tropical cyclone motion and Section VI gives data on the outward radial extention of the tropical cyclone's isotach of 30 knot winds. Other tropical cyclone information is also presented and discussed.

More detailed information is contained in the CSU Department of Atmospheric Science tropical cyclone project reports of Gray, 1975a, 1975b; George, 1975; Frank, 1976; Zehr, 1976; S. Erickson, 1977; Arnold, 1977; and other papers by Frank, 1977a, b, c; Gray, 1975a, b; Gray, 1977a, b, c; McBride, 1977; and Núñez and Gray, 1977.

1. Data and Analysis Techniques

Data Set. The information in this paper is taken from various studies of tropical cyclones using composited rawinsonde data,

climatological information, NOAA flight data and DMSP satellite photographs.

The data sources used are listed below:

1) Ten years (1961-1970) of N.W. Pacific rawinsonde data (~18,000 soundings) from 30 stations as shown in Fig. 1. This data sample is currently being expanded to 20 years.

2) Twenty years (1956-1975) of N. Atlantic rawinsonde data from the stations shown in Fig. 2.

3) All available reduced NOAA Research Flight Facility (RFF) Atlantic inner-hurricane flight data for the period of 1957-1967. This storm flight data has been described by the author and a graduate student in published papers (Shea and Gray, 1973; Gray and Shea, 1973). This aircraft data sample includes over 500 individual radial leg missions. The data itself is listed in a report by Gray and Shea (1976). This is believed to be the best available information on inner tropical storm winds, radius of maximum winds, inner radar eye radius, central pressure, etc. It is hoped that uses can be found for this in the Pacific where some degree of meshing of the aircraft data with the rawinsonde data may be possible.

4) Five years (1971-1975) of direct read-out from Guam Defense Meteorological Satellite Program (DMSP) satellite photographs of tropical cyclones and cloud clusters in the N.W. Pacific. This 1/3 nautical mile resolution data has been digitized and composited to perform quantitative analyses of the convection associated with West Pacific tropical weather systems.

5) All of the Joint Typhoon Warning Center (JTWC), Guam typhoon summaries for the 30-year period of 1946-1976.

6) Seasonal sea-surface temperature and thermocline data in 5^{o} marsden squares for the whole Pacific as recently furnished by the Navy Oceanographic Office.

7) U.S. Navy data tape documentation of Pacific typhoons and tropical storms for the period 1946-1975.

8) Digitized daily satellite data for the period of October 1966 through 1970.

9) The new global tropical storm data tape which has recently been issued from Asheville by Harold Crutcher.

10) W. Indies tropical cyclone track data as supplied by Charles A. Neumann of NOAA Miami.

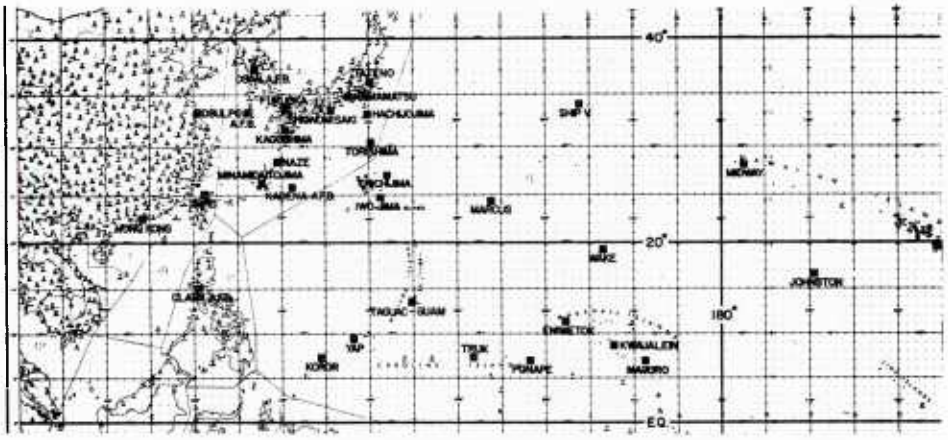

Fig. 1. Western North Pacific rawinsonde data network.

Rawinsonde Compositing Philosophy and Technique. Tropical cyclones and cloud clusters spend most of their lifetimes over the warm tropical oceans. Traditional data sources are very sparse in such regions, and daily tropical weather analyses are notoriously unreliable. The severe winds found in tropical cyclones further reduce the availability of such data. It is not possible to obtain enough rawinsonde data or surface observations around any individual storm or cluster at one time period to permit quantitative analysis of structure, dynamics or energetics.

Aircraft data have provided the best information concerning the activities in the intense central core regions of tropical cyclones. There are a number of case studies of individual storms based on Northwest Atlantic hurricane flight data (Riehl and Malkus, 1961; Miller, 1962; Gray, 1962, 1967; LaSeur and Hawkins, 1963; Sheets, 1967a, 1967b, 1968; Hawkins and Rubsam, 1968; Hawkins and Imbembo, 1976) and also statistical treatments of the flight data (Shea and Gray, 1973; Gray and Shea, 1973). However, logistical considerations have limited the ability

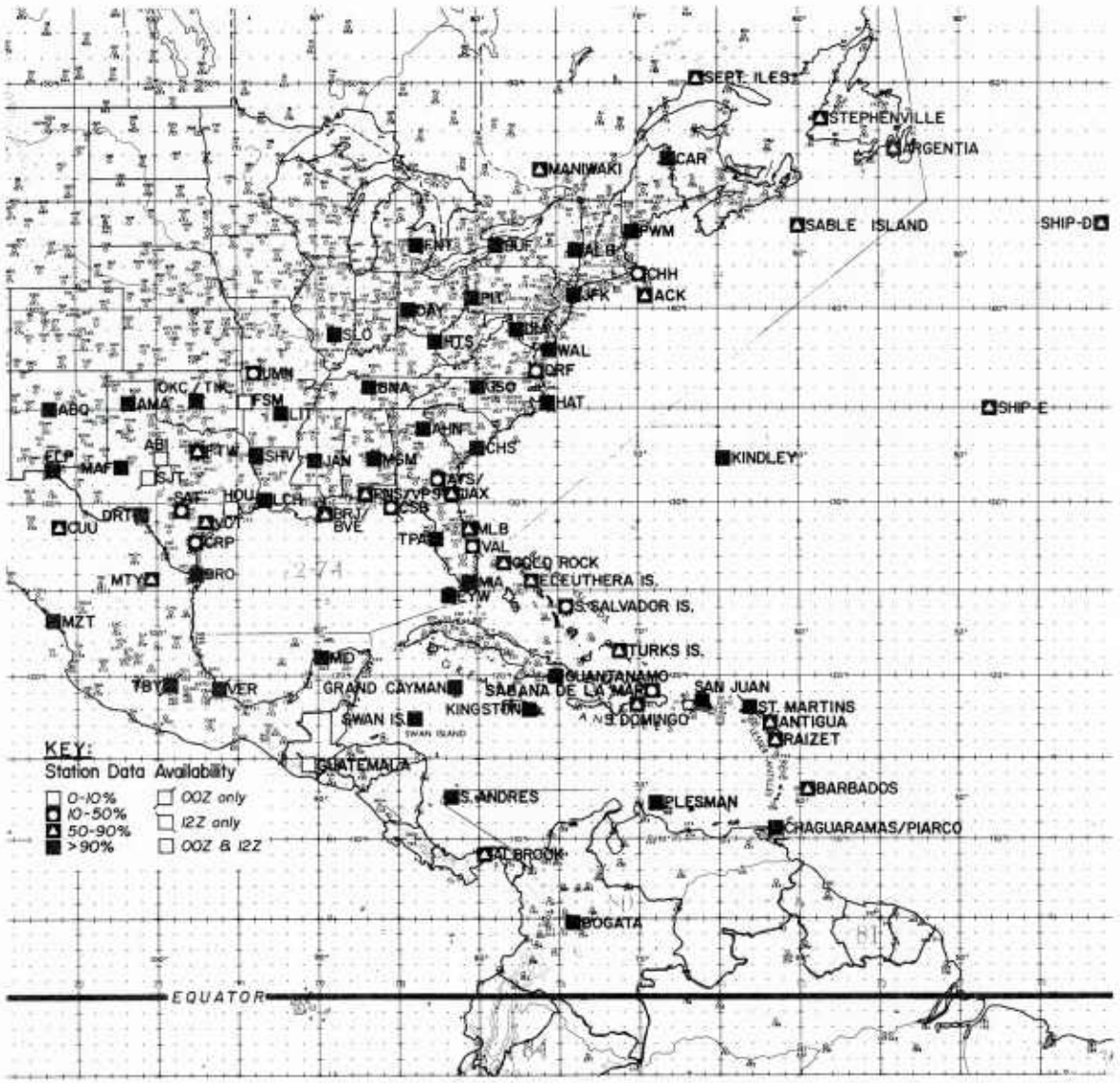

Fig. 2. North Atlantic Rawinsonde Data Network.

of aircraft to provide information concerning the outer convective regions of the storm and its broader scale environment. Aircraft data also have been limited to a few flight levels per storm time period due to the usually low number of available aircraft, maximum aircraft ceilings of 200 mb or less, and dangerous low level flight conditions.

None of the above data sources can produce an accurate vertical profile of the radial wind pattern around a system. Without such a profile it is impossible to compute meaningful budgets of energy, water vapor, momentum, vorticity, etc. In addition, vertical profiles of the other dynamic and thermodynamic variables cannot be determined fully over the mesoscale area. It is necessary to composite very large amounts of data from many similar weather systems at many time periods to obtain meaningful quantitative measurements.

Although the extreme variabilities and individual asymmetries of tropical cyclones and cloud clusters are well known, the natures of the basic dynamic and energetic processes which govern these systems must be largely invariant. Compositing allows quantiative analyses of these features. Any compositing system smoothes out many of the individual characteristics of single systems, but a great deal of information concerning asymmetrical or "eddy" qualities can be deduced by the use of proper data handling techniques.

Compositing was performed on a 15^{o} latitude radius cylindrical grid extending from sea level to 50 mb. The system circulation center was located at each time period using JTWC and NOAA Miami reports and/or satellite photographs, and the grid was positioned with the system at grid center of the lowest level. Whenever available rawinsonde soundings fell on the grid at a given time period for a given storm, each sounding was located relative to the storm center in cylindrical coordinates. Figure 3 shows the grid and the number of soundings per grid space for a typical stratification. All of the parameters to be composited, whether directly measured or computed from the directly measured parameters, were determined at the observation station locations at 19 vertical pressure levels.

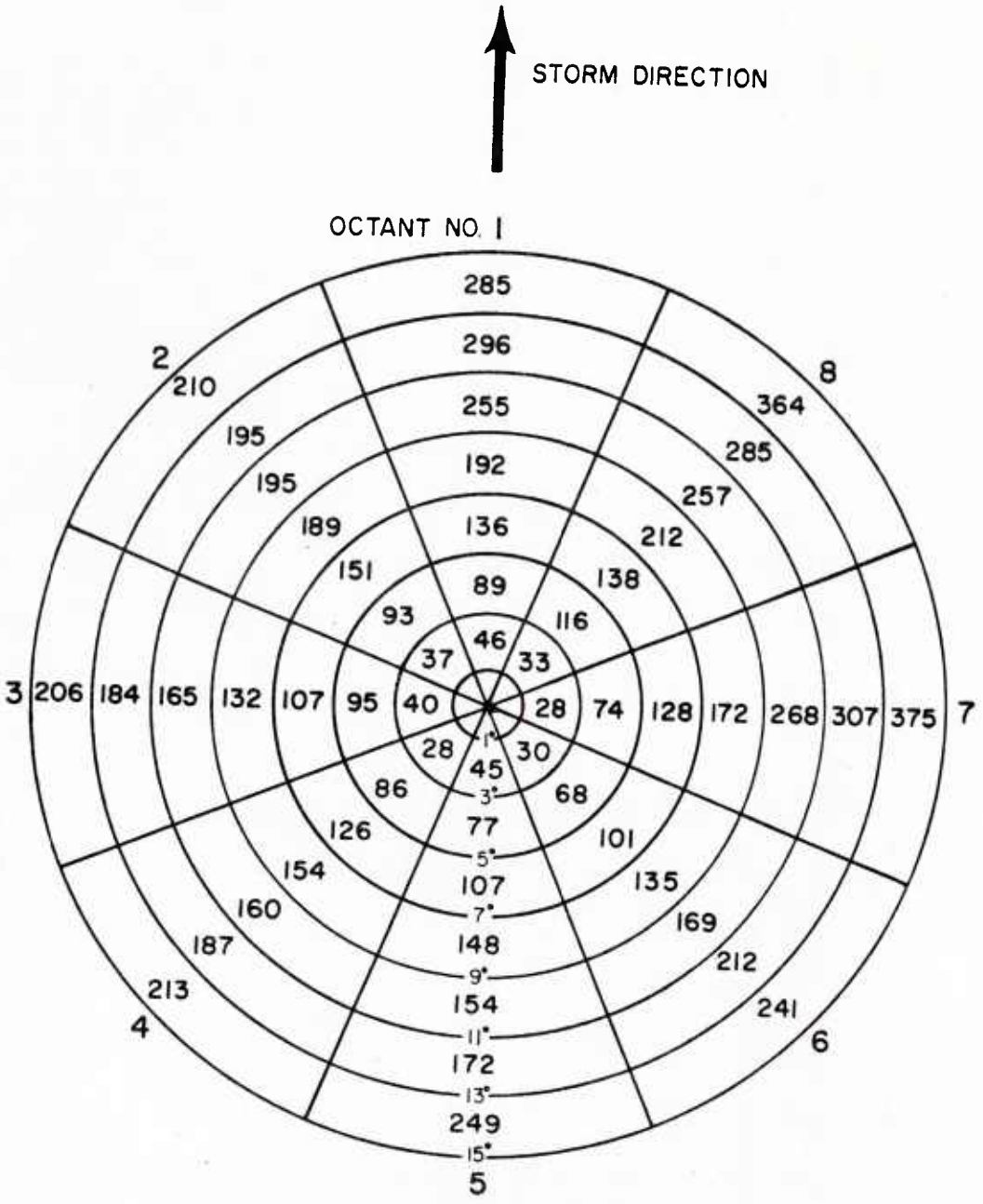

Fig. 3. Compositing grid (15° latitude radius) with the number of rawinsonde reports in each octant and each 2° radial band for a typical stratification.

The geographical alignment of the grid varied with the coordinate system used. After all parameters were either measured or computed for each sounding, the value of each parameter was assigned to a point at

the center of the grid box in which the sounding fell. All soundings which fell in that grid space for the particular group of storms and time periods being analyzed were composited.

The data set was sufficiently large to allow compositing of various subsets. Data could be grouped according to any characteristics observed in individual systems such as location, season, intensity, motion, or intensity tendency. By comparing the composites of different types of systems it was possible to quantitatively analyze the persistent differences between the groups. It was also possible to remove obviously atypical systems or time periods from a data group to improve the quality of the data set.

Rawinsonde compositing procedures involve the use of four separate reference frames:

1) With respect to the instantaneously fixed cyclone center in a N-S or geographical coordinate system.

2) With respect to the cyclone center in a geographical coordinate system with the cyclone motion subtracted out of all the winds (portrayal of data relative to the moving cyclone center in geographical coordinates).

3) With respect to the instantaneously fixed cyclone center and the direction to which the storm is moving.

4) With respect to the cyclone center and the direction to which the storm is moving with the cyclone motion subtracted out of all the winds.

See our other project reports for more information on this compositing procedure.

The relative positions of the system and the balloon changed due to their respective motions during the balloon's ascent time. These motions were estimated from the data, and the positions of each were corrected at each pressure level. In this study horizontal eddy fluxes were

estimated by compositing individual fluxes of quantities and comparing them to mean fluxes. The radial winds were initially composited and mass balanced from the surface to 100 mb by adding a small constant correction factor (ΔV_r) to each individual radial wind value in a given radial band. Changes in mass of the volume within the radial band were neglected. For each sounding the product of the corrected V_r and the quantity being analyzed was computed at each level. Such products for all of the soundings in an octant were then composited as before, giving a mean transport value for each octant at each level, $\overline{V_r Q}$, where the bar denotes time and space averaging of the $V_r \cdot Q$ products. By subtracting the product of the mean $\overline{V_r}$ and the mean quantity ($\overline{Q}$) one could achieve a good estimate of horizontal eddy transport:

$$\overline{V_r' Q'} \approx \overline{V_r \cdot Q} - \overline{V_r} \cdot \overline{Q}$$

Summary of Recent and Current Research Projects. Table 1 shows the tropical cyclone research projects which are either now in progress or have been completed since 1972 at CSU. Some of the more useful findings for operational purposes are summarized in the following chapters.

TABLE 1

Recently Completed and Current Tropical Cyclone Research Projects

Completed Studies	Subject	Region	Data Set
(Shea and Gray, 1973)	Inner Core Structure	N. Atlantic	NOAA flight data 1957-67
(Gray and Shea, 1973)	Inner Core Structure	N. Atlantic	" " " "
(Gray and Shea, 1976)	Data Summary of NOAA's Hurricane Inner-core Radial Leg Flight Penetrations 1957-1967, 1969	N. Atlantic	" " " "
Gray, (1975a, 1975b)	Tropical Cyclone Genesis	Global and N.W. Pacific	Numerous Climatological Sources
Frank, 1976	Tropical Cyclone Structure and Energetics	N.W. Pacific	∿18,000 Rawinsonde Soundings (1961-1970)
Arnold, 1977	Cyclone Intensity from Satellite Data	N.W. Pacific	1971-75 DMSP Satellite Data plus Rawinsonde Data
Frank, 1977	Eddy Processes in Tropical Cyclones	N.W. Pacific in W. Atlantic	10 yrs. Pacific and 14 yrs. Atlantic Data
Núñez and Gray, 1977	Tropical Cyclone Structure	N.W. Pacific and W. Atlantic	10 yrs. Pacific and 14 yrs. Atlantic Data
George, 1975	Tropical Cyclone Motion	N.W. Pacific	∿18,000 Soundings (1961-1970)
Gray, 1977a	Tropical Cyclone Genesis	Global	Rawinsonde and Satellite
1977b	Measurement of Cyclone Intensity	N.W. Pacific and Atlantic	Rawinsonde and Aircraft Data
1977c	Cyclone Motion	N.W. Pacific and Atlantic	Rawinsonde

TABLE 1 (cont'd)

Completed Studies	Subject	Region	Data Set
Zehr, 1976	Tropical Cyclone Genesis	N.W. Pacific	∿20,000 Soundings (1961-1970)
Erickson, 1977	Tropical Cyclone Genesis	N.W. Pacific	1971-75 DMSP Satellite Data Plus Rawinsonde Data
McBride, 1977	Tropical Cyclone Genesis	N.W. Pacific and W. Atlantic	N.W. Pacific and W. Atlantic Rawinsonde Plus NOAA Satellite Data

Current Tropical Cyclone Research Studies		
Subject		
1) Structure	N. Atlantic	Soundings from 1956-75
2) Motion	N. Atlantic	Soundings from 1956-75
3) Genesis	N. Atlantic	Soundings from 1956-75
4) Intensity Change	N. Atlantic N.W. Pacific	Same as 3) Genesis
5) Satellite Applicability	N.W. Pacific	DMSP (1971-1975)
6) Numerical Modeling of Tropical Cyclone Genesis		

II. CYCLONE GENESIS

This subject has been and is being extensively studied. Recent papers relating to this subject can be found in the reports of Zehr (1976), S. Erickson (1977), McBride (1977), Gray (1977c) and Arnold (1977). Older Colorado State University Project studies relating to the climatology of cyclone genesis can be found in the papers by Gray (1968, 1975a, 1975b), Lopez (1968), Wachtmann (1968), and Sartor (1968).

1. Climatological Considerations

Climatologically (see Gray, 1975a), the frequency of cyclone genesis by season and location appears to be well related to the seasonal product of a "dynamic potential" and a "thermal potential" or:

$$\left(\begin{array}{c}\text{Seasonal}\\ \text{Genesis}\\ \text{Parameter}\end{array}\right) \quad \alpha \quad \text{(Dynamic Potential) x (Thermal Potential)} \qquad (1)$$

The dynamic potential is related to the product of the seasonal values of:

1) ζ_r = Relative vorticity at top of planetary boundary layer or $\sim$ 950 mb,

2) f = Coriolis parameter and

3) $1/S_z$ = $1/\left|\partial \mathbf{V}_h/\partial p\right|$ or the inverse of the absolute value of the vertical shear of the horizontal wind between 950 and 200 mb.

Thus,

$$\text{Dynamic Potential} = (\zeta_r)\ (f)\ \left(\frac{1}{S_z}\right) \qquad (2)$$

The thermal potential is made up of the product of the seasonal values of:

1) E = Ocean thermal energy above 26°C to 60 m depth,

2) $\frac{\partial \Theta_e}{\partial p}$ = Vertical gradient of Θ_e between the surface and 500 mb, and

3) $\overline{RH}$ = Mean relative humidity between the levels of 500-700 mb.

Thus,

$$\text{Thermal Potential} = (E)\ (\partial\Theta_e/\partial p)\ (\overline{RH}) \tag{3}$$

Zero and negative values of the above parameters indicate no genesis potential.

There is some difficulty with using these seasonal values directly. Seasonal values are not always a close measure of what the daily parameter values can be. Thus, the seasonal relative vorticity in the Western Atlantic is slightly negative. The above seasonally determined genesis potential would not predict cyclone genesis in a region where it obviously occurs. When the seasonal values of $\left|\partial\, \mathbb{V}_h/\partial p\right|$ are small, unreasonably large values of $1/S_z$ are obtained, which are not representative of the average of the daily values. Similarly the seasonal values of $\partial\Theta_e/\partial p$ between the surface and 500 mb could be zero or negative, but individual time period values can be positive.

To cover the range of possible daily deviations of three of these parameters, arbitrary units were added to the seasonal values to simulate in an approximate sense what the average of the positive daily deviations of these values could be. Thus, five units of $10^{-6}\,\text{sec}^{-1}$ vorticity were added to all the seasonally measured values of this parameter and 5°K was added to all the seasonal values of $\partial\Theta_e/\partial p$. To prevent unreasonably large values of the genesis frequency when $\left|\partial\, \mathbb{V}_h/\partial p\right|$ approaches zero, and also to assure that the seasonal average of $\left|\partial\, \mathbf{V}_h/\partial p\right|$ is more rep-

resentative of the seasonal average of the daily values, 3 m/sec was arbitrarily added to all the seasonal vertical shear values. The minimum value of the vertical shear parameter is thus 3 units.

A Seasonal Genesis Parameter is now defined as

$$\begin{pmatrix}\text{Seasonal}\\ \text{Genesis}\\ \text{Parameter}\end{pmatrix} \propto \left[\begin{pmatrix}\text{Vorticity}\\ \text{Parameter}\end{pmatrix}\ \begin{pmatrix}\text{Coriolis}\\ \text{Parameter}\end{pmatrix}\ \begin{pmatrix}\text{Vertical Shear}\\ \text{Parameter}\end{pmatrix} \times \begin{pmatrix}\text{Ocean Energy}\\ \text{Parameter}\end{pmatrix}\ \begin{pmatrix}\text{Moist Stability}\\ \text{Parameter}\end{pmatrix}\ \begin{pmatrix}\text{Humidity}\\ \text{Parameter}\end{pmatrix}\right] \tag{4}$$

where

$\begin{pmatrix}\text{Vorticity}\\ \text{Parameter}\end{pmatrix}$ = $(\bar{\zeta}_r + 5)$, where $\bar{\zeta}_r$ is determined in units of 10^{-6}sec^{-1}.

$\begin{pmatrix}\text{Coriolis}\\ \text{Parameter}\end{pmatrix}$ = f or $2\Omega\sin\varphi$, where Ω is the rotation rate of the earth and φ denotes latitude.

$\begin{pmatrix}\text{Vertical Shear}\\ \text{Parameter}\end{pmatrix}$ = $1/(S_z+3)$ where $S_z = |\partial \mathbb{V}_h/\partial p|$ is determined in units of m/sec per 750 mb.

$\begin{pmatrix}\text{Ocean Energy}\\ \text{Parameter}\end{pmatrix}$ = E or $\int_{60\text{ m}}^{\text{sfc}} \rho_w c_w (T - 26^\circ)\,\delta z$, where ρ_w and c_w are the density and specific heat capacity of water. T is expressed in $^\circ$C. $T - 26^\circ$=zero if $T \leq 26^\circ$C. E is expressed in units of 10^3 cal/cm^2.

$\begin{pmatrix}\text{Moist Stability}\end{pmatrix}$ = $\partial\theta_e/\partial p + 5$, where $\partial\theta_e/\partial p$ is in units of $^\circ$K per 500 mb.

$\begin{pmatrix}\text{Humidity}\\ \text{Parameter}\end{pmatrix}$ = $\frac{\overline{RH} - 40}{30}$ or $(\overline{RH} - 40)/30$ where $\overline{RH}$ is the mean relative humidity between 500 and 700 mb. Parameter is zero for $\overline{RH} < 40$, and 1 for $\overline{RH} \geq 70$.

Table 2 summarizes these parameters and their role in cyclone genesis. The paper by Gray (1975a) gives more discussion of why these parameters are related to seasonal genesis frequency. Dynamic potential is expressed in units of ($10^{-11} s^{-2}$ per m/s per 750 mb), and Thermal Potential in units of (10^5 cal/cm^2 ^oK per 500 mb). Thermal Potential may also be thought of as the potential for Cb convection.

Figures 4-6 have been arranged to portray the dynamic and thermal potentials and their product for the summer season (July to September). The verification of this product (Fig. 6) is shown in Fig. 7. Values of Figs. 6 and 7 are expressed in number of cyclone genesis occurrences per 5^o latitude-longitude square per 20 years. See the report of Gray (1975a) for information on the similar verification of this genesis parameter in the other seasons.

From a conceptual view, it is important to understand the factors which lead to variations in location and seasonal frequency of cyclone genesis. But such information is often of limited assistance in making an individual day forecast of genesis in the regions and seasons where cyclones are known to develop.

2. Forecasting Individual Cyclone Genesis

At locations and in seasons which genesis regularly occurs, such as around Guam during the summer, the thermal potential is always positive and large and is not a significant factor in determining individual day genesis potential. Tropospheric vertical wind shear is usually also small. In regions and seasons where tropospheric vertical shear is small this is not a crucial factor 'by itself' in distinguishing disturbance genesis and non-genesis. Consideration must be given to other factors. Special individual case data sets of developing and non-developing

TABLE 2

Summary of Primary Genesis Parameters

Parameter	Favorable Condition	Genesis Role
1. Vorticity Parameter -- $(\zeta_r + 5)$ at ~950 mb where ζ_r is in units of $10^{-6}sec^{-1}$	Large	Produce necessary low level mass, moisture, and momentum convergence through Ekman-type boundary layer friction
2. Coriolis Parameter -- or f	Large	Allow for pressure gradient and sustaining of boundary layer winds against frictional dissipation
3. Vertical Shear Parameter -- $1/(S_z + 3)$ where $1/S_z$ is in units of $(m/sec)^{-1}$ 750 mb	Large	Allow condensation warming to be concentrated over moving disturbance; i.e. inhibit 200-500 mb ventilation energy
4. Ocean Energy Parameter -- or E	Large	Maintain surface Θ_e values in conditions of strong winds, upwelling, and large sea to air energy transfers
5. Moist Stability Parameter -- $(\frac{\partial \Theta_e}{\partial p})$ from surface to 500 mb	Large	Permit Cb cumulus convection
6. Humidity Parameter -- $\overline{RH}$ between 500 and 700 mb	Large	Allow for deep cumulus convection and high rainfall efficiency

Fig. 4 .

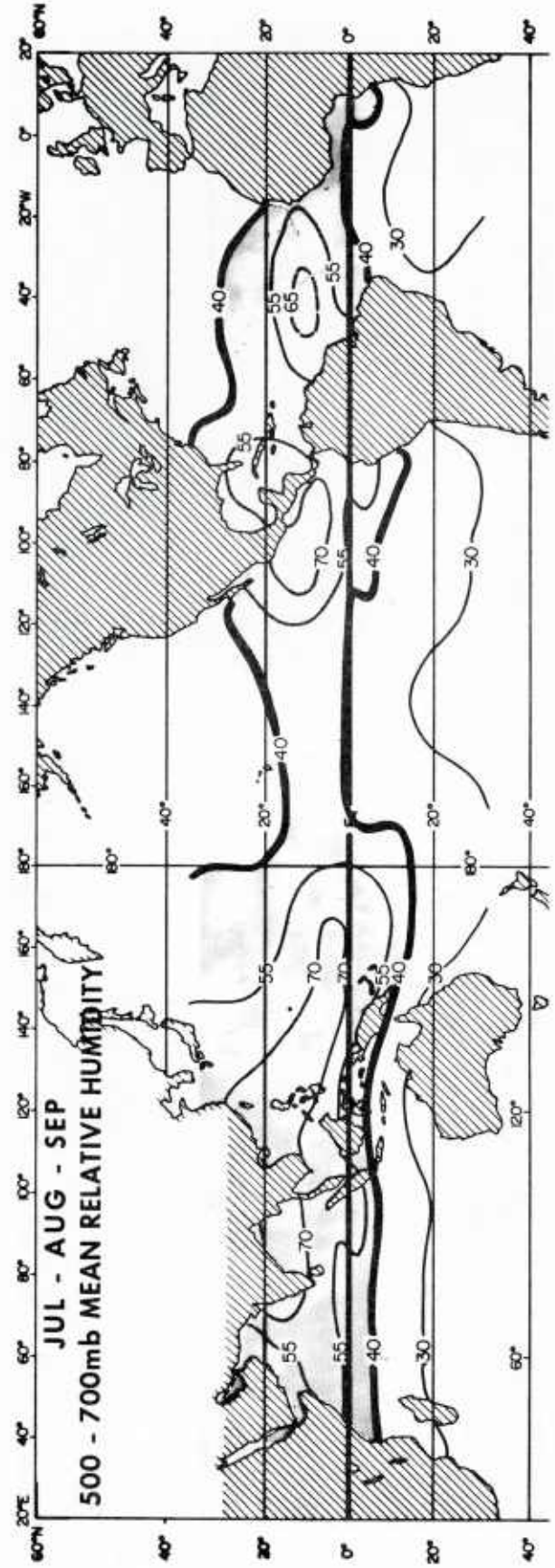
JUL - AUG - SEP
500 - 700mb MEAN RELATIVE HUMIDITY

Fig. 5 .

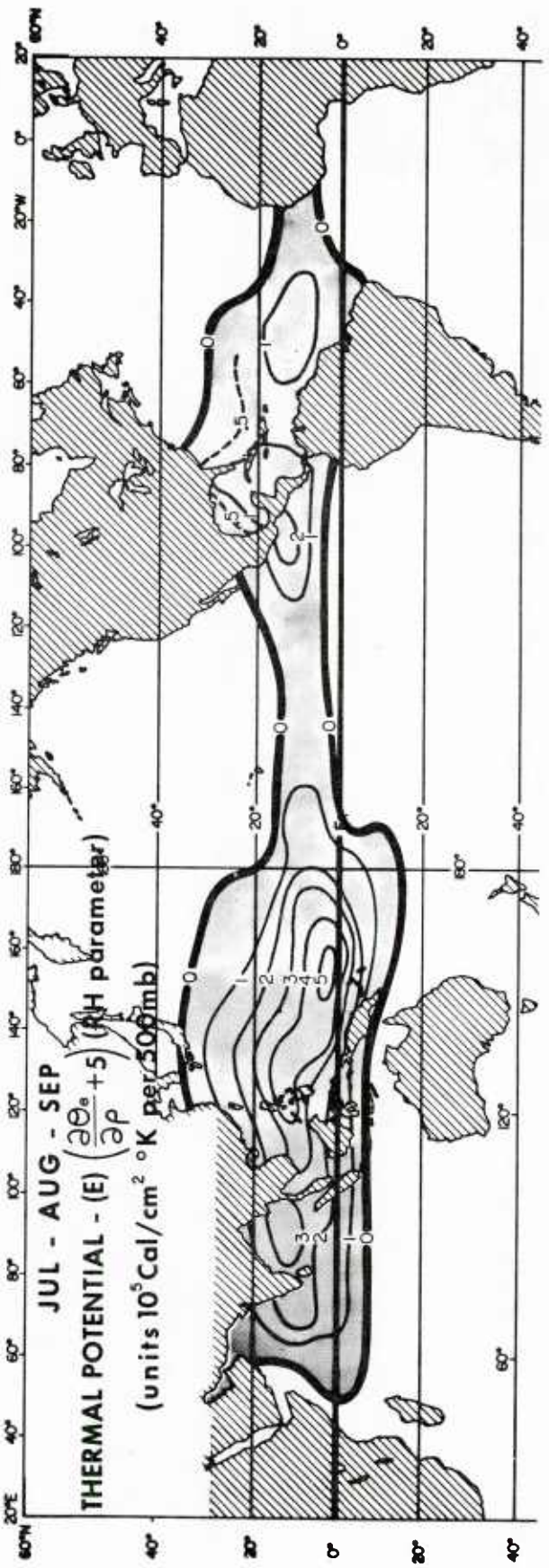
JUL - AUG - SEP
THERMAL POTENTIAL - (E) $\left(\frac{\partial \Theta_e}{\partial p}+5\right)$ (RH parameter)
(units 10^5Cal/cm^2 °K per 500mb)

Fig. 6 .

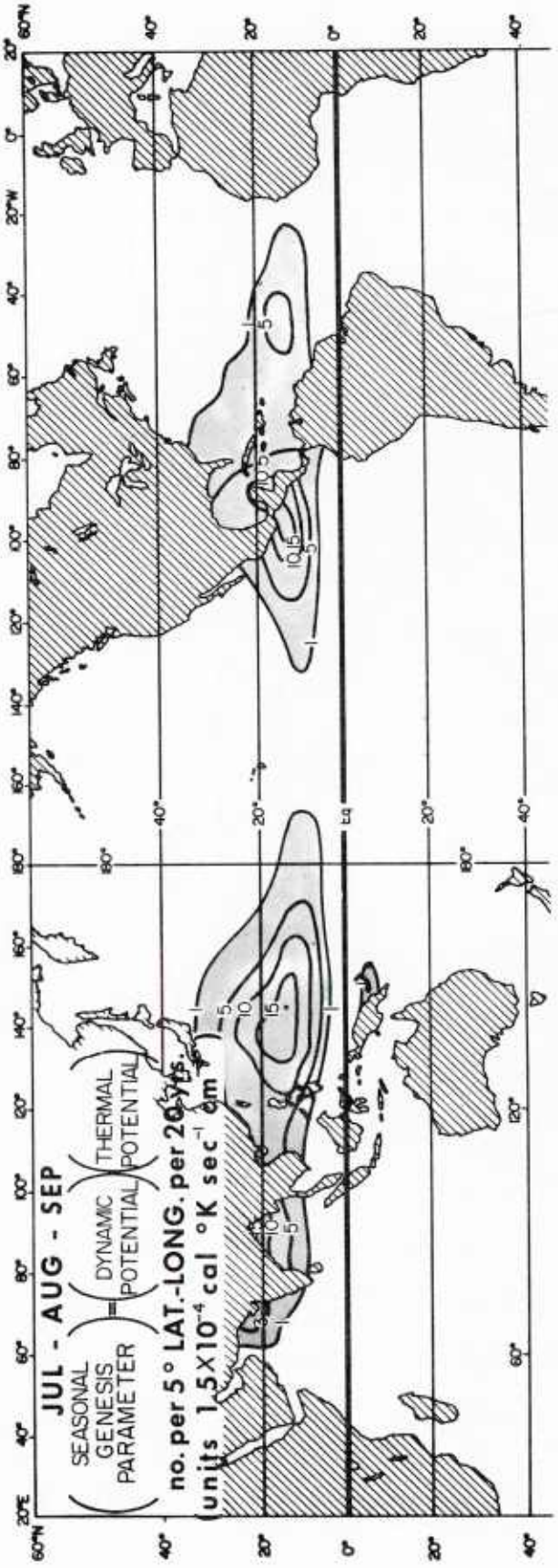
JUL - AUG - SEP
SEASONAL GENESIS PARAMETER
DYNAMIC POTENTIAL
THERMAL POTENTIAL
no. per 5° LAT.-LONG. per 20 yrs.
(units 1.5X10⁻⁴ cal °K sec⁻¹ cm⁻²)
Eq

Fig. 7 .

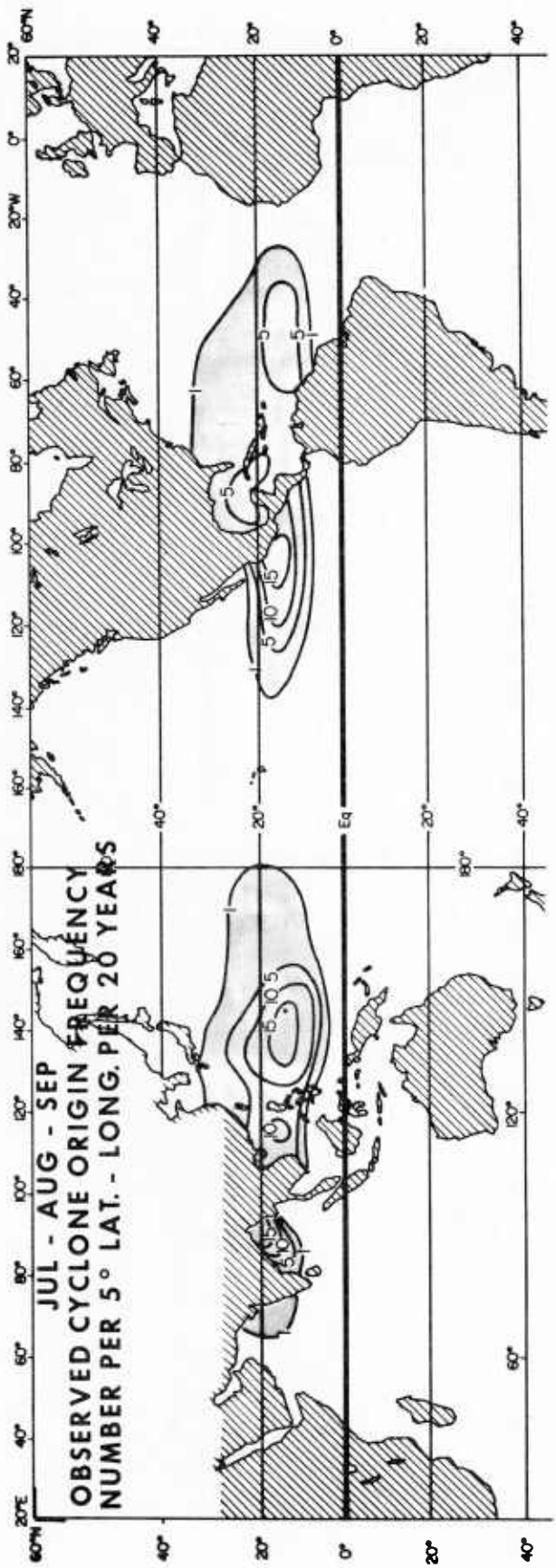
JUL - AUG - SEP
OBSERVED CYCLONE ORIGIN FREQUENCY
NUMBER PER 5° LAT. - LONG. PER 20 YEARS
Eq

disturbances have to be constructed to fully understand the day by day factors which control cyclone genesis.

We have made a large effort to come to grips with this problem by the compositing of individual disturbance cases of cyclone genesis and non-genesis and by isolating the differentiating day to day genesis features. We have constructed a number of new individual data sets. These new data sets have been extensively discussed in the reports by R. Zehr (CSU Atmos. Sci. Report No. 259, 1976), S. Erickson (CSU Atmos. Sci. Report No. 274, 1977), C. Arnold (CSU Atmos. Sci. Report No. 277, 1977), and J. McBride (11th Technical Conference on Hurricanes and Tropical Meteorology, Miami, FL, 1977). The genesis question has been observationally treated in these reports in a variety of ways.

3. Data Sets

I. R. Zehr (1976) Report. 10 years (1961-1970) and 130 cases of Western North Pacific cyclone genesis cases (designated data set 2). Over 600 rawinsonde reports are contained within 4^{o} radius of the centers of these developing cases. A greater rawinsonde sample is available at larger radii. Positioning is by the Guam Annual Typhoon Reports best track analysis combined with satellite positions since 1966.

Two sets of non-developing disturbances are used for comparison. All of these are equatorwards of 18^{o}N. One sample is of 87 non-developing cloud cluster disturbances during the summers (June through September) of 1967-1968 (designated sample 00) with a regional restriction (Fig. 8). The other is a larger data sample of approximately 400 cases of non-developing cloud-cluster disturbances throughout the years of 1967-1968 including disturbance clusters over a broader area (designated sample 0). The non-developing cases were positioned by satellite. Non-developing

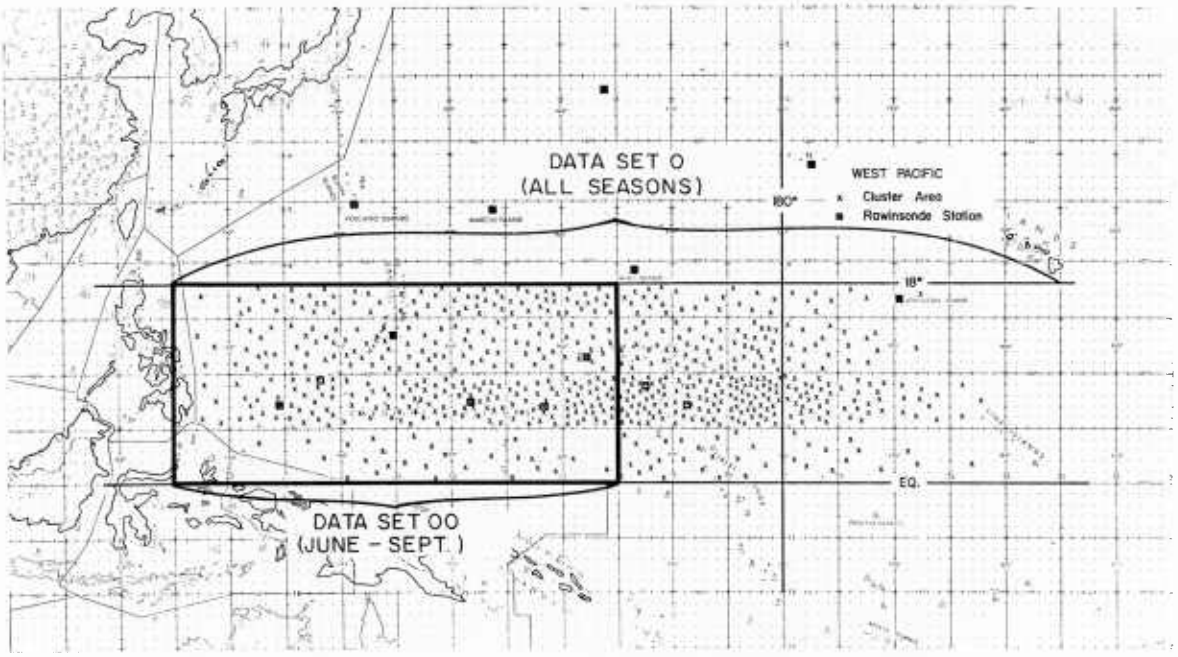

Fig. 8. X's mark positions of the clusters included in the non-developing cluster data set, Stage 0. Clusters were included which existed during all seasons. Non-developing cluster data set, Stage 00, included clusters only in the enclosed region and only during the months of June through September.

data samples 00 and 0 have 391 and 1903 rawinsonde reports within 4^{o} of their centers. Approximately twice as many rawinsonde reports are contained within 6^{o} radius of these systems.

II. S. Erickson (1977) Report. All cases are in the Western Pacific within the latitude belts of 3-19°N and longitude 125 to 178°W (see Fig. 9) during the years of 1971-1975. This data sample contains 53 cases of developing disturbance clusters (designated Early Stage 1 or ES1) and 49 cases of prominent non-developing disturbance cluster systems. The non-developing systems (designated data set 00') were tracked with the direct readout DMSP satellite pictures from Guam. All systems could be tracked for at least 1 day. The average time of tracking was 2½ to 3 days. The number of rawinsonde reports contained within

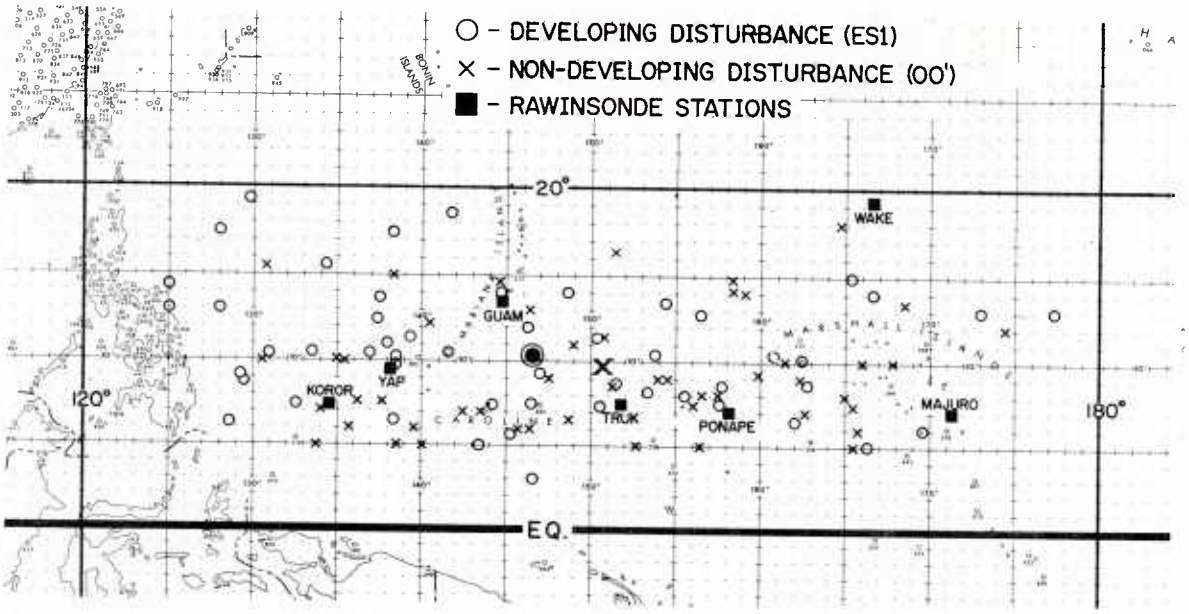

Fig. 9. X's and O's mark the initial position of the non-developing (OO') and developing (ES1) disturbances, respectively. The centroids of these positions are denoted by the large X (non-developing) and the large O (developing).

4^{o} and 6^{o} radius of the center for each of these two classes of systems is about 200 and 400 respectively.

III. McBride (1977) Paper. McBride has more extensively analyzed R. Zehr's Pacific data samples 00 and 2 plus Zehr's Pacific intensifying cyclone data sample (designated 4) which treats early cyclone genesis up to the points where the cyclones have maximum sustained winds of 50 knots. He has also assembled five addtional data sets (4 through 8) for the western Atlantic-West Indies region which are further designated by "D" for developing and "N" for non-developing. These data sets include:

N4 - Atlantic Depression: Western Atlantic depressions which do not develop into tropical storms. Positions are from the annual reports 'Atlantic Tropical Systems of 1967-76' by Staff of the National Hurricane Center published in Monthly Weather Review. Mean latitude is $\sim 21^{o}$N; Longitude is 81^{o}W; $V_{max} \sim 30$ kts.

D5 - Atlantic Prehurricane Depression: Positions for this data set and for data set D6 are from the official best tracks of the NHC. Data set D5 consists of all 12-hourly positions (up to a maximum of six positions per storm) immediately preceding data set D6. It represents the depression before it begins any significant intensification. Latitude is 21°N; Longitude is 75°W; $V_{max} \sim 30$ kts.

D6 - Atlantic Intensifying Cyclone: This data set is made up of that portion of each storm's track such that:

1) 35 knots < Estimated Maximum Sustained Winds $\leq$ 70 knots,
2) The last position where $V_{max} \leq 35$ kts is also included in the data set, and
3) V_{max} increases with every time period (12 hours) within the data set.

This data set is thus the portion of the track when the system is actually intensifying through the tropical storm stage. Mean latitude is $\sim$ 22°N; Longitude is $\sim$ 78°W; $V_{max} \sim 40$ kts.

N7 - Atlantic Cluster: In collaboration with V. Dvorak of NOAA/NESS Applications Group, positions were obtained from satellite pictures of tropical weather systems which subjectively looked like they had potential for development into tropical storms. If a circulation center for the disturbance was visible, it was defined as the position of the system; otherwise the center of mass of the cloud area was used. The mean latitude is $\sim$ 20°N; longitude is $\sim$ 82°W; $V_{max} \sim 15$ kts or less.

N8 - Atlantic Easterly Wave: N. Frank, director of the National Hurricane Center, Miami (NHC) has tracked the movement of Atlantic easterly waves since 1968. Using N. Frank's tracks in the Caribbean for the years 1968-1974 a composite was made relative to the centers of these wave disturbances. Only wave systems which had a significant amount of

cluster type convection associated with them were composited. The center of each system was defined such that the longitude was that of N. Frank's trough axis, and the latitude was the central latitude of convective activity as determined from geostationary satellite pictures. Mean latitude is $\sim 16^{o}$N; Longitude is $\sim 72^{o}$W; $V_{max} \sim$ 15 kts or less.

To retain the ability to make meaningful comparisons between systems which develop into storms and those which do not, no posiitons were included in non-developing data sets when the system center was within 1^{o} latitude of land within the following 24 hours.

The data were composited on a cylindrical coordinate grid. A parameter value described as being at 2^{o} radius is actually the composite average of all soundings falling between 1^{o} latitude distance and 3^{o} latitude distance from the system center. The number of rawinsonde reports contained within each of these eight independent data sets by radial belt is shown in Table 3.

TABLE 3

Number of rawinsonde observations included between 1-3^{o}, 3-5^{o}, and 5-7^{o} latitude distance from the center of each composite system.

	2^{o}	4^{o}	6^{o}
00 Pacific Cluster ($V_{max} \sim$ 15 kts)	142	224	283
0 Pacific Pretyphoon Cluster ($V_{max} \sim$ 25 kts)	151	281	352
4 Pacific Intensifying Cyclone ($V_{max} \sim$ 40 kts)	135	272	358
N4 Atlantic Depression ($V_{max} \sim$ 30 kts)	46	75	137
D5 Atlantic Prehurricane Depression ($V_{max} \sim$ 30 kts)	113	179	267
D6 Atlantic Intensifying Cyclone ($V_{max} \sim$ 40 kts)	111	227	299
N7 Atlantic Cluster ($V_{max} \sim$ 15 kts)	170	393	548
N8 Atlantic Easterly Wave ($V_{max} \sim$ 15 kts)	186	344	447

4. Disturbance Cloudiness and Vertical Motion as Related to Cyclone Genesis Potential

Our research project has spent much effort in determining whether significant convective and vertical motion differences exist between tropical disturbances which develop into cyclones and those which do not. Our studies show, in general, that the primary distinguishing parameters of disturbance cyclone genesis potential are not well related to the magnitude of cumulus convection and vertical motion or to disturbance moisture and temperature differences. The primary feature distinguishing genesis appears to be lower and upper tropospheric vorticity values at large radii.

Figure 10 compares the average upward vertical motion within 4^{o} radius of the center of Zehr's developing West Pacific disturbances (data set 2) with those of his non-developing cluster systems (data sets 0 and 00). Note the small differences between the two classes of systems. Figures 11 and 12 are from Erickson's independent data sample. They show mean vertical motion differences of his Early Stage One (ES1) genesis disturbances with those of his prominent cluster non-developing systems (00') for areas inside 4^{o} radius (Fig. 11) and 6^{o} radius (Fig. 12). Note again the small differences in average vertical motion between these two classes of systems.

Using DMSP satellite data, Erickson investigated many other cloud features of his two disturbance classes. These are listed in Table 4. It is seen that, in general, disturbance movement, cloud amounts, and other characteristics do not well differentiate developing and non-developing systems.

The primary cloud difference in these systems was the percentage of time that anticyclonic cirrus outflow was seen at outer radii on the

TABLE 4

Mean Physical Characteristics of Developing (ES1) and Non-developing (00') Disturbances

Physical Characteristic	Non-developing (00')	Developing (ES1)
Average Lifetime (days)	2.0	3.4*
Minimum-Maximum (days)	1-5	2.5-5.5*
Average Total Life of Storm (days)	N/A	9.5
Average Speed of Movement ($m\ s^{-1}$)	6.4	5.1
Shape (% of total cases):		
Elliptical	29.7	33.3
Wave	5.4	20.0
Circular	33.8	15.5
Irregular	31.1	31.2
Average Size (degrees radius):		
North Radius	3.5	4.0
East Radius	4.6	5.1
South Radius	3.7	4.2
West Radius	4.0	4.2
Average Radius	3.9	4.4
Average Direction Disturbance Moving to	275°	290°
Qualitative Judgement of Amount of Deep Convection(% of total cases) Classified as:		
Light	28.5	28.1
Moderate	47.9	47.8
Intense	23.6	24.1
Anticyclone Visible at Cirrus Level (% of total cases)	20.7	63.8

*Average based upon Arnold's (1977) entire pre-tropical depression stage.

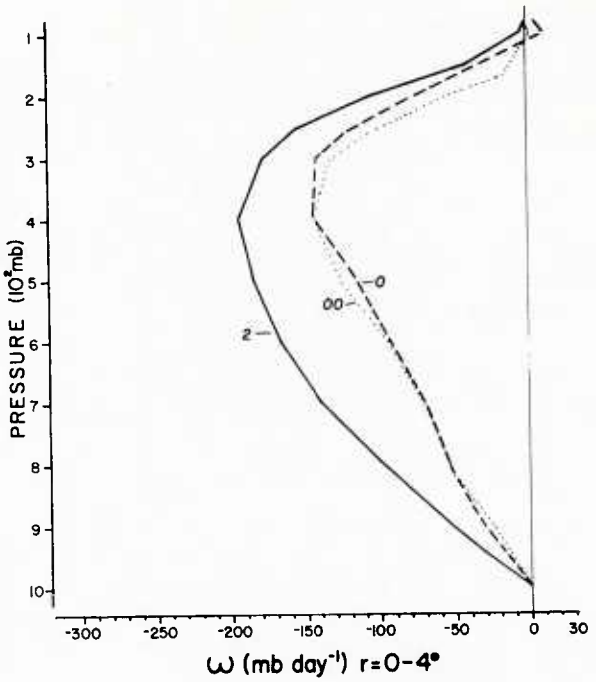

Fig. 10. Mean vertical velocity (ω) in the r = 0-4° area for the pre-typhoon cluster (2) and the non-developing clusters (0) and (00) (from Zehr, 1976).

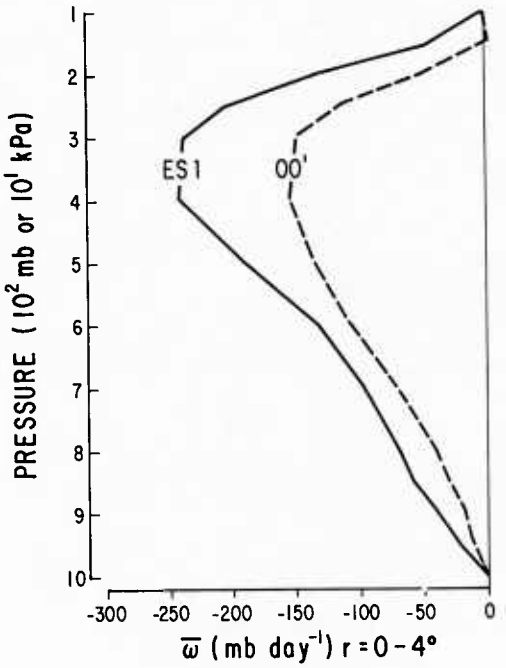

Fig. 11. Mean vertical motion within area r = 0-4° for the developing (ES1) and non-developing (00') disturbances (from S. Erickson, 1977).

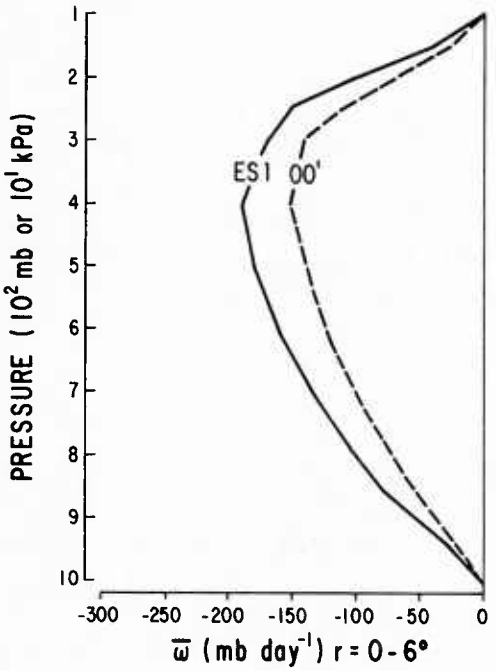

Fig. 12. Same as Fig. 11 except for r - 0-6° (from S. Erickson, 1977).

poleward side of the developing systems. Cloud amount and areal extent were not significantly related to development potential.

Of equal importance in making the case against cloud amount as a distinguishing characteristic of genesis is the large case by case variability of deep penetrative convection (which can be seen within the cirrus shield or on its edge) and of area of total cirrus cover. As seen in Figs. 13 and 14 this variability is very large for both classes of disturbance. Developing systems often have smaller amounts of deep penetrative convection and/or area of cirrus shield than do non-developing systems. Some non-developing disturbance systems can have massive amounts of deep convection and cirrus. Thus, for both the average and for the individual cases, amount of deep convection and area of cloudiness are not

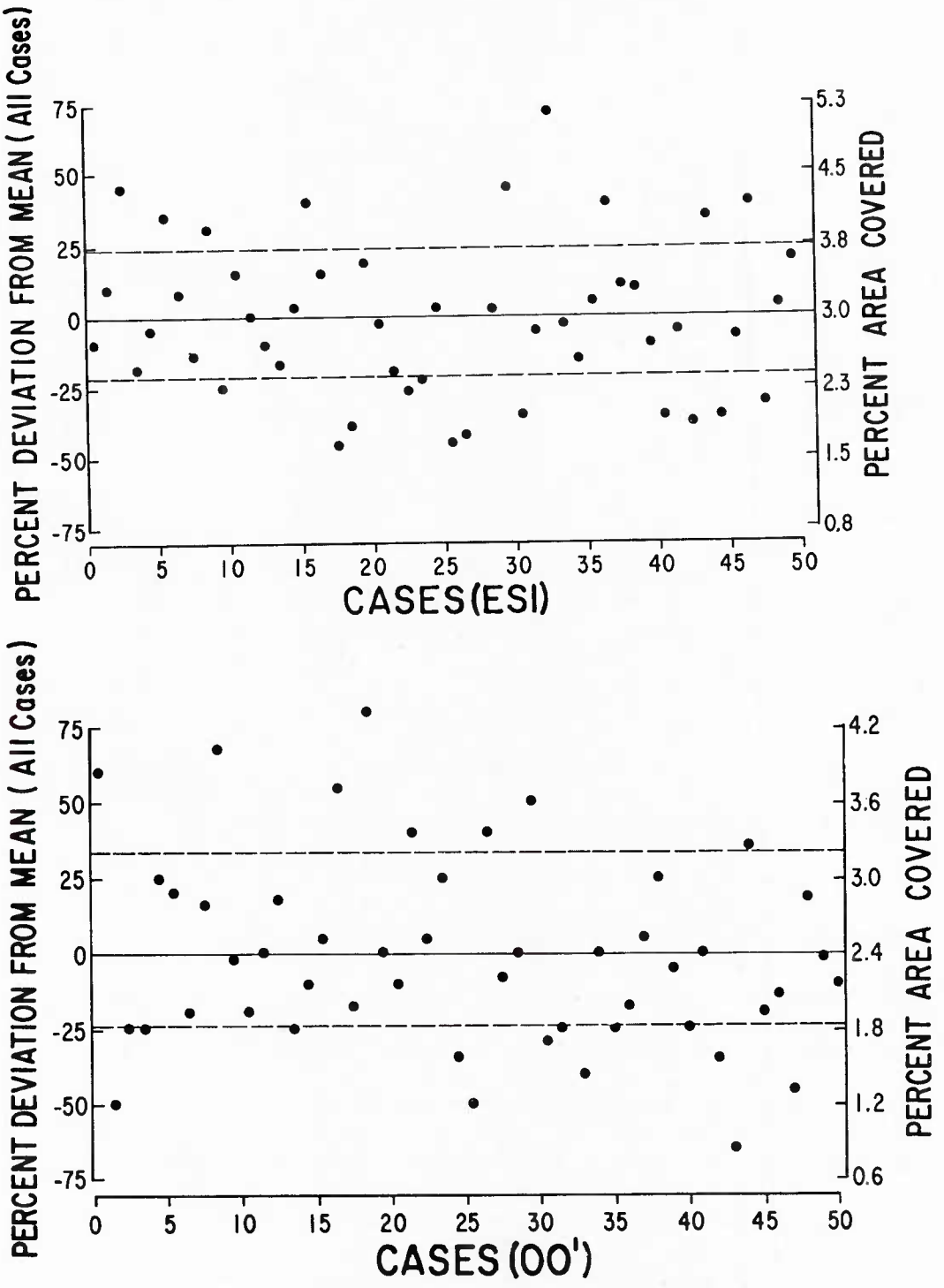

Fig. 13. A representative sample (∿ 40%) of the daily variability displayed by penetrative convection a $3^{o}x3^{o}$ area ($r \sim 4.2^{o}$) for the developing (ES1) and the non-developing (00') disturbances. The dashed lines represent the mean deviation of plotted convection samples above and below the case mean values.

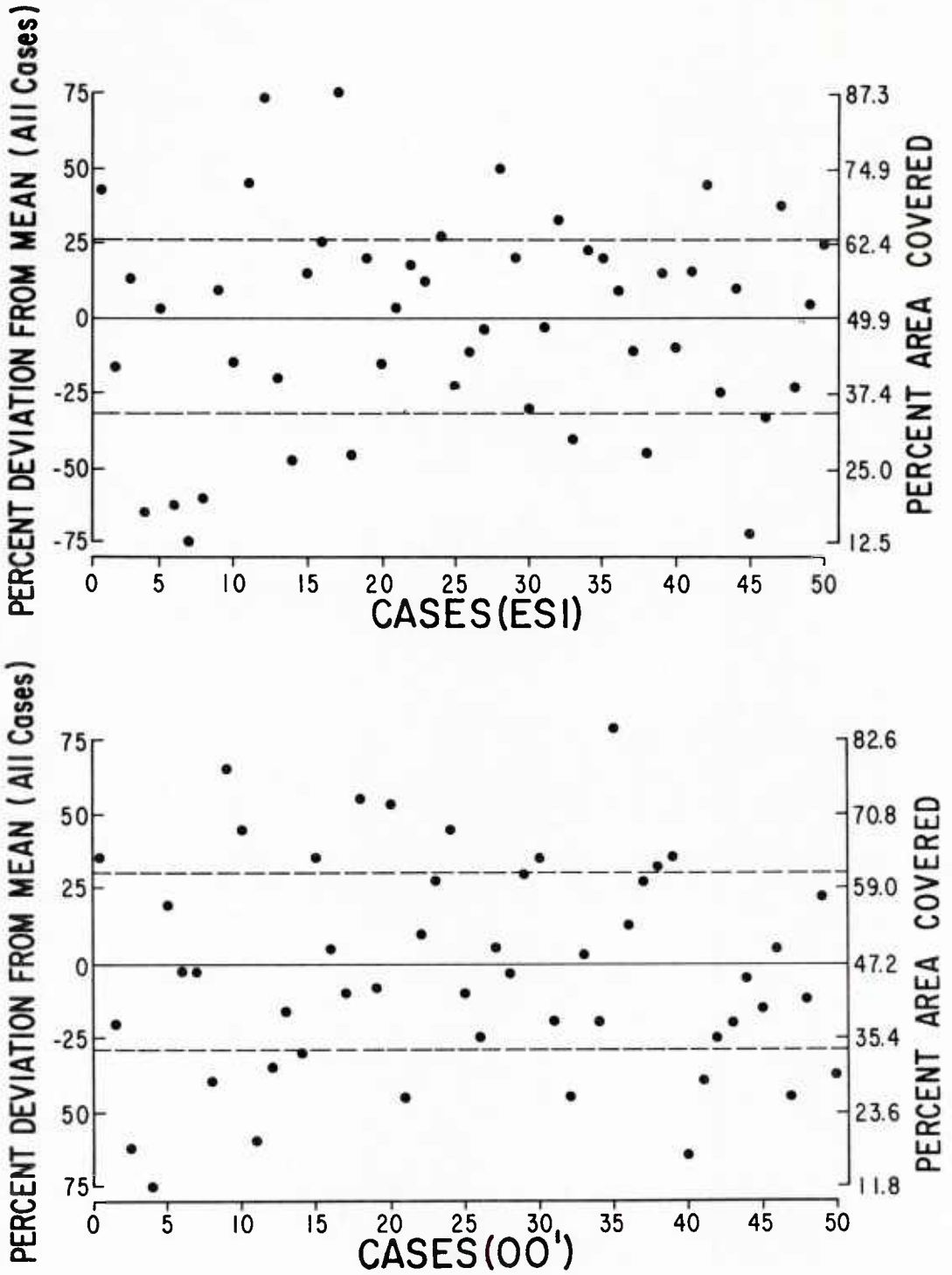

Fig. 14. A representative sample (∿ 40%) of the daily variability displayed by total cirrus within a $3^{\circ}X3^{\circ}$ area ($r_1 \sim 4.2^{\circ}$) for the developing (ES1) and non-developing (00') disturbances. The dashed lines represent the mean deviation of plotted cirrus samples above and below the case mean values.

good determining parameters of genesis potential. This is, of course, not surprising to satellite meteorologists such as V. Dvorak (1975). His skill at forecasting genesis from satellite cloud pictures is dependent primarily on cloud configuration and shape, not on cloud amount and intensity. He places a large importance on the configuration of the cirrus outflow to the poleward side of the cluster. Unidirectional upper tropospheric flow over the cluster is unfavorable for genesis.

5. Forecasting Genesis on a Daily Basis

At locations and seasons where cyclone genesis regularly occurs, such as near Guam in the summer, the thermal potential (of Fig. 5) is always positive and of large magnitude. Daily variations of this parameter do not distinguish genesis. At these times the primary distinguishing factor for cyclone genesis in individual cases is the dynamic potential.

The Coriolis parameter is important only in excluding genesis within 5^{o} of the equator. Tropospheric vertical wind shear will restrict disturbance genesis only at specific locations where it is large. Vertical shear by itself is only a limiting feature. In these situations lower and upper tropospheric relative vorticity differences surrounding the disturbance at large radii are of major importance in specifying genesis potential.

Our recent studies are showing that the primary factors differentiating the few tropical disturbances which become cyclones from the majority which do not are the relative vorticity at 900 and 200 mb averaged within 6^{o} radius of the disturbance center and the meridional

gradient of 900 to 200 mb vertical shear of the zonal wind across the disturbance [$(\partial/\partial y(-\partial u/\partial p)]$. The tropospheric vertical shear of the zonal wind at the disturbance center should be small and change sign. For genesis to occur shear should be positive to the poleward side and negative to the equatorward side of the disturbance as seen in Fig. 15. It is important that the line of zero zonal vertical shear cross near the center of the disturbance as in this figure. ITCZ genesis[1] occurs very close to this line. Examples of this change in sign of zonal vertical shear for genesis cases in other regions are shown in Figs. 16-18.

Contrasting examples of tropospheric vertical wind shear for non-developing cluster disturbances are shown in Figs. 19-21. Although vertical shear is also not large near the center of these non-developing cases, the N-S gradients of shear are much smaller than those of the developing cases.

The east to west gradient of 900 to 200 mb vertical shear of the meridional wind $(\frac{\partial}{\partial x} \frac{\partial v}{\partial p})$ can also contribute to genesis. However, this is typically smaller than the N-S shear gradient.

These shear gradients may also be thought of in terms of differences in lower and upper tropospheric vorticity. Thus, genesis is favored by the largest possible values of $\frac{\partial}{\partial y}(-\frac{\partial u}{\partial p}) + \frac{\partial}{\partial x}(\frac{\partial v}{\partial p})$, or $\frac{\partial}{\partial p}(\frac{\partial v}{\partial x} - \frac{\partial u}{\partial y})$, or $\frac{\partial}{\partial p}(Z_r)$ where Z_r is the relative vorticity. The cyclone Genesis Potential (GP) for an individual disturbance may be estimated from the magnitude of $(Z_{r_{900mb}} - Z_{r_{200mb}})$ averaged within an appropriate radius.

---

[1]Approximately 80-85% of the 100 or so global tropical cyclones which develop per year form near the ITCZ. Most of the other 15-20% develop within the trade winds, usually in association with an upper tropospheric trough to their northwest (see Gray, 1968).

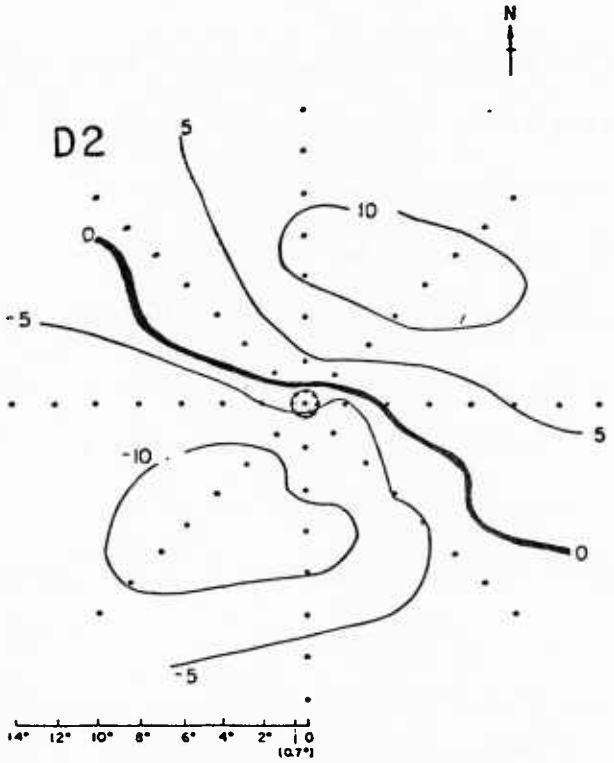

Fig. 15. Plan view of zonal shear, $U_{200mb} - U_{900mb}$ (m s^{-1}) for Pacific Pre-typhoon cluster, D2.

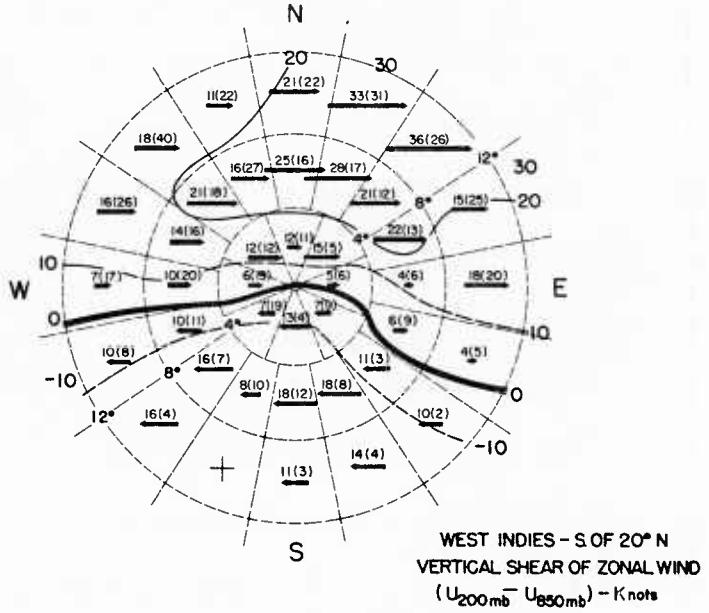

Fig. 16. Composite of average rawin information in each area relative to the center of 26 tropical disturbances which later developed into tropical storms. Length of arrows proportional to wind shear in knots (at left). Values in parentheses are number of wind reports in each area average. Distance from the center is given by the lightly dashed circular lines at 4^{o} latitude increments.

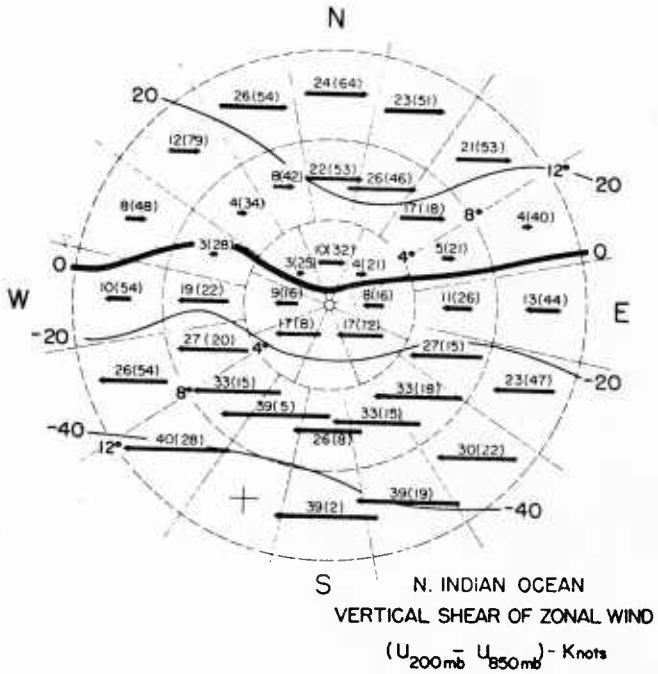

Fig. 17. Composite of average rawin information in each area relative to the center of 54 tropical disturbances which later developed into tropical storms. Length of arrows proportional to wind shear in knots (at left). Values in parentheses are number of wind reports in each area average. Distance from the center is given by the lightly dashed circular lines at 4^{o} latitude.

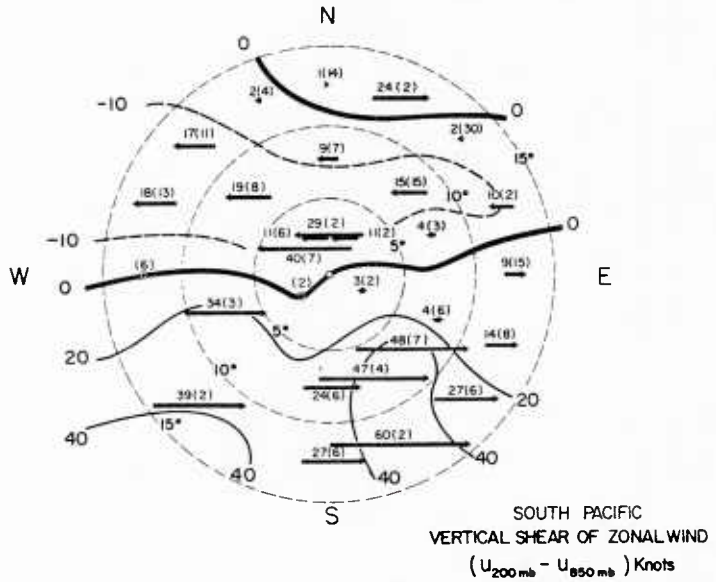

Fig. 18. Composite zonal vertical wind shear for ave. rawin information in each area relative to the center of 84 tropical disturbances in S. Pacific which later developed into tropical storms. Length of arrows proportional to wind shear in knots (at left). Values in parentheses are number of wind reports in each area average. Distance from the center is given by the lightly dashed circular lines at 5^{o} lat. increments. (Reproduced from Gray, 1968).

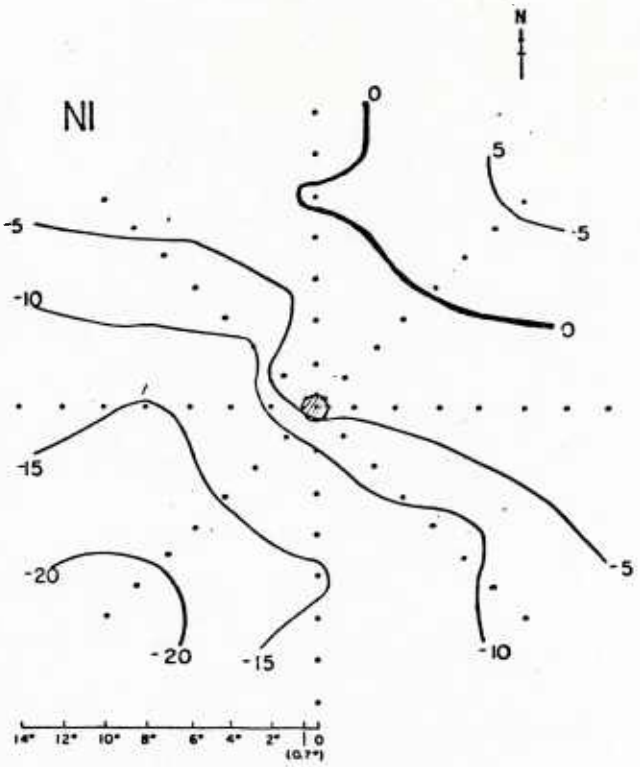

Fig. 19. Plan view of zonal shear, $U_{200mb} - U_{900mb}$ (m s^{-1}) for the non-developing Pacific clusters (00).

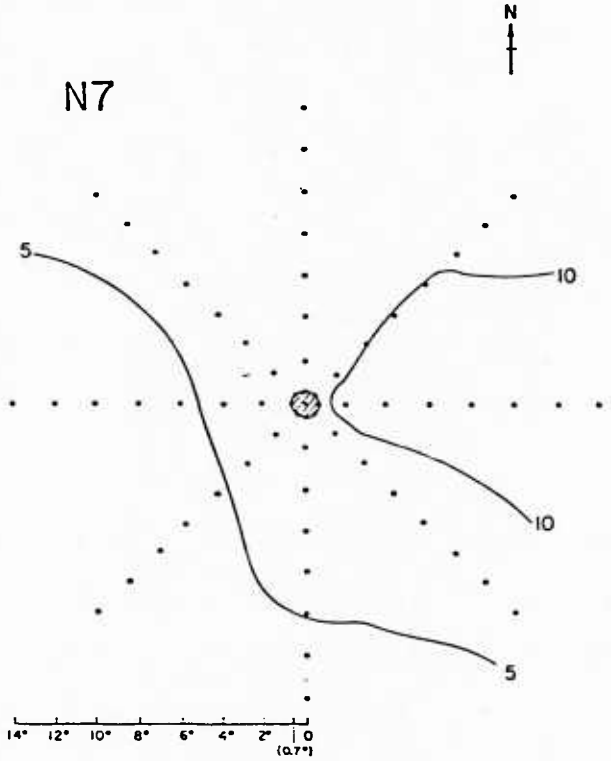

Fig. 20. Same as Fig. 19 but for non-developing Atlantic Clusters (N7).

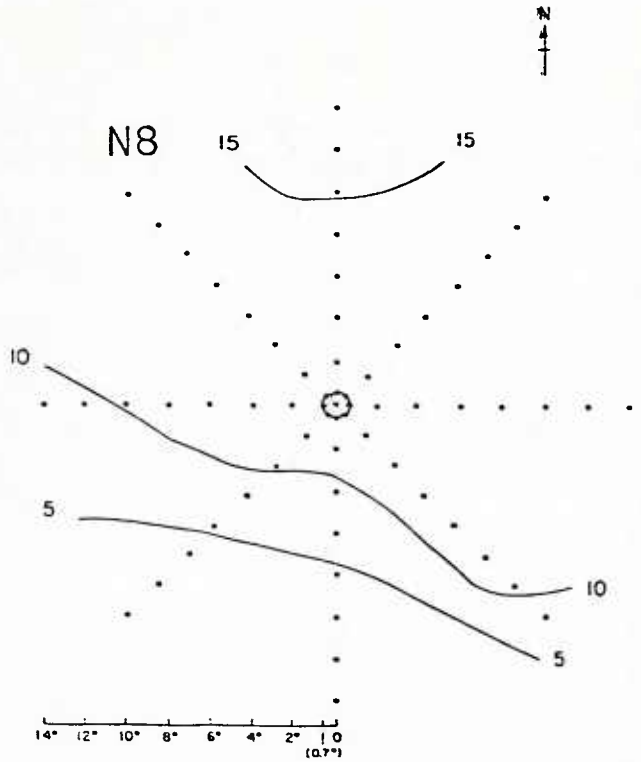

Fig. 21. Same as Fig. 19 but for non-developing Atlantic Easterly Wave (N8).

S. Erickson (1977) has calculated these upper and lower tropospheric vorticity differences by different radial bands for his developing (ES1) and non-developing (00') disturbances. Results are shown in Table 5. The best results are found for radial intervals between 0-6°. Differences are 3 to 1. No other parameter differences such as moisture, temperature, wind speed, cloudiness, vertical motion, etc. are this large.

J. McBride (1977) has also tested this Genesis Potential (GP) for Zehr's three Pacific stratifications and for his five recently composited Atlantic developing and non-developing systems. Results are shown in Table 6. All developing system classes (2, 4, D5, D6) have values of GP significantly larger (about 3 to 1) than the non-developing

TABLE 5

Mean Relative Vorticity ($\bar{\zeta}_r$) Differences Between 900 mb and 200 mb for the Developing (ES1) and Non-developing (00') Disturbances

	($\bar{\zeta}_{r_{900\ mb}}$ minus $\bar{\zeta}_{r_{200\ mb}}$)($10^{-5}s^{-1}$)	
Radial Area	Developing (ES1)	Non-developing (00')
0-2°	5.9	3.4
0-4°	3.6	1.3
2-4°	2.8	.6
0-6°	3.0	1.0
4-6°	2.5	.8

systems (00, N4, N7, N8). As with the Erickson study, other parameter differences were much smaller. Combining the developing and non-developing systems one obtains GP differences of over three to one or larger as shown in Table 7.

Vertical cross-sections of mean vorticity inside 6° radius for the two independent data samples of Zehr and Erickson are shown in Figs. 22 and 23. Note the large differences in lower and upper level vorticity for the developing cases in comparison with the non-developing cases.

Comparisons of average flow patterns between Erickson's cases of developing (ES1) and non-developing cases (00') at 950 mb and 200 mb are shown in Figs. 24 and 25. Note the stronger trade wind flow to the north of the developing systems in Fig. 24. Also note the outflow at 200 mb to the poleward side in the developing case as compared with near unidirectional flow at 200 mb with the non-developing case in Fig. 25.

TABLE 6

Genesis Potential (GP). Mean relative vorticity differences between 900 mb and 200 mb for each composite data set. Developing systems are underlined (from McBride, 1977).

$$GP = \overline{\xi}_{900mb} \text{ minus } \overline{\xi}_{200mb} \quad (10^{-5}\ s^{-1})$$

	0-2°	0-4°	0-6°
00 - Pacific Cluster	2.0	1.6	0.7
2 - Pacific Pretyphoon Cluster	4.9	3.1	2.4
4 - Pacific Intensifying Cyclone	8.6	4.7	3.0
N4 - Atlantic Depression	5.5	2.0	1.0
D5 - Atlantic Prehurricane Depression	5.2	2.8	1.8
D6 - Atlantic Intensifying Cyclone	9.8	4.2	2.8
N7 - Atlantic Cluster	-.5	.4	.7
N8 - Atlantic Easterly Wave	1.9	.5	.3

TABLE 7

Genesis Potential (GP) - Average of Developing and Non-developing Data Sets ($10^{-5}s^{-1}$)

	0-2°	0-4°	0-6°
Average NON-DEVELOPING (N1, N4, N7, N8)	2.2	1.1	0.7
Average DEVELOPING - weak systems (D2, D5)	5.1	3.0	2.1
Average DEVELOPING - all systems (D2, D5, D6)	7.1	3.7	2.5

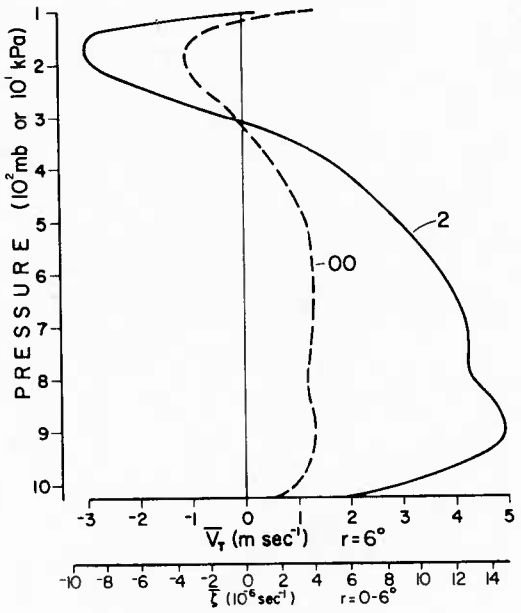

Fig. 22. Mean relative vorticity within area r = 0-6° (equivalent to mean tangential winds in r = 5-7° band) from Zehr's (1976) developing (Stage 2) and non-developing (Stage 00) disturbances.

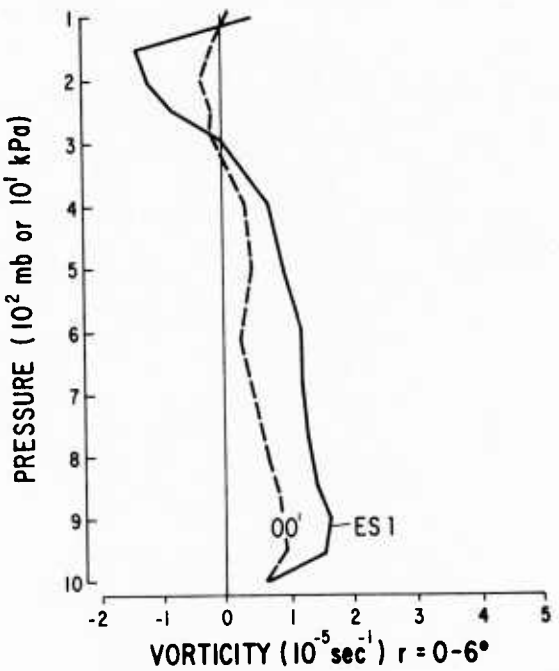

Fig. 23. Mean relative vorticity within area r = 0-6° for the developing (ES1) and non-developing (00') disturbances. S. Erickson, (1977).

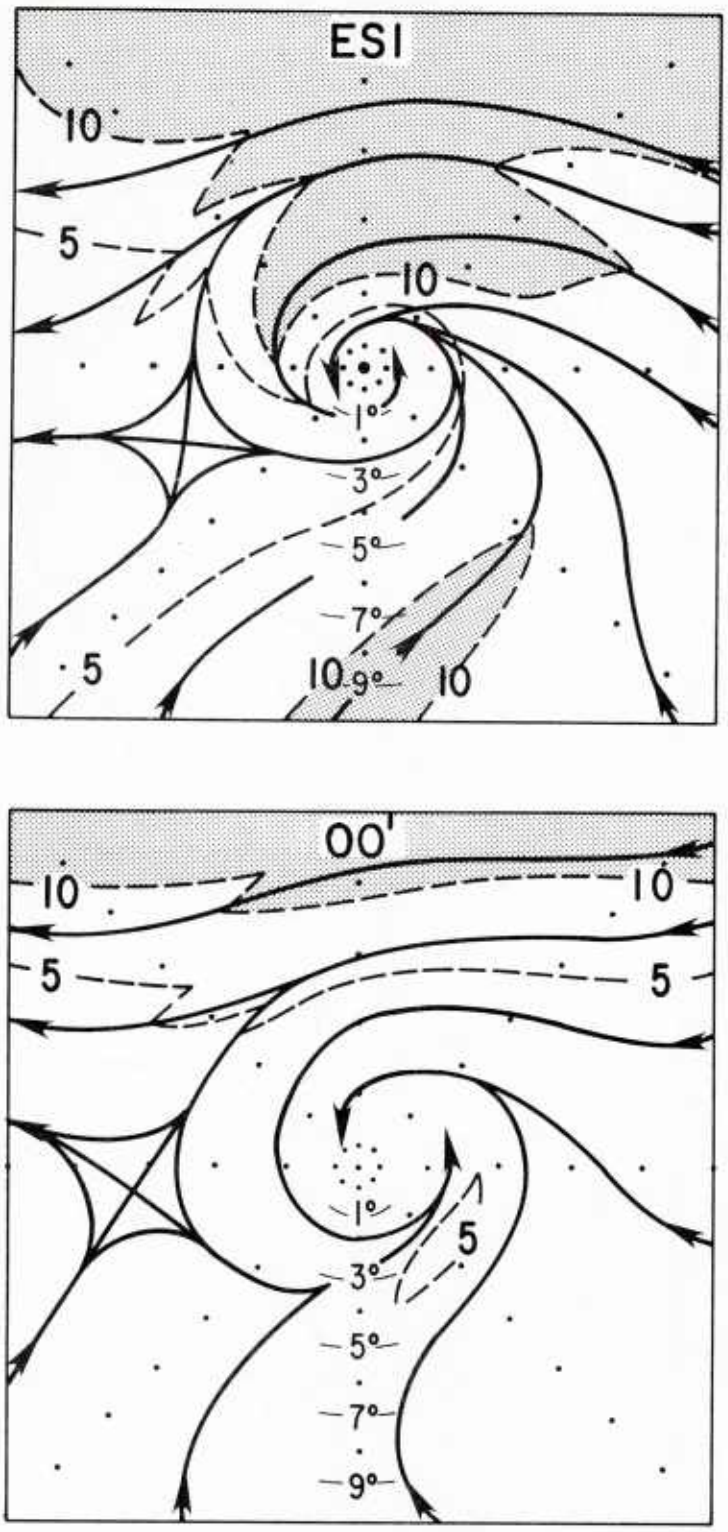

Fig. 24. Average isotach (m s^{-1}) and streamline analysis for the developing (ES1 - above) and non-developing (00' - below) disturbances at 950 mb.

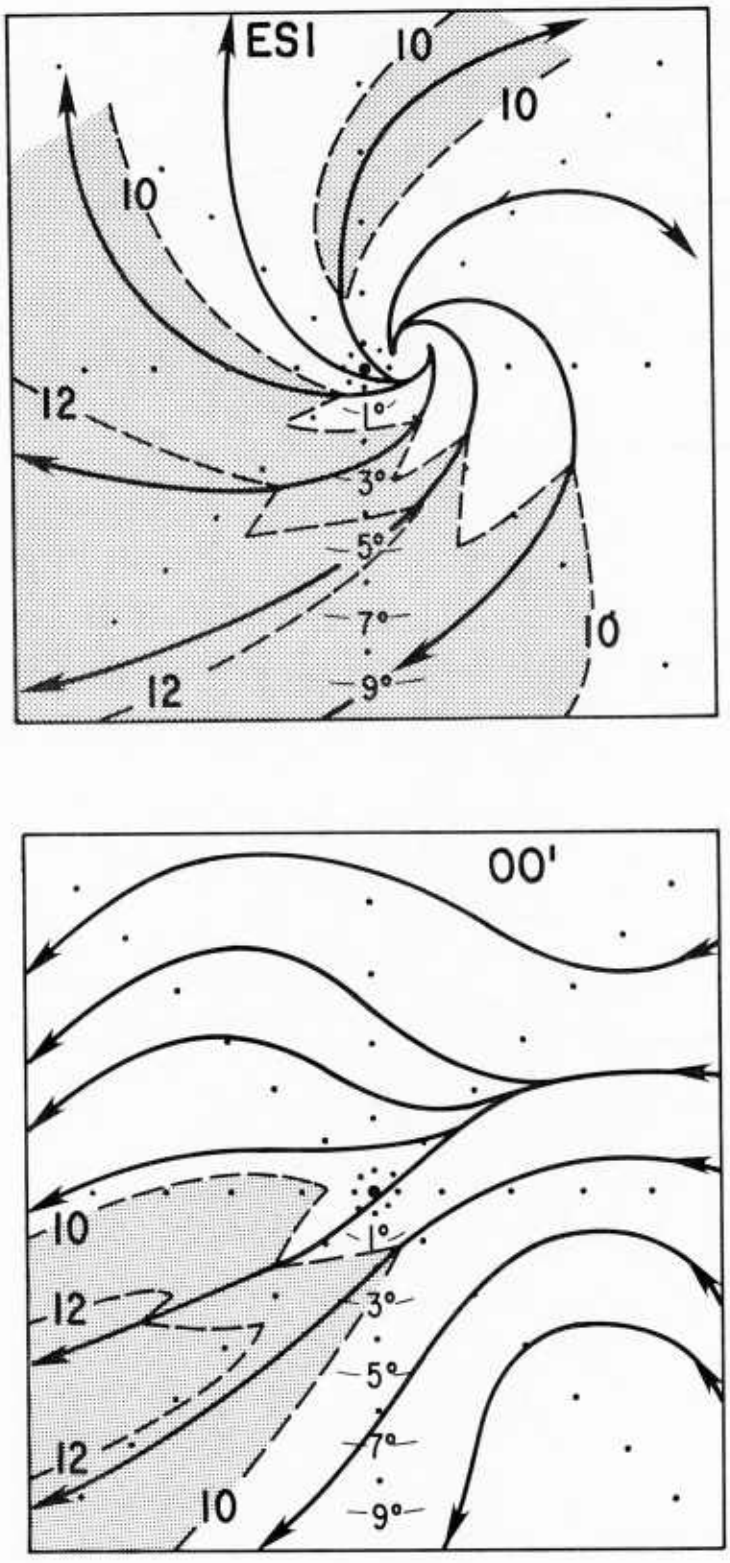

Fig. 25. Average isotach (m s^{-1}) and streamline analysis for the developing (ES1 - above) and non-developing (00' - below) disturbances at 200 mb.

There can be no doubt but that significant differences exist in the surrounding disturbance wind fields. It would appear that practical forecast schemes could be devised that would measure these surrounding disturbance vorticity differences. Thus, the mean disturbance vorticity inside 6^{o} radius can be represented by $Z_r \sim \frac{2V_\theta}{r}$ where V_θ is the tangential wind at $r = 6^{o}$ radius around the center of the disturbance. The Genesis Potential (GP) would be represented as:

$$GP \approx \frac{1}{\pi r^2} \left(\oint_{6^o} V_{\theta_{900\ mb}} \delta s - \oint_{6^o} V_{\theta_{200\ mb}} \delta s, \right. \qquad \text{or}$$

$$GP \simeq K \left(\overline{V_{\theta}}_{900\ mb} - \overline{V_{\theta}}_{200\ mb} \right)$$

where K is a constant. Genesis should be expected when $(\overline{V}_{\theta_{900mb}} - \overline{V}_{\theta_{200mb}})$ at 6^{o} becomes larger than about 5 m/s and not expected when $(V_{\theta_{900mb}} - V_{\theta_{200mb}})$ is less than approximately 3 m/s. This relationship needs more specific case testing, however.

As lower and upper tropospheric maps are the primary analysis levels in the tropics and since the geostationary satellite will often be able to furnish winds at these levels, specially constructed 6^{o} radius templates could be placed over weather maps at the disturbance centers and the average wind components tangent to this circle at 900 and 200 mb estimated. A rapid numerical evaluation of this genesis parameter could thus be obtained. We are presently making an evaluation of this GP on individual cases and hope to have a workable calibration of this parameter within the next year.

6. Discussion

It appears that cyclone genesis is dependent not upon the magnitude of tropical disturbance convergence and rainfall but rather upon the strengths of the surrounding low level cyclonic circulation and upper tropospheric anticyclonic circulation.

Genesis might be thought of from the point-of-view of conditions which lead to an increase of absolute angular momentum (m_a) within a cylindrical area of the disturbance region out to 6^o radius. Thus,

$$\int \frac{\partial m_a}{\partial t}\ \delta m = -\int_{100\ mb}^{Sfc}\int_{0}^{2\pi} m_a\, v_r\ \delta\theta\ \frac{\delta p}{g} \quad + \quad \int r F_\theta\ \delta M \qquad (5)$$

(1) (2) (3)

(Mean rate of change of Momentum Within Disturbance Region) (Import of Angular Momentum at the 6^o Radius Boundary) (Dissipation of Angular Momentum Within the Disturbance Region)

where

$$m_a = rV_\theta + \frac{fr^2}{2}$$

$$\delta M = \int_{100mb}^{Sfc}\int_{0}^{2\pi}\int_{0}^{6^o} r\ \delta r\ \ \delta\theta\ \ \frac{\delta p}{g}$$

V_r, V_θ = radial and tangential winds

F_θ = tangential friction

Cyclone genesis requires positive values of term (1) [term (2) significantly larger than term (3)]. The observational data of Zehr (1976) and S. Erickson (1977) allow us to calculate these terms for the developing (2, ES1) and non-developing (00 and 00') disturbances

at the 6° radius. Results indicate sizable differences in the inward angular momentum transport between these classes of systems. The developing systems have much stronger inward transport of momentum. In the developing systems (2, ES1) the gain of angular momentum is significantly larger than the dissipation. This is not so with the non-developing (00, 00') systems. This subject is now being extensively investigated by J. McBride. Results should be available by next year. Kinetic energy and other budgets are also being made.

The large scale positioning of the disturbance's surrounding lower and upper tropospheric flow patterns is a crucial factor in the specification of cyclone genesis. Sadler (1967a, 1967b, 1974, 1976a,b) has presented much evidence of the importance for genesis of the positioning of a surrounding upper tropospheric trough to the northwest of pre-cyclone disturbances. The resulting concentrated outflow channels to the north of the incipient disturbance favor genesis, and the presence of the trough strengthens upper level anticyclonic flow and hence increases the Genesis Potential. Cyclone genesis poleward of 18-20° seldom occurs unless an upper tropospheric trough is present to the northwest.

H. Riehl[2] (1975) has often noted that many cases of Gulf of Mexico cyclone formation are associated with the passage of an upper-level westerly wind trough to the north of an incipient disturbance. Riehl has consistently emphasized the importance for genesis of favorable sub-tropical or middle latitude upper tropospheric flow features.

---

[2]Personal communication 1957-1962.

Yanai[3] (1961) has also emphasized the role of favorable large-scale surrounding flow features as a requirement of genesis.

The favorable positioning of surrounding wind fields are not well related to the amount of disturbance convection. This is consistent with the observation that heavily raining tropical disturbances often do not form cyclones while other less intense disturbance systems often do. Thus, it would appear that cyclone genesis can never be realistically modeled through schemes which deal only with differences in the direct condensation processes of the disturbances. It is much more important that the surrounding wind field differences be modeled.

---

[3] Personal communication 1962-1970.

III. COMPARISON OF TYPHOON AND HURRICANE STRUCTURES

A great deal of current tropical cyclone research involves the use of numerical models of the storms. To assess the results of such efforts it is important to determine whether the models accurately simulate the structure and dynamic processes of tropical cyclones. Advances in our knowledge of tropical storms based on observational studies are therefore important to those involved in modeling research. In addition, improved understanding of storm/environment interactions should lead directly to improvements in storm intensity change and motion forecasts.

In a recent NEPRF report Gray and Frank (1977) discussed the structure of West Pacific typhoons based on 10 years of composite rawinsonde data (Fig. 1). Similar analyses have now been performed for West Indies hurricanes by Núñez and Gray (1977) using 14 years (1961-1974) of rawinsonde data (Fig. 2). This section compares the large scale structures and angular momentum and kinetic energy budgets of the above two types of storms. Since differences between storms in the two regions must be due to differences in the large scale circulations, a comparison of typhoons and hurricanes yields some insight into the relationships between a storm and its environment. The typhoon data set includes all West Pacific storms with Central pressures $\leq$ 980 mb, while the West Atlantic sample is composed of all storms with maximum wind $\geq$ 65 knots. The data sets and compositing techniques have been discussed in Gray and Frank (1977) and Frank (1977a).

1. Thermodynamic Fields

Temperature Anomaly. Figures 26 and 27 show the temperature

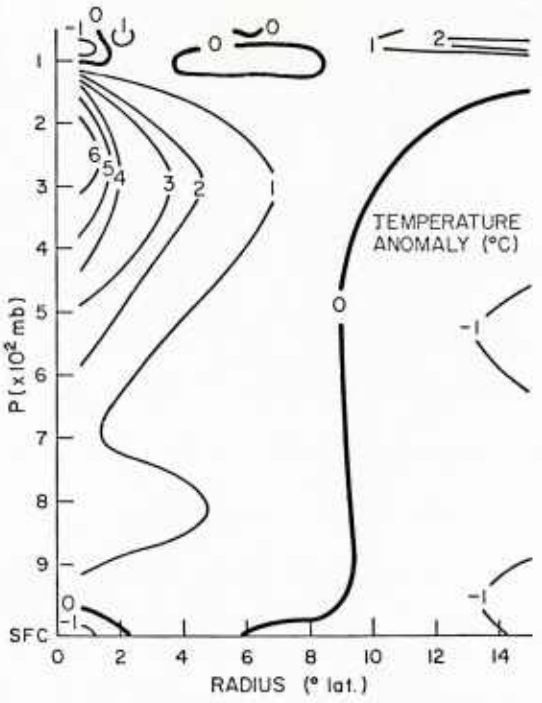

Fig. 26. Temperature anomaly in ^{o}C for the mean steady state typhoon. A mean temperature for the 9^{o} to 15^{o} east and west latitude belt was computed and deviations from it were then calculated.

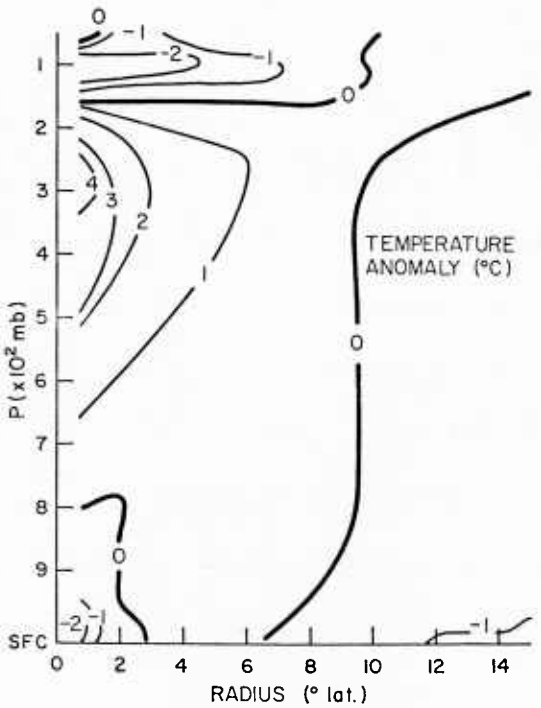

Fig. 27. Same as Fig. 26 but for the mean steady state hurricane.

anomaly for the typhoon and the hurricane. Temperature anomaly has been calculated in the following manner: a mean temperature is determined by averaging the temperature values between 9 and 15 degrees to the east and west of the hurricane position. Deviations from this mean temperature are then computed.

There is a marked similarity between the two temperature anomaly patterns. Both are shown to be warm core throughout most of the troposphere. The warmest temperature is detected at about 300 mb for the hurricane and slightly higher for the typhoon (250 mb). Due to high wind conditions, there are few data points inside 0.7^{o} of latitude radius, but Gray and Shea (1973), Gray and Shea (1976) and several case studies have shown that the temperature in the eye can exceed that at 0.7^{o} by about $7\text{-}8^{o}$ or more. These temperatures cannot be measured with our rawinsonde network.

Near the surface we can detect a somewhat larger cooling anomaly for the hurricane than for the typhoon. This may be indicative of a smaller ocean to atmosphere sensible heat flux. This is also suggested by the fact that the mean typhoon position lies over waters where the depth of the 26^{o}C isotherm varies between 60 and 90 m while for the hurricane the depth varies between 30 and 60 m (see Gray, 1975a). Consequently, on the average, there might be less sensible heat available to the West Indies systems.

A cold core region can be detected at the upper tropospheric and lower stratospheric levels for both systems. This cooling is probably a result of overshooting by Cb towers and radiational cooling off the top of the cirrus deck. For the hurricane this region can be detected at a somewhat lower level and covers a larger radial extent.

Relative Humidity. Figures 28 and 29 show nighttime relative humidity cross sections of the typhoon and the hurricane. Relative humidity values for the hurricane are in general 10% drier than those for the typhoon at equivalent radii and heights. The typhoon also shows a moister inner core with relative humidities in excess of 90% up to about 400 mb, while in the hurricane these values are not found higher than 575 mb. It would appear that entrainment will have slightly greater restraining effects on cumulonimbus convection within the hurricane's inner 2^{o} radius. Beyond 6^{o} radius relative humidities approach environmental values.

It should be mentioned that the typhoon develops within a more favorable environment. Gray, Ruprecht and Phelps (1975) found Western Pacific clusters and clear regions to have significantly higher middle level relative humidities than corresponding regions in the West Atlantic. Boundary layer relative humidities in the West Atlantic clear area were about 15% lower than in the West Pacific.

2. Wind Fields

Radial Winds. Two dimensional cross sections of radial wind (V_r) for the typhoon and the hurricane are shown in Figs. 30 and 31. These winds have been adjusted to achieve mass balance. Maximum inflow occurs at 950 mb for both systems. At 0.7^{o} radius, inflow seems to be much shallower for the hurricane. However caution must be exercised because the data set at this radius is small. From a radius of 2^{o} on, the patterns are quite similar showing a layer of inward radial winds extending to around 300 mb and an outflow layer centered near 150 mb. The outflow layer extends farther out for the typhoon.

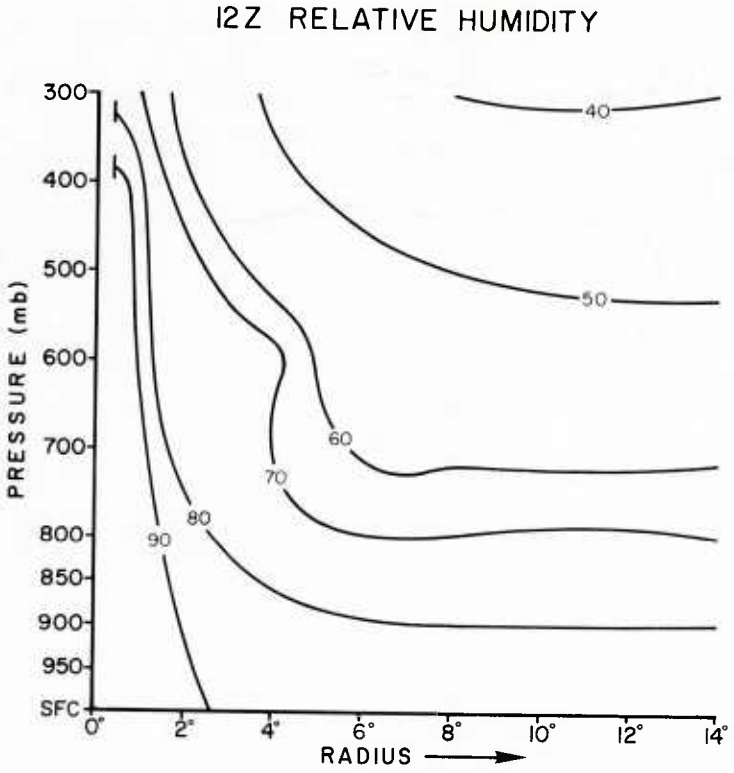

Fig. 28. 12Z relative humidity for the mean steady state typhoon (∿ 2200 local time).

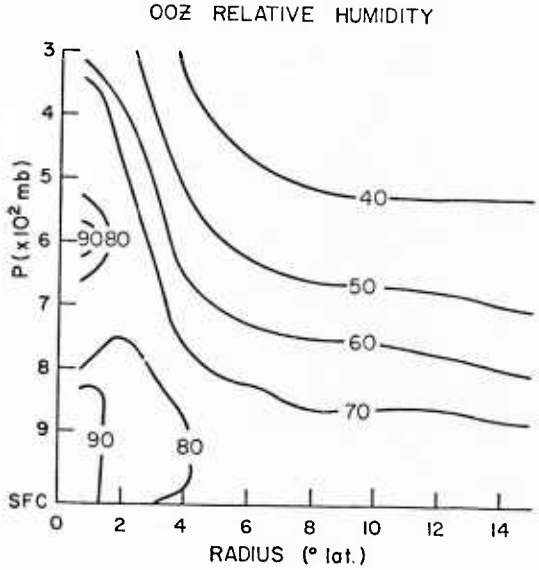

Fig. 29. 00Z relative humidity for the mean steady state hurricane (∿ 1900 local time).

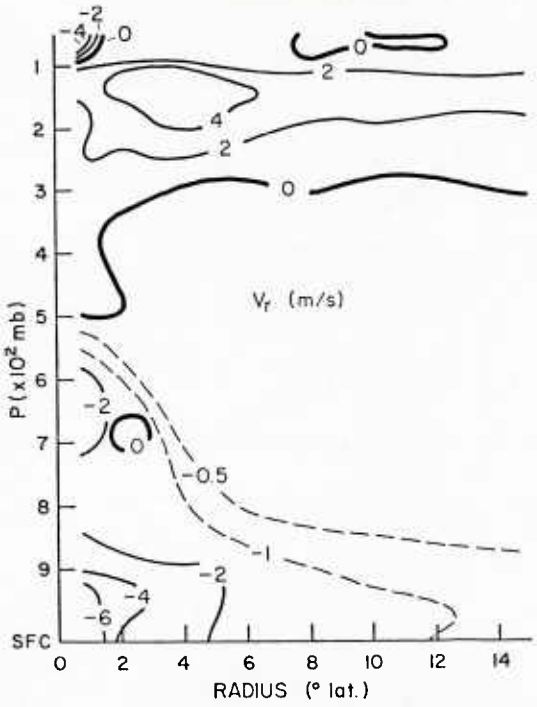

Fig. 30. Two dimensional cross section of radial winds (V_r) for the mean steady state typhoon .

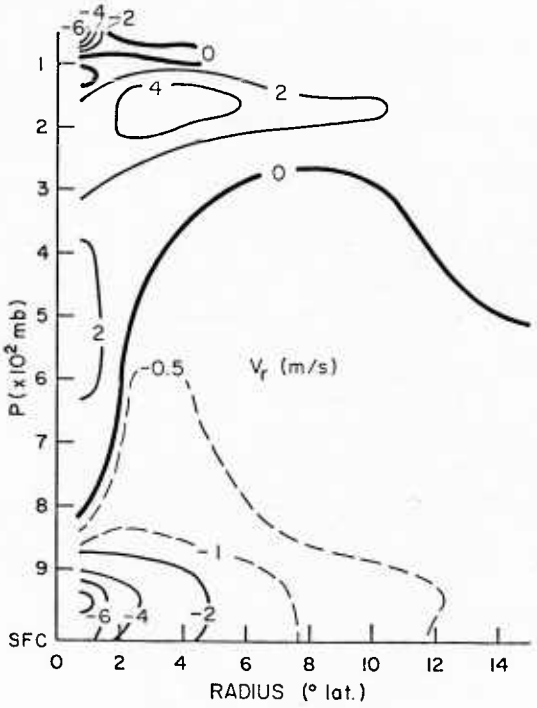

Fig. 31. Same as Fig. 30 but for the mean steady state hurricane.

Plan views of the radial wind at 150 mb in stationary geographical coordinates are offered for comparison in Figs. 32 and 33. This is the maximum outflow level for the typhoons. Although the patterns have a close resemblance, it can be noted that the mean typhoon has two strong outflow jets, one to the northeast and another to the southwest. The southwest jet has a greater magnitude. For the hurricane the northeast jet is about four times stronger than the southwest jet. In both cases the outflow jets have a preferred geographical position which is independent of the system's motion.

Tangential Wind. Mean tangential wind (V_θ) cross sections for both systems are shown in Figs. 34 and 35. Maximum cyclonic flow is found in both cases to be at 850 mb, where the effective top of the frictional boundary layer is located. Cyclonic rotation extends through the depth of the troposphere only inside the 2^o radius. The magnitude of the tangential wind at any radius is smaller for the hurricane system reflecting the smaller average size of the Atlantic storms.

The anticyclonic maximum occurs around 150 mb in both tropical cyclone systems, but the hurricane's anticyclonic circulation is more attenuated. The $V_\theta = 0$ line serves as a boundary between cyclonic and anticyclonic circulation. In the West Indies storms it intersects the sea surface at 13^o radius, indicating that the hurricane's broad scale circulation is smaller than the typhoon's.

Inside 14^o radius the average vertical shear of the tangential wind for the typhoon is 15 - 20 m/s between 950 and 150 mb (Frank, 1976). For the hurricane this shear is only 10 - 15 m/s.

Inflow Angle. The mean inflow angle for a radial band can be computed employing the mean radial (V_r) and tangential (V_θ) winds.

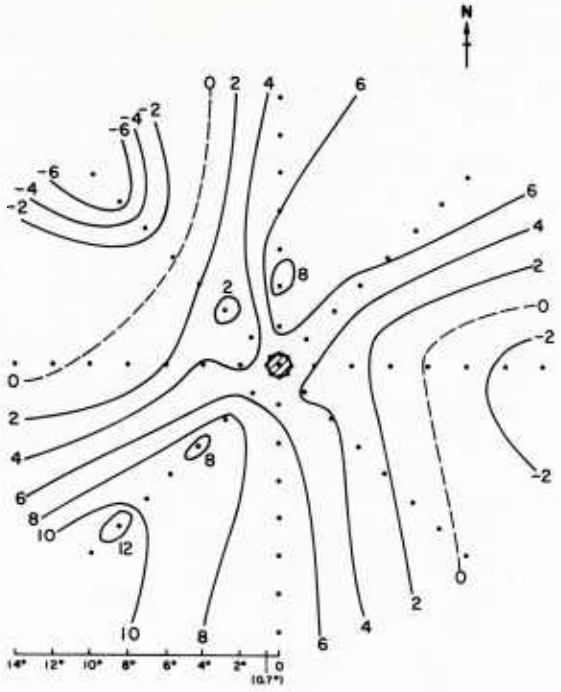

Fig. 32. 150 mb plan view of radial wind in stationary geographical coordinates for the mean steady state typhoon. North is towards the top of the figure. Values in m/sec.

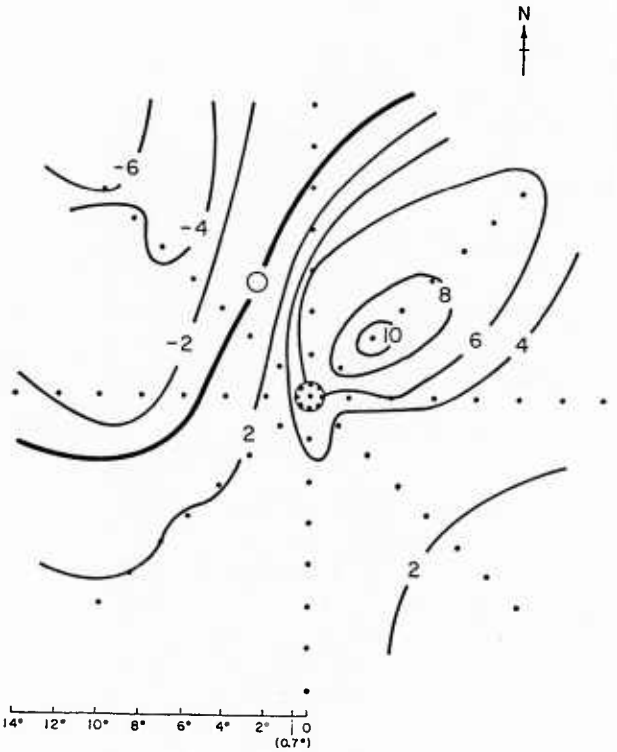

Fig. 33. Same as Fig. 32 but for the mean steady state hurricane. Values in m/sec.

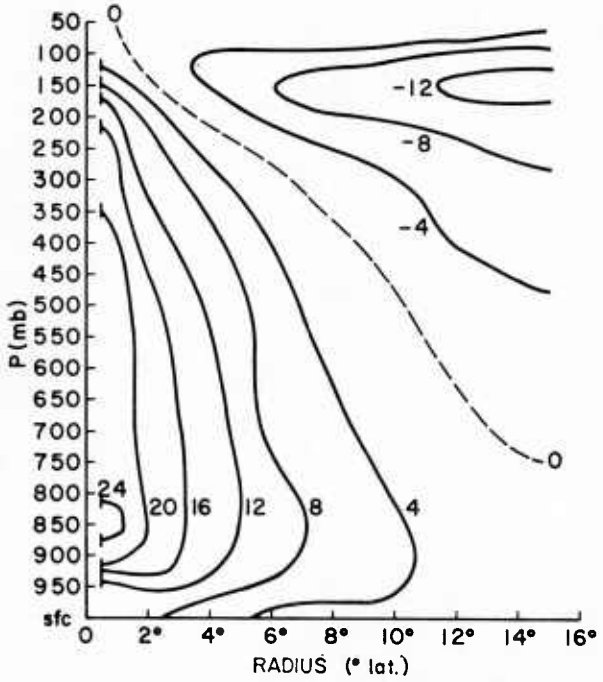

Fig. 34. Two dimensional cross section of tangential winds (V_θ) for the mean steady state typhoon. Values in m/sec.

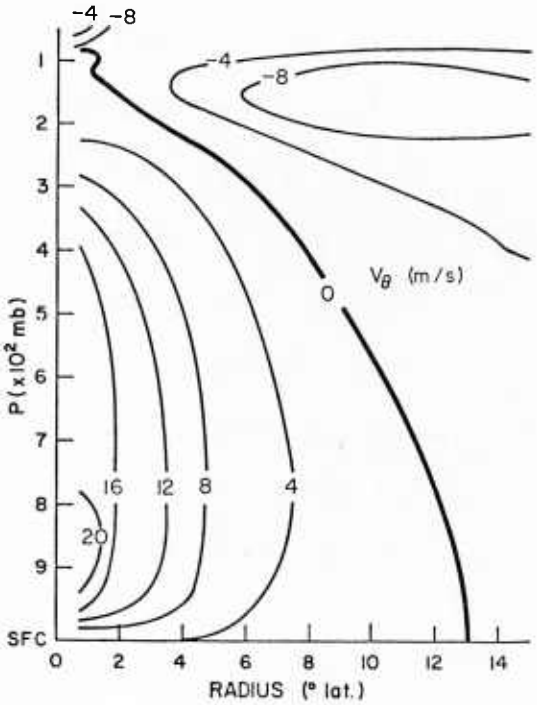

Fig. 35. Same as Fig. 34 but for the mean steady state hurricane. Values in m/sec.

Frank (1977a) calculated the inflow angles for the typhoon at 2^{o}, 4^{o} and 6^{o} radius. His values at 950 mb agreed with the 16^{o} reported by Ausman (1959) at the ocean's surface from ocean ship data. The inflow angles at the surface were almost identical at 2^{o}, 4^{o} and 6^{o}. Values averaged about 24^{o}. The inflow angles for the hurricane agree closely with those for the typhoon. At the surface, however, the hurricane's inflow angle is about $\sim 30^{o}$. It is believed that this is due - at least in part - to the greater number of elevated land stations found in the West Indies data set and the resulting greater surface friction.

The average inflow angle for each storm quadrant was calculated in moving storm relative coordinates for both systems at 2^{o}, 4^{o} and 6^{o} radius, (the storm's direction of motion towards 360^{o}). These quadrants were labeled front, left, back and right. The front quadrant, for example, is centered around the direction of storm motion. The storm motions have been subtracted from the winds in this coordinate system. Figures 36 and 37 show the mean inflow angle in each quadrant for the typhoon and the hurricane at 2^{o} radius. In the boundary layer the front and right quadrants have a greater inflow angle than the left and back. This relationship is also true at 4^{o} and 6^{o} (not shown). When interpreting these results, we should bear in mind that the inward mass flux can increase without the inflow angle increasing. Greater inflow can result under the previously mentioned restriction if the total wind speed increases.

3. Angular Momentum Budgets

The conservation of relative angular momentum equation in cylindrical stationary coordinates is:

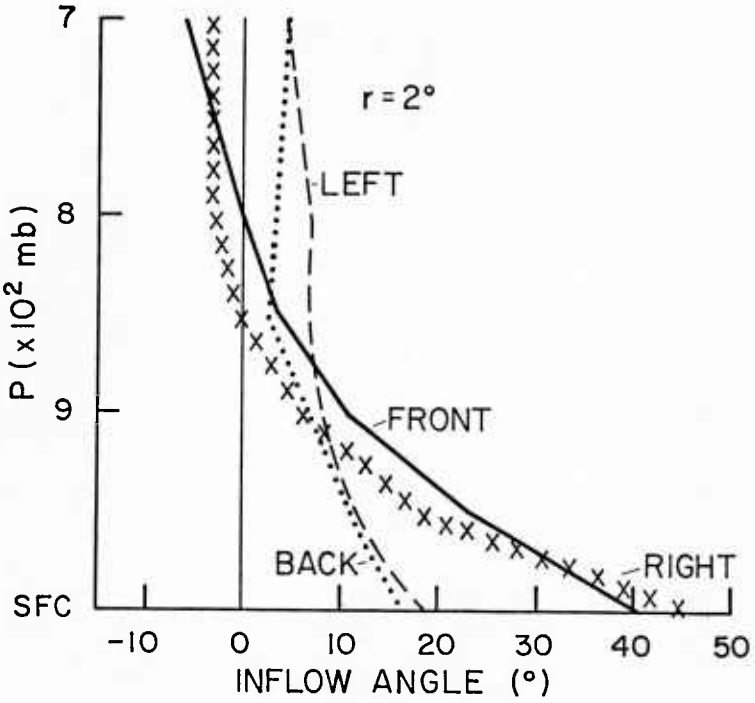

Fig. 36. Inflow angle per quadrant for the mean steady state typhoon at 2° radius.

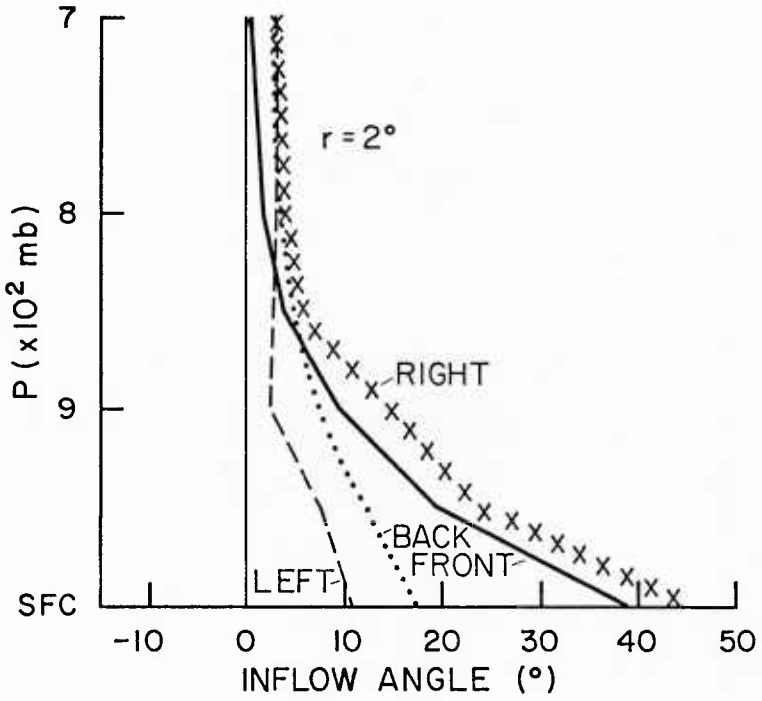

Fig. 37. Same as Fig. 36 but for the mean steady state hurricane.

$$\frac{dm}{dt} = - r\, fV_r - \frac{1}{\rho}\frac{\partial p}{\partial \theta} + rF_\theta \qquad (6)$$

where $m = V_\theta r$ is the relative angular momentum, and

$$F_\theta = \frac{1}{\rho}\,\frac{\partial \tau_{\theta z}}{\partial z} \,. \qquad (7)$$

Steady state is assumed, and terms involving $\partial/\partial\theta$ drop out when integrated around a circle. Vertical flux terms also integrate to zero assuming no flux at 100 mb. Therefore, the large scale vertically integrated angular momentum balance is:

$$\overline{\nabla \cdot V_r V_\theta r} = - \overline{frV_r} + F_\theta r \qquad (8)$$

The term on the left is the convergence of m due to the radial circulation. This flux is estimated by compositing individual values of $\overline{V_\theta V_r}$ (over bar represents time and space averaging). By subtracting the flux due to the mean circulation ($\overline{V_r}\ \overline{V_\theta}$) it is possible to estimate the eddy flux. As noted by Riehl (1961), horizontal momentum fluxes near the center can be estimated well from the mean circulation. At greater radii, however, the transport becomes increasingly dominated by eddy fluxes (Fig. 38). About 60% of the total momentum import at 10^o radius is accomplished by eddy fluxes resulting from advection in the lower and middle troposphere and from the strongly divergent anticyclonic flow in the upper level outflow jets. These jets are necessary if the outflow is to satisfy the simultaneous constraints of conservation of angular momentum and generation of kinetic energy (Anthes, 1974). Both the W. Pac. storms and W. I. hurricanes have large eddy influxes of m in the upper troposphere, although the values are higher for the W. Pac. storms due to the larger mean size (and hence radial mass flux) of the typhoon.

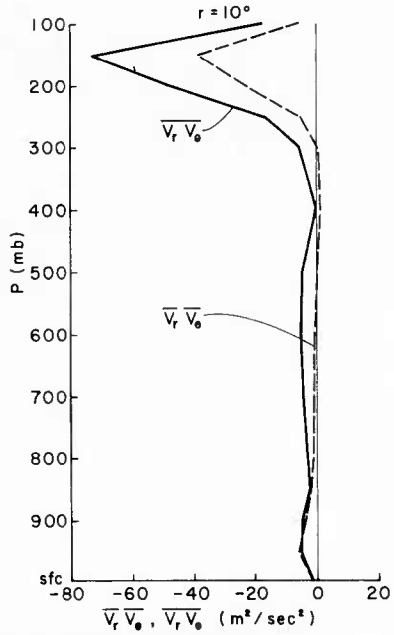

Fig. 38. Total horizontal flux of relative angular momentum divided by radius ($\overline{V_r V_\theta}$) and flux by mean circulation ($\overline{V_r}\ \overline{V_\theta}$) at r = 10° W. Pac. region, stationary coordinates. The difference between the curves is the eddy flux.

Most m budget studies of tropical cyclones have assumed that the Coriolis torque term ($-fV_r r$) in Eq. 8 integrates to zero for a steady state storm. This is valid in the inner core region where f varies little across the storm area, but at larger radii any net southerly/northerly wind causes an eddy spin-down/up of the tangential circulation.

The southerly meridional flow is much stronger in the W. Pac. region than in the W.I. area. Therefore, the net Coriolis torque term is larger in the former region as shown in Figs. 39 and 40. These figures show the vertically integrated terms of Eq. 8 for each region as computed except for some smoothing of the W.I. horizontal convergence term. The budgets do not exactly balance. The frictional dissipation has been computed using a variable drag coefficient (Frank, 1977b), and the higher dissipation values in the W. Pac.

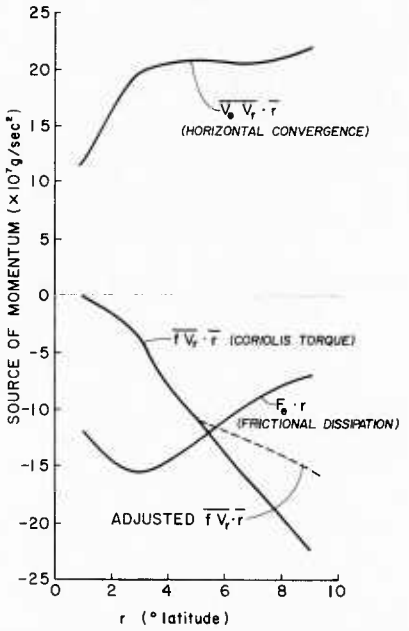

Fig. 39. Vertically integrated angular momentum budget terms for West Pacific region: horizontal convergence ($V_\theta V_r r$), surface dissipation ($F_\theta \cdot r$) and net Coriolis torque ($fV_r r$). Dashed line is adjustment to Coriolis term to achieve balance.

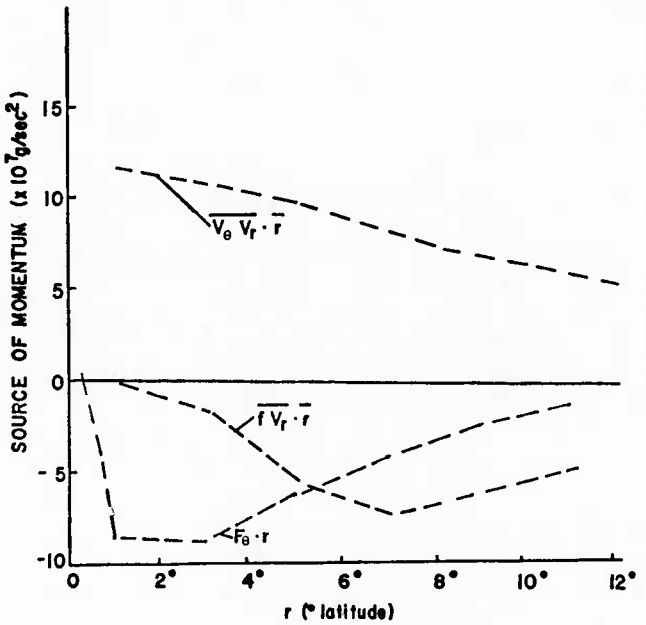

Fig. 40. Same as Fig. 39 but for the West Indies storms.

result from the greater size and intensities of the storms found there.

At inner radii there is general balance between the frictional dissipation and horizontal convergence of momentum. At larger radii, however, the budget is increasingly dominated by the eddy Coriolis torque and the horizontal convergence with the latter term resulting largely from eddy fluxes as shown. In view of the importance of these eddy terms, the accuracy of 2-dimensional models of tropical cyclones must be questioned.

4. Kinetic Energy Budgets

There have been several empirical studies of tropical cyclone kinetic energy (K.E.) budgets (Hawkins and Rubsam, 1968; Miller, 1962; Riehl and Malkus, 1961; Palmén, 1958; and Palmén and Jordan, 1955). These researchers generally concluded that the eddy horizontal transports and generation of kinetic energy were small and did not play an important role in the storm energy budgets. Numerical modeling studies (Ooyama, 1969; Rosenthal, 1970) have reinforced this viewpoint by showing that the models do not require outside sources of kinetic energy to generate and maintain a mature tropical cyclone.

The results of this study indicate that eddy processes are of great importance in the overall energetics of tropical cyclones and their environments. The outer storm circulation region exhibits substantial net generation and export, resulting primarily from transient eddy processes.

The conservation of kinetic energy equation is:

$$\frac{\partial \overline{K}}{\partial t} = - \overline{\nabla \cdot \underset{\sim}{V} k} - \overline{\frac{\partial \omega K}{\partial p}} - \overline{\underset{\sim}{V} \cdot \nabla \phi} + \overline{\underset{\sim}{V} \cdot \underset{\sim}{F}} \qquad (9)$$

where K = kinetic energy per unit mass

ϕ = gz = potential energy

F = frictional processes

No fluxes of K or mass are allowed at 100 mb, and $\omega = 0$ at the sea surface. The term on the left of Eq. (9)is the local rate of change of kinetic energy and is zero for the assumed steady state. The first term on the right is the horizontal flux divergence of kinetic energy. The second term is the vertical flux divergence of K, and third term is the generation of kinetic energy by down gradient flow. The last term is the frictional dissipation.

Results are shown in Figs. 41-44 for the W. Pac. and W. I. regions, respectively. The W. Pac. storms export large quantities of kinetic energy, and eddies become the dominant export mode at large radii (Fig. 41). The transports and eddy fluxes are found almost entirely in the upper troposphere and reflect the presence of the outflow jets (Fig. 42). Based on the fluxes shown in Fig. 42, the W. Pac. storms generate (and export) an excess of about 4.8 w/m^2 averaged over the $0\text{-}10^{o}$ radius region. The W.I. storms export far less kinetic energy (Fig. 44) and the total transports are only slightly greater than the mean circulation fluxes. Eddy export of K in the upper troposphere is still important at outer radii (Fig. 44), but it is nearly balanced by an eddy influx near 400-300 mb. The origin of this influx of K is not clear. W.I. storms generate a net excess of about 1.7 w/m^2 over the $0\text{-}10^{o}$ region.

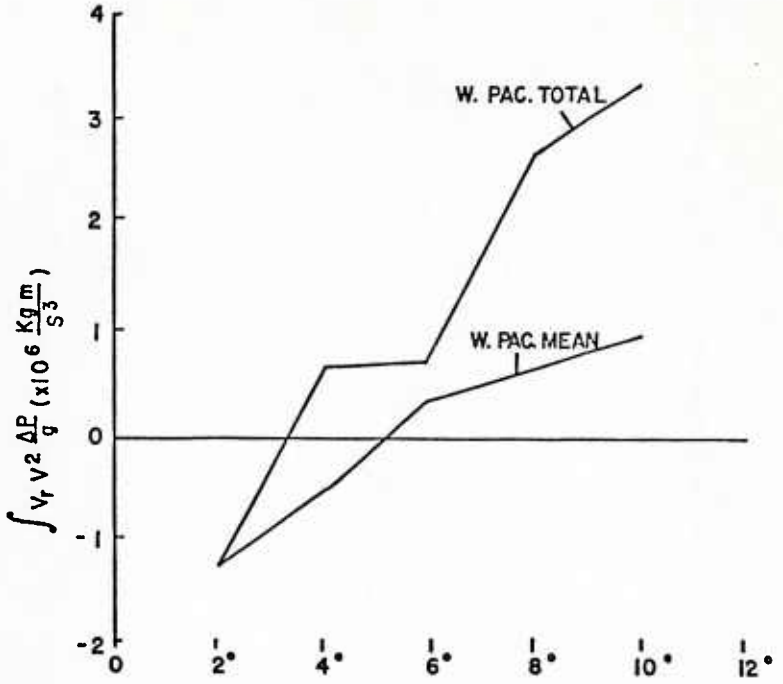

Fig. 41. Total vertically integrated horizontal flux of kinetic energy times 2 ($\overline{V_r V^2}$) and flux by mean circulation ($\overline{V_r}\ \overline{V^2}$), West Pacific.

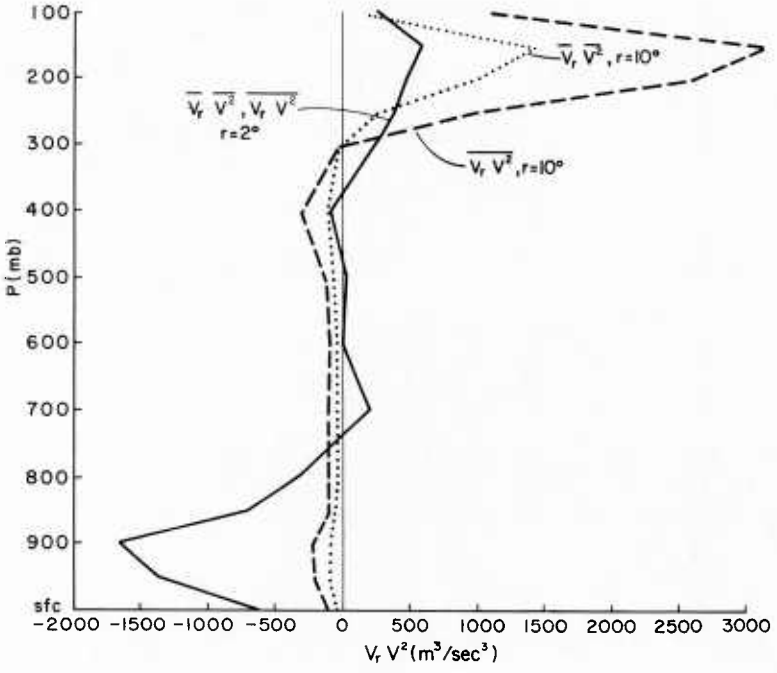

Fig. 42. Total flux of kinetic energy times 2 ($\overline{V_r V^2}$) and flux by mean circulation ($\overline{V_r}\ \overline{V^2}$), r = 10°, West Pacific.

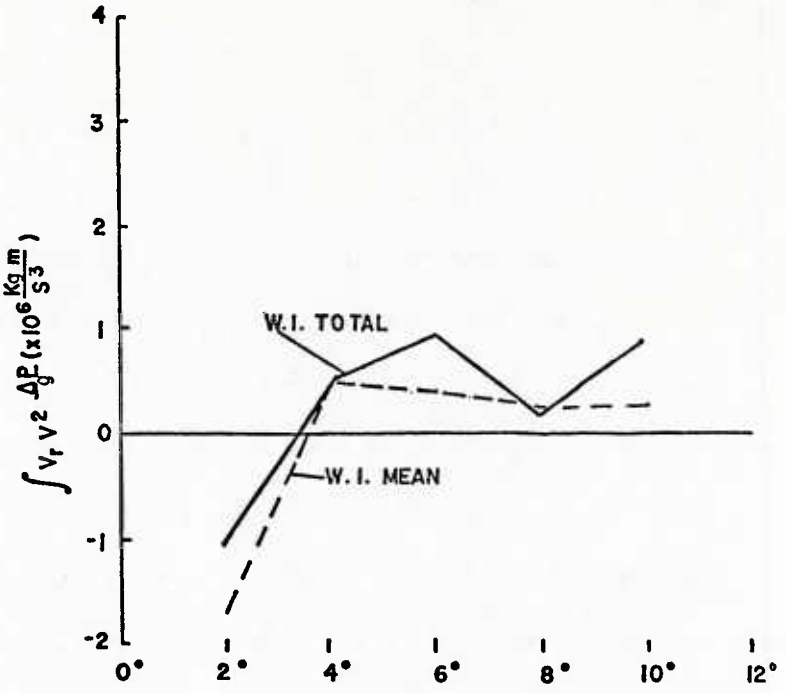

Fig. 43. Same as Fig. 41 but for the West Indies region.

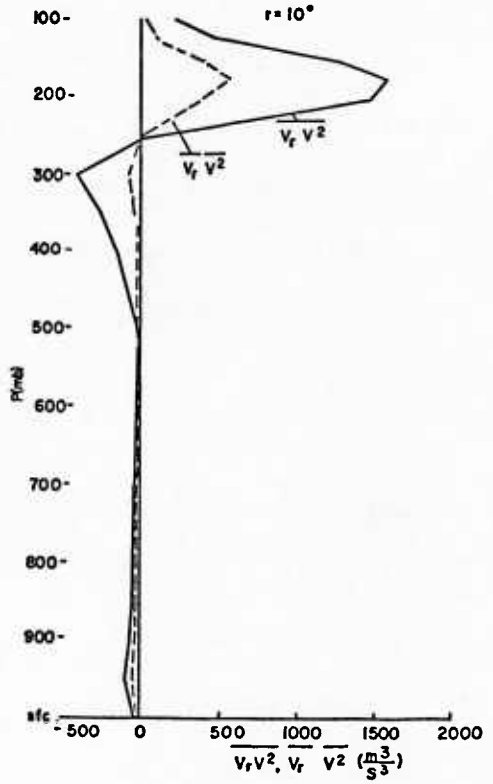

Fig. 44. Same as Fig. 42 but for the West Indies region.

It is not possible to measure $\overline{V \cdot \nabla\phi}$ for each sounding. Therefore, the generation by the mean circulation ($\overline{V_r} \cdot \overline{\partial\phi/\partial r}$) was computed. This product was also computed for each octant at each level and averaged for the W. Pac. data. This latter quantity minus $\overline{V_r} \cdot \overline{\partial\phi/\partial r}$ gives an estimate of the standing eddy generation. Transient eddies of radial generation of K and azimuthal eddy generation ($\overline{V_\theta' \cdot \partial\phi'/r\partial\theta}$ were estimated as residuals. The mean generation is greatest in the inflow and outflow layers with the upper maximum becoming the more important at outer radii. Standing eddy generation is negligible at all radii.

Frictional dissipation of kinetic energy in the boundary layer (sfc-900 mb) was estimated by the bulk aerodynamic method using the equation:

$$\text{Dissipation} = \frac{C_D V^3}{\Delta z} \qquad (10)$$

A variable drag coefficient was used (Frank, 1977b). Internal dissipation of K above the boundary layer cannot be computed. This additional sink is probably substantial. The importance of internal dissipation due to clear air turbulence and wave momentum fluxes has been emphasized by Trout and Panofsky (1969) and Lilly (1972). Convective processes probably dissipate substantial amounts of energy as well. Some studies, from lack of knowledge to the contrary, have estimated the inner core region ratio of internal dissipation to surface dissipation (I.D./S.D.) as about 1 to 1 (Riehl and Malkus, 1961), 1/1 (Miller, 1962) and 0.5/1 (Hawkins and Rubsam, 1968). However, all of these studies solved for internal dissipation as a residual in kinetic energy budgets which neglected eddy generation. Their results probably give underestimates of internal dissipation.

Table 8 shows the vertically integrated K.E. budgets for the 2-10° regions of W. Pac. typhoons and W.I. hurricanes. The values of all three terms are higher in the Pacific by about a factor or two. The residuals must equal the sum of the transient eddy generation and internal dissipation terms (the horizontal eddy fluxes are included in the convergence term).

If internal dissipation (I.D.) is assumed to equal surface dissipation (S.D.), the budgets would appear as shown in Table 9. I.D. = S.D. is probably a conservative, if somewhat arbitrary, assumption. Table 9 shows that the transient eddy generation of kinetic energy probably equals or exceeds the generation by the mean circulation.

TABLE 8

Kinetic Energy Budgets from 2-10° Radius (w/m^2). Positive Numbers = Sources of K.

	W.PAC.	W.I.
$-\overline{\bar{V}} \cdot \overline{\nabla\phi}$ (Mean Generation)	5.0	2.4
$\overline{\bar{V}} \cdot \overline{\nabla K}$ (Convergence)	-5.3	-2.4
$\overline{F} \cdot \overline{V}$ (Surface Dissipation)	-2.9	-1.2
Residual (= Eddy Generation plus Internal Dissipation)	-3.2	-1.2

5. Conclusions

The average hurricane and typhoon have quite similar structures. Both systems show maximum inflow at 950 mb and outflow around 150 mb. A deep inflow layer at outer radii which decreases in depth inside 2° is observed for both systems. Mean radial winds exceed 2 m/s in the boundary

TABLE 9

Kinetic Energy Budgets from 2-10° Radius (w/m^2) Assuming That Internal Dissipation = Surface Dissipation. Positive Numbers = Source of K.

	W.PAC.	W.I.
$-\overline{V} \cdot \overline{\nabla\phi}$ (Mean Generation)	5.0	2.4
$\overline{V} \cdot \overline{VK}$ (Convergence)	-5.3	-2.4
$\overline{F} \cdot \overline{V}$ (Surface Dissipation)	-2.9	-1.2
Assumed Internal Dissipation	-2.9	-1.2
Transient Eddy Generation	-6.1	-2.4

layer only inside 5° radius. Outflow occurs in jets which show a preferred geographical location. Only inside 2° radius is the circulation cyclonic throughout all the troposphere. Notable asymmetries in the inflow angles of both systems have been detected with the front and right quadrants showing greater inflow angles.

There are some interesting differences between the two cyclones. The hurricane exhibits a smaller temperature anomaly at mid-tropospheric inner radii. Nevertheless, there is a wider region of upper tropospheric cooling in the West Indies storms. On the average, the hurricane's relative humidity values are 10% lower than the typhoon's. A strong northeast outflow jet is observed for the hurricane while the typhoon has two jets, the southwestward one dominating. As expected, both the cyclonic and anticyclonic circulations in the hurricane are of smaller magnitude. The average hurricane shows the greatest inflow angles in the right quadrant and the smallest angles on the left. Corresponding quadrants for the typhoon are the front and back, respectively.

It has been shown that eddy processes are fundamentally important in the angular momentum and kinetic energy balances of tropical cyclones. Horizontal fluxes of these quantities can greatly exceed transports predicted by the 2-dimensionally averaged mean circulation, especially in the highly asymmetrical outflow layers. In the presence of any mean meridional wind, there is a net Coriolis torque effect on the circulation at large radii. The horizontal eddy fluxes of momentum and energy appear to be highly dependent on the large scale wind fields as well.

Tropical cyclones are net sources of kinetic energy, largely due to the strong generation of energy by transient eddy processes. Eddy generation and internal dissipation of kinetic energy are probably at least as important as generation/dissipation by the mean circulation.

Due to the importance of asymmetrical storm features in the overall momentum and kinetic energy balances, it seems doubtful that 2-dimensional models can provide very realistic simulations of tropical cyclones.

IV. TROPICAL CYCLONE CLOUD AND INTENSITY RELATIONSHIPS AS DERIVED FROM DMSP SATELLITE INFORMATION

1. Introduction

Although very significant strides have been made in the utilization of satellite picture data for cyclone intensity determination (as demonstrated by V. Dvorak, 1975) operational forecasters usually also desire verifying aircraft intensity information when cyclones are nearing populated coastal regions. Intensity estimates based on a relationship between maximum sustained winds and central pressure are unreliable on an individual case basis. As shown in Fig. 45, pressure and maximum sustained winds as derived from inner core 500-900 mb NHRL hurricane flights in the 1950's and 1960's are only statistically related (Shea and Gray, 1973). A significant variation of maximum winds between cyclones with similar central pressures is possible. In addition, a quite variable relationship exists between maximum sustained winds and radius of maximum winds as portrayed in Fig. 46. Large variation also exists between eye diameter and central pressure as seen in Fig. 47. Cyclone intensity relations with other parameters are difficult to determine.

Although recent cyclone intensity estimates from satellite picture configurations have been found satisfactory in the majority of cases (e.g. Dvorak, 1975) the relationship between cloudiness configuration and intensity is quite complex, and significant errors can occur in individual situations. C. Arnold (1977, Colorado State University Atmospheric Science Report No. 277) has documented some of these cases

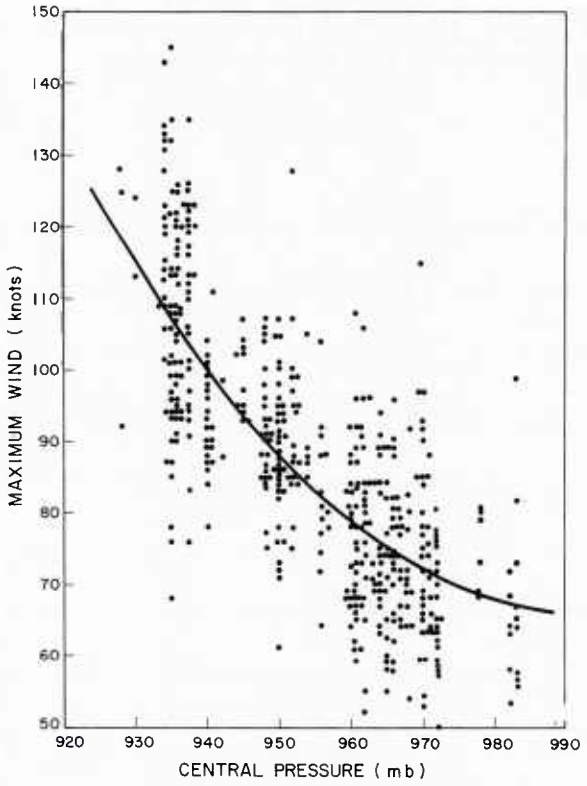

Fig. 45. Variation of the maximum wind with central pressure. The best fit curve is indicated by the heavy line (from Shea and Gray, 1973).

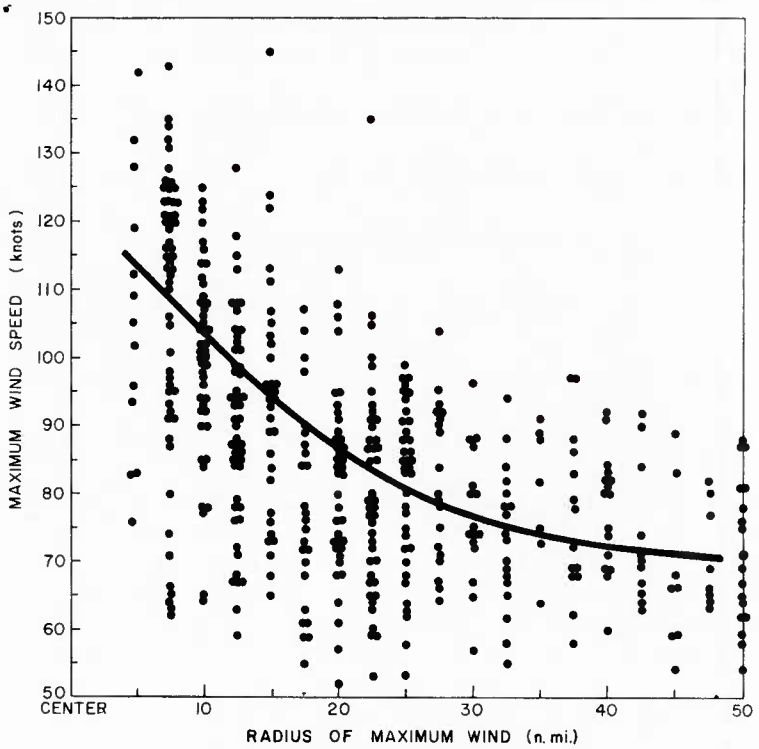

Fig. 46. Variation of the maximum wind with radius of maximum wind. The best fit curve is indicated by the heavy line (from Shea and Gray, 1973).

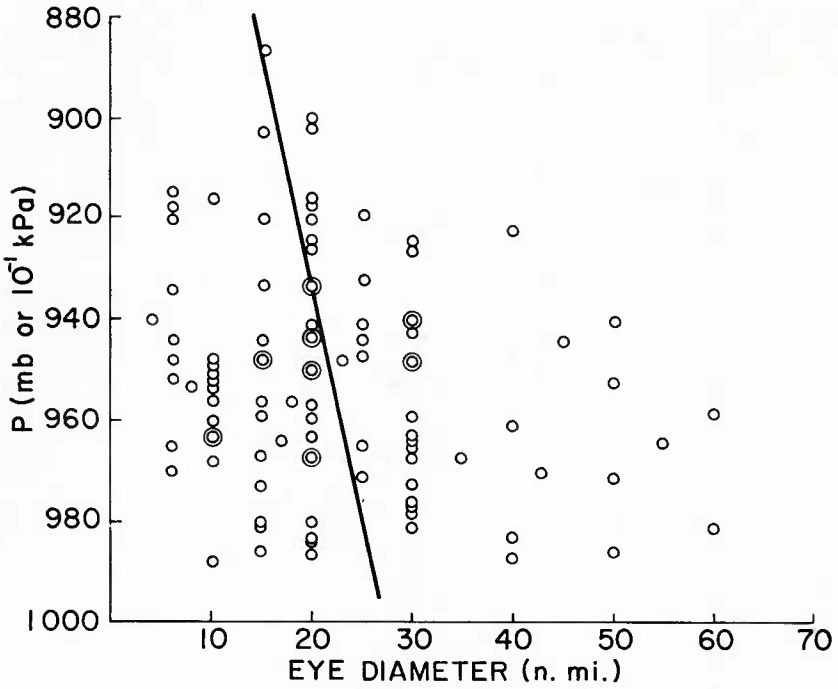

Fig. 47. Variation of eye diameter with central pressure. The best fit line is indicated by the heavy line. (Arnold, 1977).

for recent West Pacific cyclones. He has also made a thorough investigation of the relationships between DMSP satellite observed cloud amounts and cyclone intensity. The rest of this chapter discusses some of his findings.

2. Description of Arnold's Data Sets

Satellite data consisted of positive transparency DMSP photos obtained from the USAF DMSP site located on the island of Guam in the Western North Pacific (WESTPAC), via the University of Wisconsin DMSP data archive. Data was obtained for the period May 1971 through 1975 and included as much of the life cycle of each tropical cyclone as could be obtained by the Guam site.

For the period indicated above there were normally two, and at times three, DMSP polar orbiting sun-synchronous satellites in 450 nautical

mile orbits. They had daytime ascending nodes (AN) which were at approximately 0800 local sun time (LST) and approximately 1200 LST. With two such satellites the Guam site would normally obtain two daylight and two night passes from each satellite for a total of eight day/night passes. Not many tropical cyclones were missed.

During this period of time there were basically two types of DMSP imagery available.

1) daytime visual or VHR with a spatial resolution at subpoint of 1/3 n mi, and spectral band width 0.4-1.2 μ m, and

2) day/night infrared or IR with a thermal resolution as good as 1.6 K per gray shade, a spatial resolution of 2 n mi at subpoint and spectral bandwidth 8-13 μ m. The temperature range of IR is 210 K to 310 K with 16 shades of gray linearly distributed through this temperature range. The normal temperature resolution is 6.25 K per gray shade.

Each storm was classified into one of five stages according to its current intensity as described in Table 10.

Two data sets were created using the CSU Atmospheric Science Department's Optical Data Digitizer and Display (or OD^3). The OD^3 provides the capability for digitizing positive transparencies.

The first data set (I) was created from the VHR (1/3 n mi visual) data based on a partially subjective analysis of meso-convective elements and an objective measurement of these elements using the OD^3 with a desk top CDC 2100 computer programmed to provide fractional percent area covered by a given cloud type. The subjective analysis was done by exploiting the wide dynamic range (brightness range or contrast) of DMSP VHR data in combination with IR data. With high contrast positive transparency film meso-convective elements (groups of deep convective cells) can easily be distinguished from other cirrus and lower level cloud types. Texture, shading and shadows all were used to locate these

TABLE 10

Composite Stage Characteristics of Rawinsonde Data Sets

Rawinsonde Stages	Corresponding Stages used in this Paper	Estimate of Central Pressure (mb)	Estimate of Maximum Sustained Surface Winds	Number of Individual Storms	Mean Lat.	Mean Long.	Direction of Movement	Speed of Movement (m/s^{-1})
Developing Cluster (Stage 2 of Zehr, 1976)	I	1005	15	130	10	153	287	5.5
Tropical Depression (Frank, 1976)	II	1002	25	∿126	17	139	308	5.2
Tropical Storm (Frank, 1976)	III	990	50	∿200	19	136	319	4.9
Typhoon (Frank, 1976)	IV	965	80	∿175	22	136	326	5.0
Super-Typhoon (Frank, 1976)	STY	935	115	85	21	137	329	5.2

relatively small areas of deep convection. Infrared was used to confirm selected meso-convective elements. These elements were first outlined with pencil on the film and later traced onto paper. From these tracings a determination of the deep penetration of Basic Convective Elements of the visual pictures could be made.

A second data set (II) utilized digitizing procedures with the IR data. Calibration of each piece of IR data was accomplished with a 16 step gray scale, the percent area of the top or coldest three shades of gray representing temperatures less than 222.5°K. This temperature range effectively measured most cirrus clouds assuming a maximum sensor error reading of 5 C too cold (DMSP User's Guide).

Examples which show the Basic Convective Elements (BCE) obtained from the tracing procedure outlined above are shown in Fig. 48. The Visual (VHR) picture used for this case is shown in Fig. 51. The corresponding IR data enhanced with a color densitometer and then photographed in black and white to emphasize selected IR temperature ranges is shown in Fig. 49 (total cirrus) and Fig. 50 (coldest shade of cirrus).

An overlay rectangular grid (Fig. 52) centered on the storm and aligned north-south was used with each system. The overall grid size and the size of an individual grid box were determined by the typical storm size and by the data resolution, respectively. Individual grid boxes were 160 x 170 n mi rectangles.

Fractional areas of convection and cirrus (σ) were determined for the center box, 1x1 ($r \sim 0\text{-}1.4^{\circ}$); the inner 9 boxes, 3x3 ($r \sim 0\text{-}4.2^{\circ}$); and the total 25 boxes, 5x5 ($r \sim 0\text{-}7.1^{\circ}$). From this data the σ or

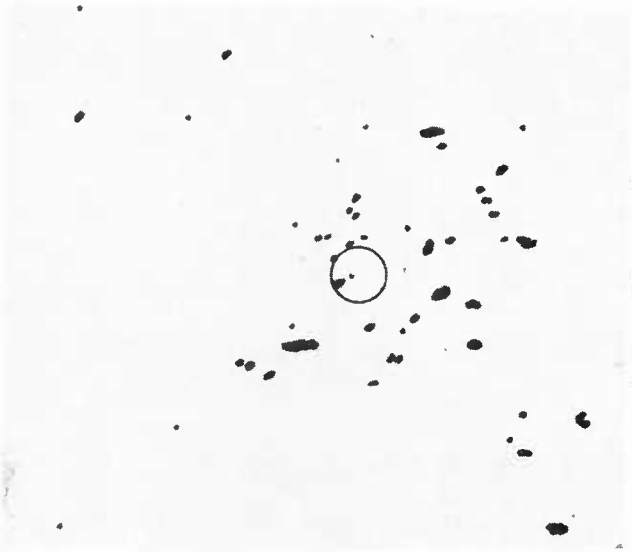

Fig. 48. Meso-convective elements of a developing cluster (Stage I) obtained from the tracing data set. Storm's circulation center is within the circle. 1" = 484 km.

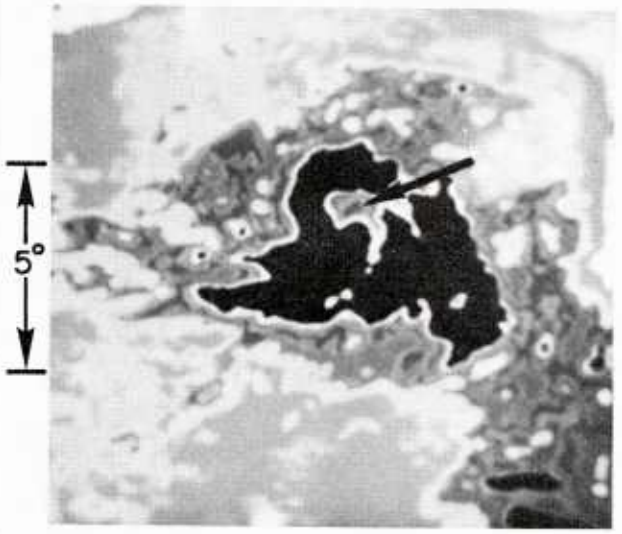

Fig. 49. Total cirrus (darkest shade) obtained from the infrared data set. for the cluster in Fig. 48. Arrow points to storm's circulation center. 1" = 484 km.

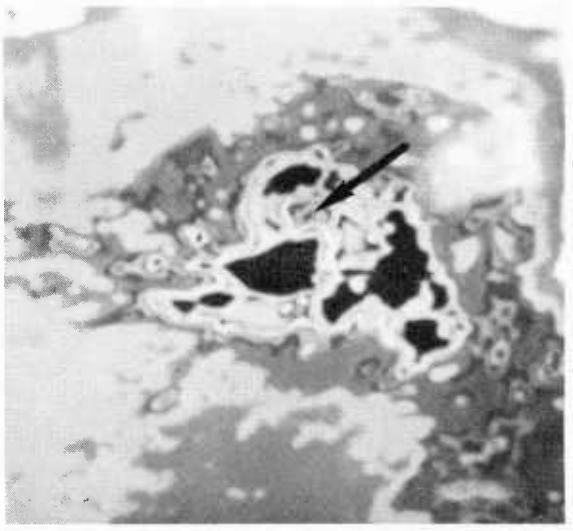

Fig. 50. Coldest shade (darkest shade) of cirrus ($\underline{T}$< 210K) obtained from the infrared data set for the cluster in Fig. 48. Arrow points to storm's circulation center. 1" ∿ 484 km.

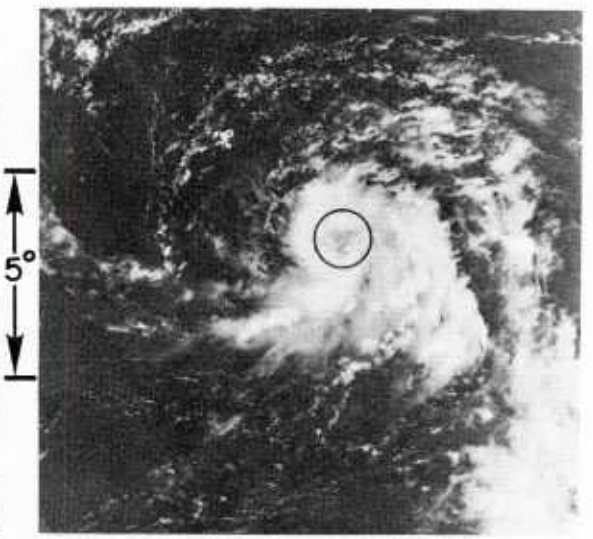

Fig. 51. The visual satellite picture used for Fig. 48. A developing cluster (Stage I of future Typhoon Nancy), 15 October 1972, 0109Z. Storm's circulation center is within the circle, 1" = 484 km.

fractional cloud area values could be determined for the 3x3 excluding the 1x1, called the outer 8 (r ∿ 1.4-4.2°) as well as the 5x5 excluding the 3x3, called the outer 16 (r ∿ 4.2-7.1°) (see Fig. 53).

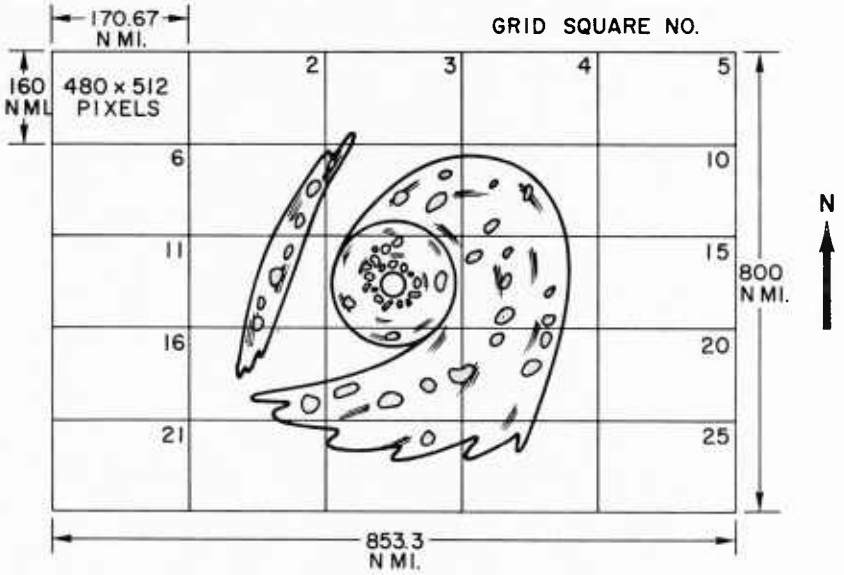

Fig. 52. Overlay grid centered on storm's circulation center and oriented north-south used to create visual and infrared data sets.

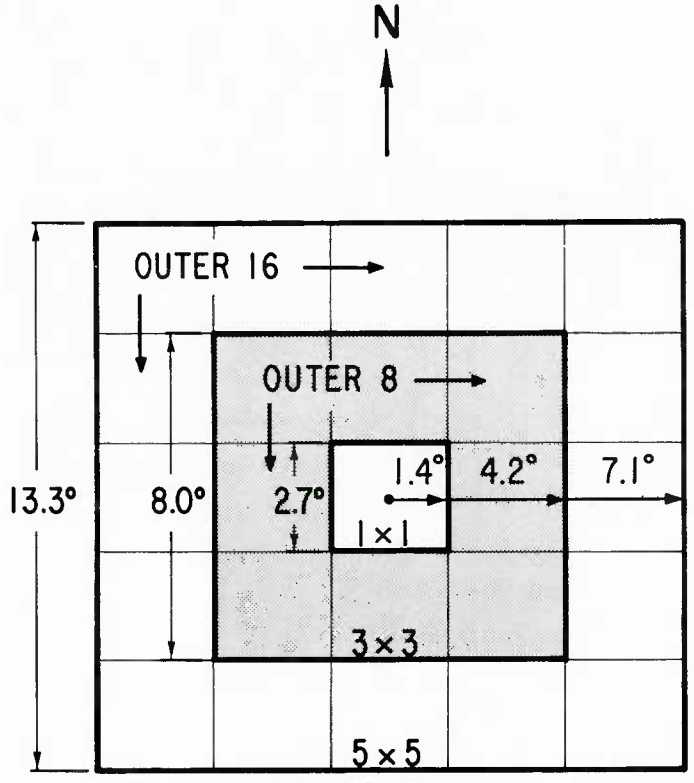

Fig. 53. Same as Fig. 52. Shows approximate radial equivalents of 1x1, 3x3 and 5x5 regions.

3. Results

Table 11 portrays the percent area coverage by the Basic Convective Elements (BCE-see section 5), total cirrus, and coldest shade of cirrus by cyclone region and intensity class. The Standard Deviation (SD) of these cloud amounts is also shown.

As a developing cluster (Stage I) intensifies into a tropical depression (Stage II) there appears to be a small increase in the concentration of deep convection about the circulation center. There is correspondingly a small decrease in convection at outer radii (outer 8 and outer 16).

As the cyclone continues to intensify from the tropical depression (Stage II) to the super typhoon stage, deep convection, as revealed in both the tracing data and the top shade of IR, appears to increase gradually at all radii. However, percentage (σ) values for the BCE area within the outer 16 region of Stages II, III and IV are not significantly different, and hence no statistical trend can be ascertained. Peripheral banding has continued to increase while at the same time inner core convection has become more organized into well defined eye walls. Convection within the inner core continues to increase, and spiral bands begin to form at outer radii with an observed increase in both convection and cirrus production.

Within the storm area (5x5 region) there is a 47% increase in visible deep convection and a 13% increase in the total cirrus from a developing cluster (Stage I) to a super typhoon (STY). The amount of deep convection found within the 3x3 area of a typhoon is 3.7%.

TABLE 11

Percent of Area Covered by Convective and Cirrus Clouds

Storm Stage:		I			II			III			IV			IV TY P>950 mb	IV STY P≤950 mb
Storm Region		N	$\bar{\sigma}$	SD	N	$\bar{\sigma}$	SD	N	$\bar{\sigma}$	SD		$\bar{\sigma}$	SD	$\bar{\sigma}$	$\bar{\sigma}$
1 x 1	(1)	54	5.4	3.6	48	5.2	2.8	39	4.9	2.4	88	4.6	2.5	4.6	4.5
(r ∿ 0-	(2)	68	74.6	27.5	48	79.2	18.7	41	80.1	26.5	92	91.4	14.1	89.1	92.3
1.4°)	(3)	68	30.6	32.7	48	32.0	29.4	41	34.6	32.0	92	68.3	30.8	61.0	71.7
3 x 3	(1)	54	3.2	1.7	48	2.1	0.9	39	2.2	1.1	88	4.5	2.4	3.7	4.5
(r ∿ 0-	(2)	68	49.9	24.5	48	46.9	20.9	41	47.5	24.5	92	62.8	23.1	61.2	65.1
4.2°)	(3)	68	16.1	13.7	48	10.7	12.7	41	13.2	13.1	92	32.8	20.3	28.9	33.8
5 x 5	(1)	54	1.9	1.0	48	1.3	0.5	39	1.4	0.7	88	2.5	1.3	2.0	2.8
(r ∿ 0-	(2)	64	32.9	18.0	48	30.3	18.1	40	30.9	18.5	90	42.0	20.2	39.8	43.2
7.1°)	(3)	64	8.5	7.2	48	6.4	9.3	40	7.4	7.6	90	17.0	11.8	14.1	19.0
Outer 8	(1)	54	2.9	1.7	48	1.8	1.0	39	2.0	1.1	88	3.8	2.4	3.8	4.6
(r ∿ 1.4-	(2)	68	46.8	25.5	48	42.9	22.4	41	43.4	25.2	92	59.2	24.7	57.7	61.7
4.2°)	(3)	68	14.3	13.3	48	8.0	11.3	41	10.5	11.7	92	28.3	19.9	24.9	29.1
Outer 16	(1)	54	1.2	0.8	48	0.8	0.5	39	1.0	0.7	88	1.4	1.1	1.3	1.8
(r ∿ 4.2-	(2)	64	22.7	15.3	48	21.0	18.3	40	21.6	17.2	90	30.6	20.1	27.8	30.9
7.1°)	(3)	64	4.4	4.1	48	4.0	8.4	40	4.1	5.5	90	8.5	8.9	5.8	10.7

1 = Basic convective element (Data Set I . 2 = Total cirrus (Data Set II . 3 = Coldest shade of cirrus (T ≤210K) (Data Set II.

N = Sample size $\bar{\sigma}$ = Average percent area covered by cloud SD = Standard deviation of sample.

4. Stratifications

Numerous stratifications of the satellite data were made from which composited statistics were computed.

1) Cluster (Stage I) vs. Typhoon (Stage IV) Cloudiness, same Storm.

Cluster cloudiness and later typhoon cloudiness for the same storm show a moderate degree of correlation. The linear correlation coefficient was 0.61 for the 5x5 area. This suggests that small (cloud area) clusters exhibit a tendency to become small (cloud area) typhoons, and large clusters similarly tend to become large typhoons. Any such tendency naturally violates the idea that storm cloud diameter and intensity are related.

2) Early vs. Late Clusters (Stage I).

Clusters were separated into early and late stages, the former being representative of clusters 3-5 days before they were classified as depressions. The latter were representative of clusters 1-2 days before they become depressions. Early clusters were found to have approximately 8% more cloudiness than late clusters.

3) Trade Wind vs. Equatorial Trough Clusters (Stage I).

Clusters which developed north of $\sim 15^{o}$N latitude were considered to be of the trade wind variety. These were compared to those which formed south of 15^{o}N. This stratification revealed that trade wind clusters had approximately 40% less cirrus and convection than equatorial trough clusters.

4&5) Deepening vs. Filling Typhoons - Rapid Deepening vs. Deepening Typhoons.

Fully developed storms were examined to determine any relationship which may exist between pressure tendency and cloudiness. Deepening typhoons were found to have about 23% more cirrus

and only 8-10% more deep convection than filling storms. Rapidly deepening typhoons (central pressure falling by greater than 15 mb/12h) were found to have 8% more convection than deepening typhoons (central pressures falling by less than 15 mb/12 h).

6) Past Pressure Tendency vs. Current Cloudiness.

When past pressure tendency (previous value) was compared to current cloudiness values, the correlation was nearly zero. Thus, while current pressure tendency appears somewhat correlated with cloudiness, there is no apparent direct relationship with past tendency and current cloudiness.

7) Past Cloudiness vs. Current Intensity.

Only a weak correlation could be found between previous 0-48 h mean cloudiness and current intensity.

8) Cloudiness vs. Storm Direction of Movement and 9) Cloudiness vs. Storm Speed.

Tropical storm and typhoon cases were combined and divided into two classes based on direction of movement:

1) Storm moving towards $270^{o} \pm 45^{o}$.
2) Storm moving towards $360^{o} \pm 45^{o}$.

A second group likewise divided evenly into three classes based on storm speed:

1) Speed less than or equal to 10 kts,
2) Speed greater than 10 kts but less than or equal to 15 kts and
3) Speed greater than 15 kts.

Composited cirrus and convective element areas were computed for the 3x3 regions of both stratifications. No significant differences in cloudiness could be established between storms moving in different directions or between storms having different speeds. The degree of

variability associated with each class of each stratification appeared to be independent of direction or speed.

5. Characteristics of Basic Convective Elements (BCE)

This convective form appears to be a basic one in tropical cyclones. Deep convective cells over western Pacific tropical waters typically are found to exist as groups of multiple cells of about 20-30 km diameter. This was found to be particularly true in W. Pacific tropical cyclones.

The average number of convective elements per storm picture and per unit area in the 1x1 box, the outer 8 boxes, and the outer 16 boxes reveal the same trends as observed in the percentage of area covered by the convective elements and the top shade of cirrus (Table 11). In the inner box we observe a decrease in BCE count with greater storm intensity. This is thought to result from the increasing difficulty in observing these cells as they become embedded in increasingly denser cirrus. The average numbers of BCE's in the outer 16 between storm stages are not significantly different. The average BCE size for all stages based on data set I (tracing data set) was approximately 250 n mi^2 or approximately a 30 x 30 km area. S. Erickson (1977) has reported finding similar size convective elements in both his developing and non-developing clusters. He found the average size to be $\sim$ 26-34 km in diameter. There are slightly more convective elements to the east of the storm center than to the west. Likewise, there are slightly more cells to the south than to the north. The northwest quadrant of the storm reflects a primary minimum in convection.

6. Location of Initial Cyclone Centers Relative to Cluster Convection

A large body of satellite information is now available in both the Western Atlantic and Pacific to indicate that the location of the center of newly forming tropical cyclones is not typically within the disturbance's active convective region (Fett, 1965[4], 1966; Hubert, 1968[5]; Oliver and Anderson, 1969; Dvorak, 1975; Wright, 1976; Arnold, 1977; Erickson, 1977; plus other data). Instead the center occurs:

1) within the clear region just to the west or northwest of the cluster as seen in Fig. 54a,

2) in the clear region between two different disturbance clusters as seen in Fig. 54b, or

3) between active convective regions in the same cluster as seen in Fig. 54c.

The dotted areas of these figures show typical regions of concentrated warming due to dynamically forced subsidence. These locations are places where the disturbance's upper-level outflow impinges upon the circulation of an upper level trough, the outflow from another cluster, or the outflow from different cloud groups within the disturbance. The outflows merge with each other and cause a mechanically forced downward motion. It is hypothesized that it is only at locations where dynamically forced subsidence occurs that enthalpy increase can be of sufficient magnitude to initiate a cyclone. See Arnold (1977) for documentation.

---

[4]Personal communication.

[5]Personal communication.

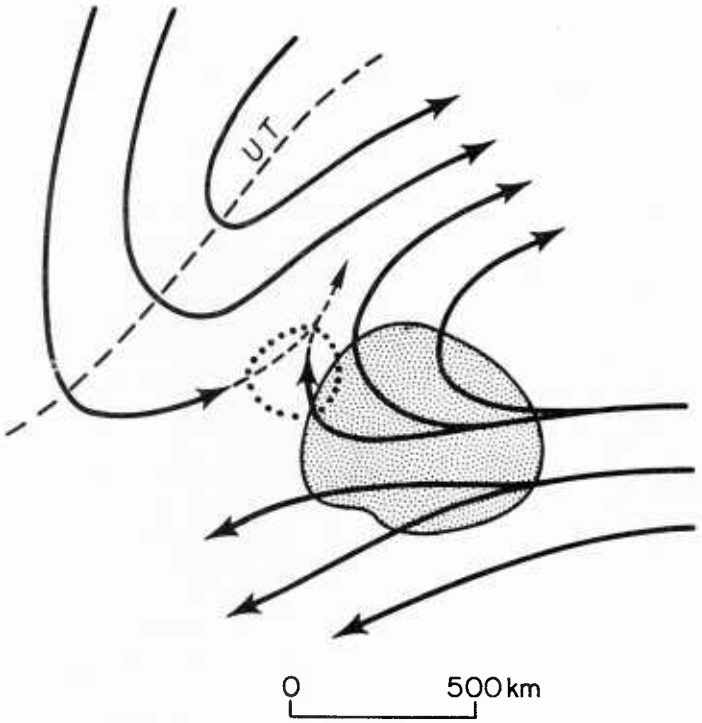

Fig. 54a Idealized portrayal of 200 mb flow features associated with intensifying tropical disturbance where the initial cyclone center occurs in the dotted region adjacent to the cloud area (shaded) and an Upper Trough (UT) is present to the northwest.

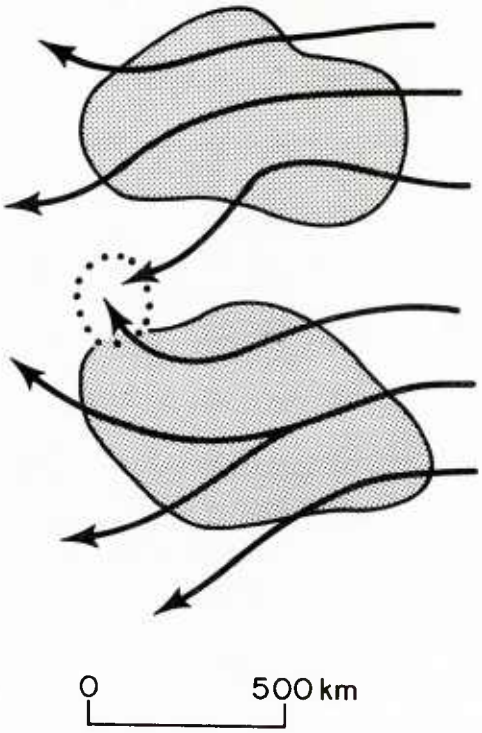

Fig. 54b. Schematic of how the outflow from two disturbances could produce large flow convergence in the dotted region between the disturbances.

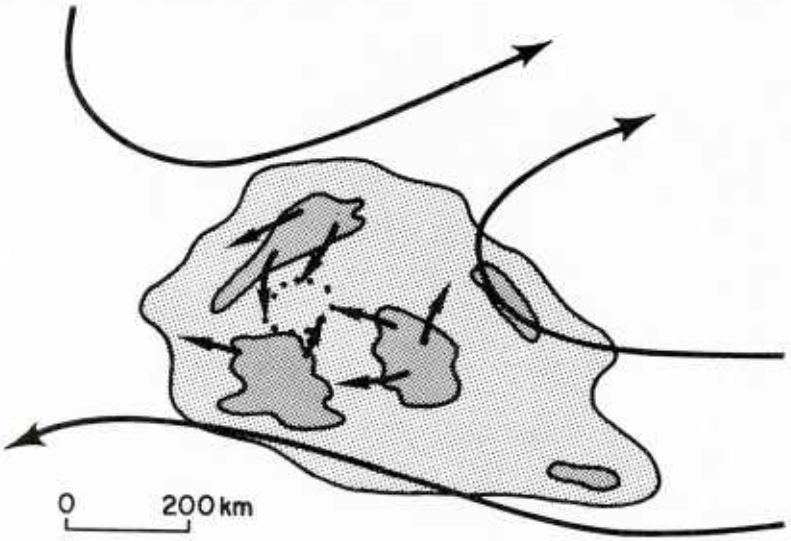

Fig. 54c. Conditions where dynamically forced subsidence occurs within the disturbance cirrus shield (light shading) but between active convective elements (heavy shading). The cirrus level outflow from the convective areas meet in the dotted circle region.

7. Variability in Cloudiness

Perhaps the single most important result of Arnold's analysis is the documentation of the large day to day and diurnal variability in both deep convection and cirrus. This variability occurs within the same storm and between storms. Storms which begin, for example, as small clusters may evolve into large sprawling typhoons. Likewise, large clusters may become typhoons with small regions of cloudiness. Clusters with little convection may eventually contain enormous spiral arms with numerous convective elements, and fully developed storms may contain little convection.

Figure 55 shows the percent deviation from the mean for the area covered by deep convection (data set I) within the 3x3 area for the typhoons. All cases have been included and have been randomly ordered. It is evident that there is considerable variability in cloudiness. Similar variations in individual system cloudiness are also observed for the weaker cyclones and disturbances. This variability occurred with all cloud types and at all different locations within the cyclones. Similar graphs were made for small storms and for large storms of the same intensity. The degree of variability in both groups is quite large and essentially the same. A large diurnal variability in cloudiness has also been observed. This has also been reported by Browner et al. (1977).

Summary. It was concluded that deep cumulus convection, cirrus and total cloud coverage, and to a large extent the banding characteristics of storms are often not well related to storm intensity except in a statistical sense. Arnold (1977) concludes that the Dvorak method (Dvorak, 1975) of cyclone intensity estimation has shown the best skill of any

cloud and intensity scheme so far devised. It has been extensively used on an operational basis for the past 6 or 7 years. This scheme works best for the weak and average strength storms and less well for the strong and extremely fast developing ones. Even though the Dvorak method may work reasonably well as much as 75-80% of the time, it is the other 20-25% of cases which can cause serious forecasting problems. This occasional breakdown of the storm cloud-intensity relationship is quite consistant with the large range in cloudiness found by Arnold for cyclones of similar intensity.

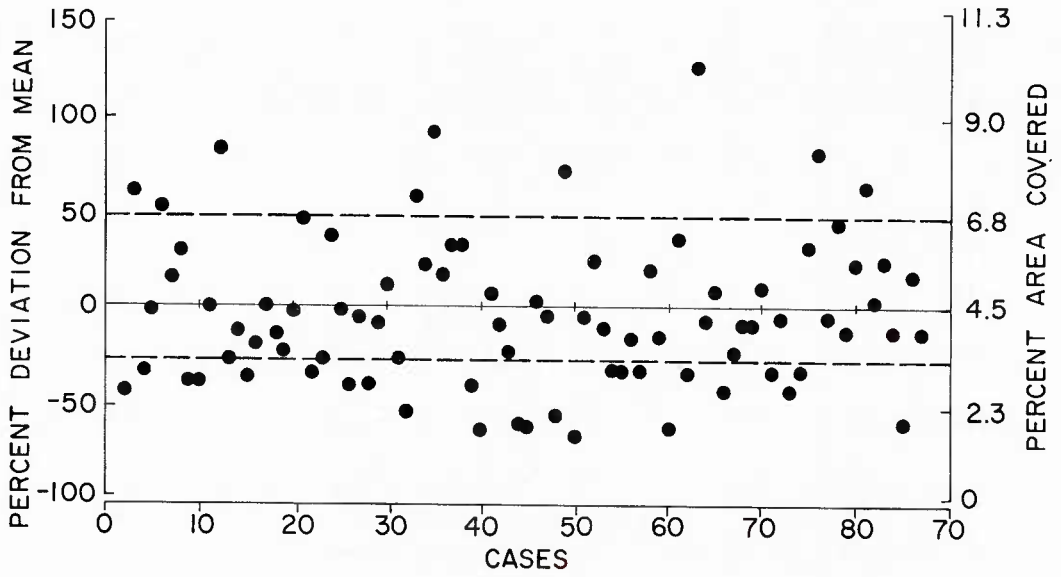

Fig. 55. Percent deviation from the average area of all deep convective elements within the 3x3 ($r \sim 0\text{-}4.2^{\circ}$) region of the typhoon (Stage V). The order of the cases is random. Dashed lines above and below the mean show the mean positive and negative deviations, respectively.

V. CYCLONE MOTION

1. Steering Current Determination

Our recent Colorado State University studies of cyclone motion in the Western North Pacific (George and Gray, 1976, see the project report by George, 1975, for more details) have shown that statistically, tropical cyclone motion is directly related to the surrounding wind and height fields. The general concept of a steering flow appears to be quite valid for up to 13 different classes of cyclones. This steering concept has been basically accepted and applied when possible by forecasters for a number of years. But up until now, little direct quantitative verification of this steering hypothesis has been provided except by Miller (1958). There are differences between his conclusions and ours. The primary difficulty in obtaining such relationships is a data one. At individual time periods, measurements of surrounding steering flow are subject to large errors. One must average over many cases in order to obtain a reasonable sample.

Tropical cyclone direction in the West Pacific appears to be very well related (in a statistical sense) to the mean 1-7^{o} radius 500 mb surrounding wind direction, while cyclone speed is best related to the 1-7^{o} radius 700 mb surrounding wind speed. Close relationships also exist between the 1-7^{o} actual and geostrophic wind fields at these levels. These two fields can, in general, be used interchangeably. We have just started to test these relationships in the Western Atlantic. The following section discusses our initial findings of these steering flow relationships for the West Atlantic.

Fourteen years (1961-1974) of West Indies (W.I.) rawinsonde data have recently been accumulated at Colorado State University (CSU)

and early results are now becoming available. This West Indies data set includes soundings from 92 stations (Fig. 2) of Chapter I.

Cyclone Motion Analysis. The grid is rotated to the direction of the cyclone motion so that in the compositing technique the cyclone motion is always at zero or 360°. The relative number of rawinsonde reports around the center are quite uniform in both oceans. From the data sample in the two relevant coordinate systems (stationary and moving), two new environmental wind vectors at each of the 64 grid points are calculated. These new vectors are defined as the wind components perpendicular (V_N) and parallel (V_L) to the cyclone motion. Analysis is performed to determine the relationships between the surrounding mean wind direction and speed and the cyclone's motion.

Two intensity, two speed, two latitude and two direction categories have been run so far. Other stratifications will be made later. Table 12 lists these initial stratifications and gives results. Figure 56 portrays the results in graphical form. In general, more than a thousand rawinsonde reports are available inside 7° radius for each stratification. The reports are well distributed by octant and radial interval about the cyclone center. Only the U.S. coastal stations of Fig. 1 have been included in this motion composite. Inland stations have not been used.

The results are quite similar to those obtained in the Western Pacific. All eight stratifications showed the cyclone moving 13 to 32% faster than the 700 mb 1-7° radius mean wind speed. In the Pacific all of the 13 different stratifications (see George and Gray, 1976 for details) showed the cyclone moving at speeds of 7-24% greater than the 700 mb 1-7° radius mean wind speed.

TABLE 12

West Atlantic Rawinsonde Stratifications of Cyclone Motion

Stratifications	Mean Cyclone Center Velocity (m/sec)	700 mb 1-7° Radius Mean Wind Velocity (m/sec)	Ratio Cyclone Motion to 1-7° 700 mb Mean Wind	Cyclone Motion Relative to the 500 mb 1-7° Radius Mean Wind Direction (degrees right or left of mean wind)
By Cyclone Max. Wind Intensity				
≥ 65 knots	4.44	3.54	1.25	3°L
35-65 knots	4.14	3.39	1.22	7°L
By Cyclone Speed				
>8 knots	6.64	5.12	1.30	10°L
< 8 knots	2.49	1.89	1.32	8°L
By Latitude				
> 20° Lat. (Ave. 25.6°)	3.87	3.24	1.19	10°L
< 20° Lat. (Ave. 17.2°)	4.40	3.89	1.13	3°L
By Cyclone Direction				
Towards 225-315°-West (Ave. Dir. 284°)	4.56	3.51	1.30	8°R
Towards 315-045°-North (Ave. Dir. 009°)	4.88	3.70	1.32	17°L
		AVERAGE	1.25	6°L

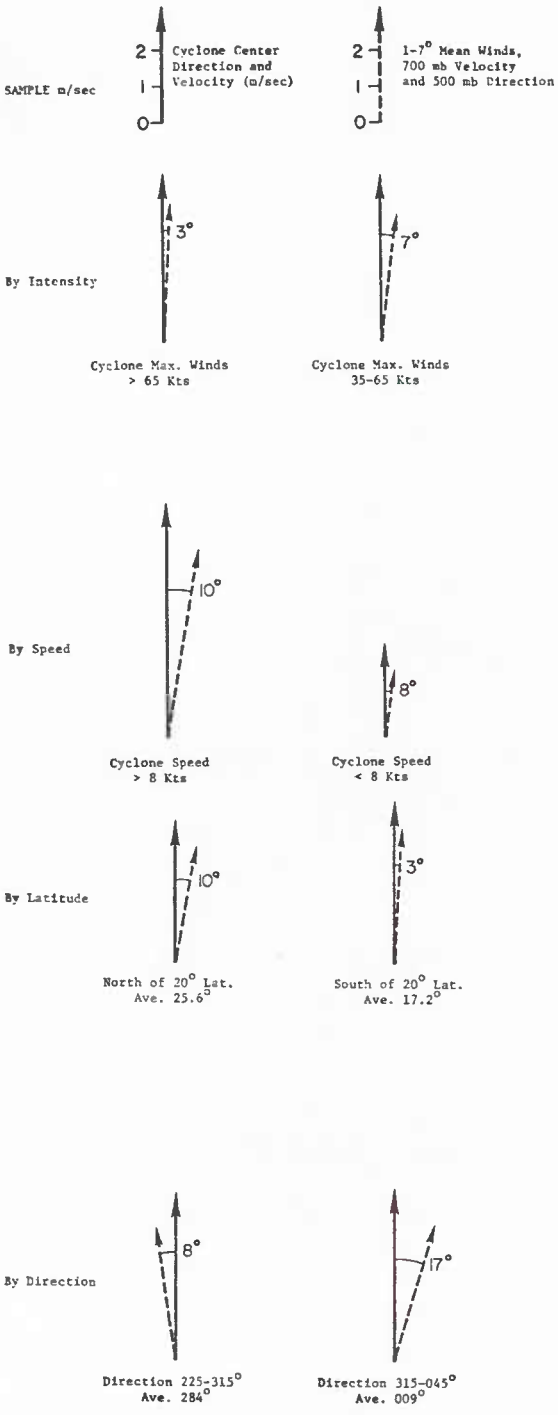

Fig. 56. West Atlantic mean storm motion and mean wind vectors.

Seven of the eight West Atlantic stratifications showed the cyclone moving 3-17° to the left of the 500 mb 1-7° radius mean wind field. One of the eight stratifications (storms moving to the west) indicated the cyclone moving to the right of the 500 mb 1-7° radius mean wind. In the Western Pacific all 13 stratifications showed the cyclone moving from 12-23° to the left of the 500 mb 1-7° radius mean wind. Thus, the West Atlantic stratifications agree well with those of the West Pacific. The only exception is the westerly moving cyclones which the data indicate move 8° to the right of the 500 mb 1-7° radius mean wind. This latter case is being examined more carefully.

When each region's data sets are combined into regional averages, the cyclone motion speed relative to the 700 mb 1-7° wind speed, and cyclone direction relative to the 1-7° 500 mb direction are in quite good agreement (Table 13). It appears that the agreement between the data of both regions and the individual stratifications is better than one might have expected. Tropical cyclone motion appears to be quite well correlated with the large scale 1-7° radius (∿ 1550 km diameter) surrounding middle tropospheric motion fields. These results are not surprising to us and should not be to experienced tropical cyclone forecasters who have been using steering flow concepts for a number of years. The move to the left of the steering current is a surprise, however. It is of interest to note that the West Pacific cyclones appear to move more to the left of the mean current than do West Atlantic cyclones.

Some degree of future improvement in cyclone forecasts might be forthcoming for the 15-25% or so of tropical cyclones which follow a-typical tracks if this steering current could be more accurately measured than at present. Special aircraft flights might be required to gather the necessary data.

TABLE 13

Comparison of mean cyclone speed and direction in the West Atlantic and West Pacific

	Cyclone Motion Relative to 700 mb 1-7° Wind Speed	Cyclone Direction to Left of 500 mb
West Atlantic Average (2362 Soundings)	1.25	6°
West Pacific Average (2011 Soundings)	1.16	16°

Recurvature Forecasting. Our recent research on typhoon recurvature (George and Gray, 1977) indicates that these phenomena may be better forecast 1-3 days in advance with the use of upper tropospheric (200 mb) information than with the conventional 700-500 mb level information. Recently C. Guard (1977) of the JTWC has (following our earlier CSU research on this subject) further explored the use of the 200 mb level for recurvature forecasting. He has developed a more refined forecasting method on cyclone recurvature which appears to increase the skill of forecasting this phenomena in the Western Pacific. We are planning to carry out more studies of tropical cyclone motion using upper tropospheric wind analysis and/or a combination of upper and lower tropospheric levels. As the new geostationary satellite data increases our wind information at these levels, we should attempt to determine the possibilities of more extensive use of upper levels in motion and intensity study.

VI. TROPICAL CYCLONE RADIUS OF 30 KNOT WINDS

Sea traffic is greatly affected by the high seas generated by typhoon winds. To maximize safety and minimize the expenses of re-routing ships, the horizontal extent of high winds must be forecast. In particular, the radius of 30 knot surface winds is an important parameter. This section uses Western North Pacific and Western Atlantic rawinsonde data to estimate the probability of encountering surface winds $\geq$ 30 knots at various points relative to the centers of typhoons and hurricanes. The dependence of the 30 kt isotach on storm intensity and size are explored, and asymmetries relative to the storm's direction of motion are discussed.

Analysis Procedure. All of the rawinsonde stations are over land, and local topography influences are variable and difficult to estimate. Therefore, the best method of obtaining surface winds over the ocean is to estimate them from observations of winds at a level above the boundary layer. In this study 850 mb winds are used. This is the approximate level of maximum winds in typhoons (Frank, 1977a). Since winds at ship deck or 10 m height are significantly lower than those at 850 mb, a correction factor had to be applied to the 850 mb winds. Bates (1977) found the 10 m winds over water in hurricanes to be about 72% of the winds at 1000 m. Here it is assumed that 10 m winds are 75% of the 850 mb winds - i.e. - a 40 kt wind at 850 mb corresponds to a 30 kt wind at the sea surface (defined as the 10 m ship deck level).

A few soundings recorded winds at the surface (over land) but not at 850 mb. In those cases, the winds at 850 mb were estimated by:

$$V_{sfc} = (C)\ (V_{850\ mb})$$

where C is an emperical constant. Based on the author's rawinsonde data composites, different values of C were chosen for the two data regions:

$$C = .47 \text{ (West Pacific)}$$

$$C = .53 \text{ (West Indies)}$$

Rawinsonde wind data around a hurricane always includes a low wind bias. Since the balloon can't be launched in very high wind conditions, the data sample tends to underestimate the true frequency of high wind occurrences. This phenomenon is most important at inner radii. Beyond a radius of 3^{o} latitude or so this bias is probably insignificant, but it should be recognized that the mean winds and frequency of 30 kt wind occurrences is increasingly underestimated as one approaches the center.

The data sample is composed of all the soundings of the authors' West Pacific (10 years) and West Indies (14 years) rawinsonde data networks (see Figs. 1 and 2). As such it usually includes numerous soundings common to each storm. Extremely long-lived storms or those which traverse the denser portions of the data networks are therefore weighted the most heavily. It is assumed that this type of bias has negligible effect on the results presented due to the very large number of storms studied.

Results. Table 14 shows the frequency of occurrence of winds $\geq$ 30 kts as a function of radius around West Pacific storms of various intensity. Table 15 shows the same information for West Indies storms. Beyond 6^{o} radius in the Pacific (4^{o} in the West Indies) 30 knot winds are encountered no more than 10% of the time. Inside those radii there is a clear trend towards more high winds with increasing central core

TABLE 14

Percent of Total West Pacific Soundings With Estimated Sea Surface Winds ≥30 Knots For Various Storm Intensities. Numbers in Parenthesis Give Number Observations

Maximum Winds Knots	Radius (°latitude) 1-2°	2-3°	3-4°	4-5°	5-6°	6-7°	7-8°
<35	5	5	5	7	2	2	0
No. of Observa. -	(41)	(42)	(77)	(99)	(105)	(105)	(129)
35-49	22	20	5	6	1	5	3
	(36)	(60)	(93)	(114)	(145)	(149)	(179)
50-64	26	20	13	9	6	4	1
	(35)	(49)	(64)	(94)	(126)	(145)	(141)
65-79	32	38	36	13	11	8	2
	(19)	(42)	(75)	(87)	(109)	(125)	(155)
80-99	80	49	29	11	6	4	2
	(20)	(35)	(65)	(71)	(99)	(130)	(129)
≥ 100	58	50	29	18	11	6	5
	(55)	(84)	(134)	(182)	(223)	(251)	(292)

TABLE 15

Percent of Total Soundings With Estimated Sea Surface Winds ≥ 30 Knots For Various Storm Intensities in West Indies. Numbers in Parenthesis Give Number of Observations

Maximum Winds Knots	Radius (^{o}latitude) 1-2^{o}	2-3^{o}	3-4^{o}	4-5^{o}	5-6^{o}	6-7^{o}	7-8^{o}
<35	1	0	0	0	0	0	0
No. of Observa.	(75)	(138)	(182)	(205)	(258)	(314)	(350)
35-49	8	9	3	0	2	0	2
	(38)	(45)	(63)	(85)	(112)	(97)	(125)
50-64	26	9	2	3	1	1	0
	(19)	(55)	(63)	(96)	(82)	(85)	(112)
65-79	36	22	9	3	2	1	0
	(28)	(45)	(87)	(90)	(99)	(105)	(117)
80-99	50	16	7	5	3	00	0
	(14)	(32)	(41)	(57)	(79)	(88)	(100)
≥100	46	38	20	10	2	1	0
	(33)	(56)	(69)	(94)	(135)	(157)	(163)

intensity. The greater size and intensity of the typhoon is evident from a comparison of Tables 14 and 15.

Figures 57 and 58 show the average 850 mb winds for the two regions. Recall that a 40 kt wind at 850 mb is about equal to a 30 kt wind at the sea surface. This line is dashed in. There is only a weak correlation between the wind speeds at 7-8° radius and the maximum winds near the center. Mean winds in excess of 40 kts are found only inside 2° radius of the strongest storms, although the winds inside 3° radius or so are probably underestimated as previously mentioned.

The extent of 30 knot winds is quite variable for a given central intensity class of storms. One measure of the size of a storm is the mean radius of the highest closed isobar (HCI) on the surface analysis. Table 16 shows the frequency of 30 knot surface wind occurrences for three storm intensity classes which have been further stratified according to the radius of the highest closest isobar (HCI). This data is for West Pacific storms only.

Within a given intensity class the 30 knot wind occurrences at each radius, as expected, become more frequent with increasing storm size. There is also a tendency for the mean storm size to increase as the maximum winds become stronger, but the radius of the HCI is quite variable within each intensity grouping.

The winds at large radius in tropical cyclones are in approximate gradient balance, and the storms' motion is closely specified by the 500-700 mb large-scale geostrophic wind component (George & Gray, 1976). Therefore, a symmetrical storm pressure perturbation imposed upon a large-scale gradient results in increased winds on the right

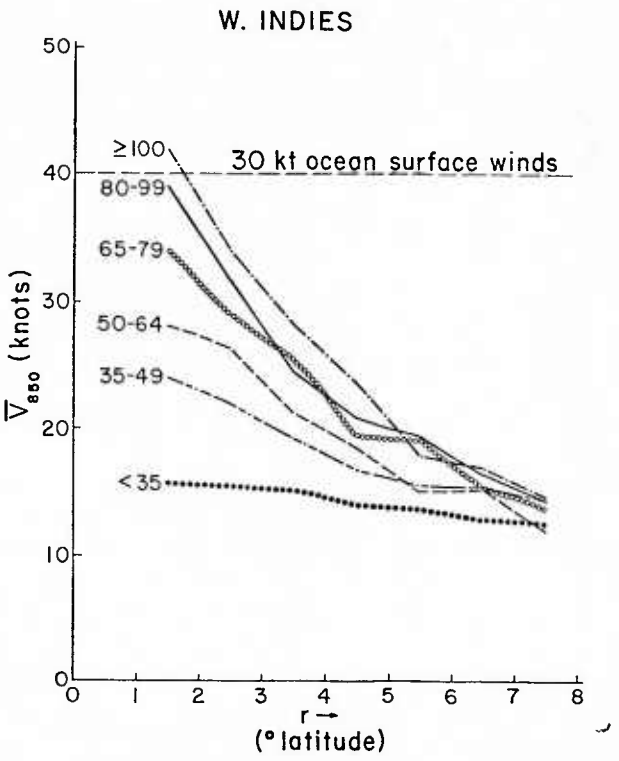

Fig. 57. Mean 850 mb winds around West Indies storms with different maximum winds. The number at the left of each line is the maximum wind range (knots) for that class of storms. Dashed line corresponds to estimated 30 knot winds at the sea surface.

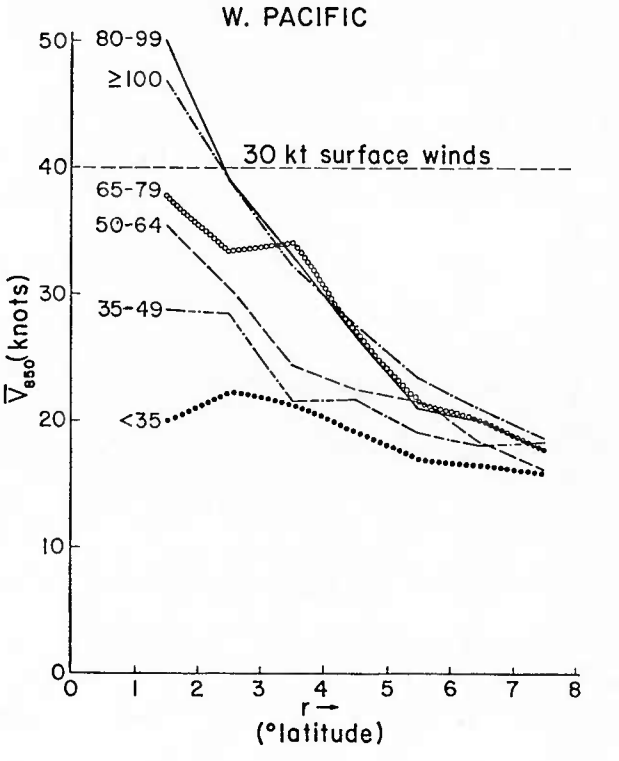

Fig. 58. Same as Fig. 57 but for the West Pacific storms.

TABLE 16

Radius of highest closed isobar as related to percent of sea surface winds exceeding 30 knots. Upper numbers are percent of soundings with estimated surface winds ≥ 30 knots.

A. Maximum Winds: 35-65 Knots

Radius of Highest Closed Isobar (HCI) In Degrees of Latitude	Radius (°latitude) 1-2°	2-3°	3-4°	4-5°	5-6°	6-7°	7-8°
0-3°	7	17	7	3	3	3	0
No. of Observa.	(27)	(42)	(82)	(86)	(120)	(129)	(139)
4-6°	38	23	9	12	4	4	5
	(39)	(61)	(64)	(104)	(129)	(143)	(147)
≥7°	0	25	11	0	11	33	0
	(2)	(4)	(9)	(10)	(9)	(12)	(24)

B. Maximum Winds: 65-90 Knots

Radius HCI	Radius (°latitude) 1-2°	2-3°	3-4°	4-5°	5-6°	6-7°	7-8°
0-3°	22	28	14	3	2	5	0
No. of Observa.	(9)	(25)	(35)	(31)	(54)	(55)	(84)
4-6°	56	38	31	13	13	6	3
	(18)	(21)	(52)	(69)	(89)	(93)	(96)
≥7	100	67	57	12	14	11	7
	(3)	(3)	(14)	(17)	(14)	(27)	(8)

C. Maximum Winds > 90 Knots

Radius HCI	Radius (°latitude) 1-2°	2-3°	3-4°	4-5°	5-6°	6-7°	7-8°
0-3°	64	27	17	23	7	0	7
No. of Observa.	(11)	(15)	(30)	(30)	(43)	(53)	(55)

TABLE 16 (cont'd)
C. Maximum Winds ≥ 90 Knots (cont'd)

Radius (^{o}latitude)

Radius HCI	1-2^{o}	2-3^{o}	3-4^{o}	4-5^{o}	5-6^{o}	6-7^{o}	7-8^{o}
4-6^{o}	74	50	37	13	9	7	1
No. of Observa.	(19)	(38)	(71)	(100)	(112)	(122)	(149)
≥7	100	91	52	48	21	13	9
	(12)	(23)	(29)	(31)	(58)	(71)	(78)

side and diminished winds on the left (looking downstream). One would expect the occurrences of 30 knot winds to reflect this asymmetry.

Tables 17 and 18 show the left vs. right percent frequencies of 30 knot winds for West Pacific and West Indies storms, respectively. The right side maximum is observed at all radii studied (0-8^{o}) and seems to increase with storm intensity. George (1976) found that the wind asymmetry occurred only inside of 10^{o} radius in W. Pacific typhoons (Figs. 59 and 60), and this radius would probably be less for the smaller West Atlantic cyclones. The degree of asymmetry depends upon the magnitude of the large-scale pressure gradient. Since the speed of storm motion is also proportional to this environmental gradient, the left-right wind asymmetry should be directly proportional to the speed of storm motion. This is a topic for future research.

Tropical cyclone winds in the low levels are usually about equal at any radius in front of and behind the storm. Therefore, mean wind data such as those presented in Tables 14 and 15 and Figs. 57 and 58 can be applied to those sectors without correction for rate of storm motion.

TABLE 17

Percent of Estimated Sea Surface Winds ≥ 30 Knots on Left and Right Sides of Storms. West Pacific. Number in Parenthesis is Total Observations

Maximum Winds Knots	Radius (°latitude)													
	1-2°		2-3°		3-4°		4-5°		5-6°		6-7°		7-8°	
	L	R	L	R	L	R	L	R	L	R	L	R	L	R
35-64	30 (30)	33 (12)	10 (40)	38 (34)	6 (02)	5 (38)	5 (74)	13 (67)	2 (88)	5 (96)	5 (95)	7 (103)	2 (106)	3 (113)
65-99	36 (11)	75 (16)	21 (29)	64 (25)	20 (51)	45 (53)	4 (55)	22 (64)	6 (84)	14 (73)	4 (97)	10 (91)	1 (106)	2 (98)
≥100	71 (14)	55 (22)	42 (33)	65 (31)	26 (53)	39 (41)	16 (61)	25 (71)	9 (77)	14 (80)	3 (70)	9 (89)	2 (86)	9 (118)

TABLE 18

Same as Table 4 For West Indies Storms

Radius (^{o}latitude)

Maximum Winds Knots	1-2°		2-3°		3-4°		4-5°		5-6°		6-7°		7-8°	
	L	R	L	R	L	R	L	R	L	R	L	R	L	R
35-64	11 (19)	18 (22)	6 (35)	11 (44)	0 (45)	6 (48)	0 (75)	2 (63)	1 (76)	0 (62)	0 (76)	2 (62)	0 (87)	2 (81)
65-99	17 (12)	60 (20)	0 (25)	27 (26)	0 (43)	20 (55)	4 (29)	7 (58)	3 (64)	2 (64)	0 (69)	1 (71)	0 (83)	0 (77)
≥100	25 (8)	58 (19)	29 (21)	35 (20)	5 (19)	32 (37)	0 (27)	16 (45)	0 (55)	4 (53)	0 (51)	1 (69)	0 (51)	0 (77)

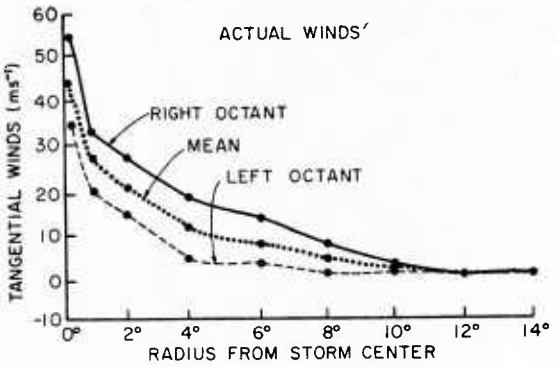

Fig. 59. 700 mb tangential wind profiles of actual and relative winds depicting the asymmetry between the right and left octants of West Pacific tropical cyclones for the LAT > 20°N stratification, (George, 1976).

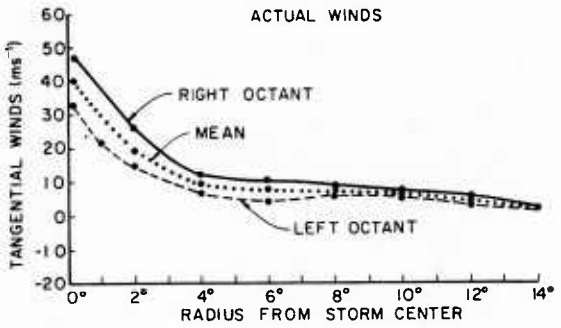

Fig. 60. Same as Fig. 59 except LAT $\leq$ 20°N.

ACKNOWLEDGEMENTS

The authors wish to express their gratitude to Raymond Zehr, Major Charles P. Arnold, Captain John E. George, Captain Steven L. Erickson, John L. McBride and Edwin Núñez for much discussion and information concerning their research findings. Mr. Edwin Buzzell has been responsible for the numerical data processing. Thanks are also extended to Mrs. Barbara Brumit and Mrs. Dianne Schmitz for their assistance in manuscript preparation. We are also very appreciative of the US Naval Environmental Prediction Research Facility of Monterey, California and Mr. Samson Brand for financial assistance and encouragement of our Colorado State University tropical cyclone research efforts.

BIBLIOGRAPHY

Anthes, R. A., 1974: The dynamics and energetics of mature tropical cyclones. Reviews of Geophysics and Space Physics, 12, 495-522.

Arnold, C. P., 1977: Tropical cyclone cloud and intensity relationships. Atmos. Sci. Paper No. 277, Colo. State Univ., Ft. Collins, CO, 154 pp.

Ausman, M., 1959: Some computations of the inflow angle in hurricanes near the ocean surface. Univ. of Chicago Dept. of Meteorology Research Report, 19 pp.

Bates, J., 1977: Vertical shear of the horizontal wind speed in tropical cyclones. NOAA Technical Memorandum ERL WMPO-39, 19 pp.

Browner, S. P., W. L. Woodley and C. G. Griffith, 1977: Diurnal oscillation of the area of cloudiness associated with tropical storms. Mon. Wea. Rev., 105, 856-864.

Dvorak, V. F., 1975: Tropical cyclone intensity analysis and forecasting from satellite imagery. Mon. Wea. Rev., 103, 420-430.

Erickson, S. L., 1977: Comparison of developing vs. non-developing tropical disturbances. Atmos. Sci. Paper No. 274, Colo. State Univ., Ft. Collins, CO, 81 pp.

Fett, R. W., 1964: Some characteristics of the formative stage of typhoon development: A satellite study. National Conference on Physics and Dynamics of Clouds, Chicago, IL, March 24-26, U.S. Weather Bureau, Washington, DC, 10 pp.

Fett, R. W., 1966: Upper-level structure of the formative tropical cyclone. Mon. Wea. Rev., 94, 9-18.

Frank, W.M., 1976: The structure and energetics of the tropical cyclone. Colo. State Univ., Atmos. Sci. Paper No. 258, Ft. Collins, CO, 180 pp.

Frank, W. M., 1977a: Structure and energetics of the tropical cyclone, I: Storm structure. Mon. Wea. Rev., 105, 1119-1134.

Frank, W. M., 1977b: The structure and energetics of the tropical cyclone, II: Dynamics and energetics. Mon. Wea. Rev., 105, 1135-1150.

Frank, W. M., 1977c: Convective fluxes in tropical cyclones. J. Atmos. Sci., 34, 1554-1568.

George, J. E., 1975: Tropical cyclone motion and surrounding parameter relationships. Colo. State Univ., Atmos. Sci. Paper No. 214, 105 pp.

BIBLIOGRAPHY (cont'd)

George, J. E. and W. M. Gray, 1976: Tropical cyclone motion and surrounding parameter relationships. J. Appl. Meteor., 15, 1252-1264.

George, J. E. and W. M. Gray, 1977: Tropical cyclone recurvature and nonrecurvature as related to surrounding wind-height fields. J. Appl. Meteor., 16, 34-42.

Gray, W. M., 1962: On the balance of forces and radial accelerations in hurricanes. Quart. J. Roy. Meteor. Soc., 88, 430-458 pp.

Gray, W. M., 1967: The mutual variation of wind, shear and baroclinicity in the cumulus convective atmosphere of the hurricane. Mon. Wea. Rev., 95, 55-73.

Gray, W. M., 1968: Global view of the origin of tropical disturbances and storms. Mon. Wea. Rev., 96, 669-700.

Gray, W. M., 1975a: Tropical cyclone genesis. Colo. State Univ., Atmos. Sci. Paper No. 234; Ft. Collins, CO, 119 pp.

Gray, W. M. 1975b: Tropical cyclone genesis in the western North Pacific. ENVPREDRSCHFAC Technical Paper No. 16-75, Monterey, CA, 66 pp.

Gray, W. M., 1977a: Cyclone intensity determination through upper tropospheric reconnaissance. Paper prepared for the 11th Technical Conference on Hurricanes and Tropical Meteorology, Miami, FL, 6 pp.

Gray, W. M., 1977b: Tropical cyclone motion and steering flow relationships in the Western Atlantic and the Western Pacific. Paper prepared for the 11th Technical Conference on Hurricanes and Tropical Meteorlogy, Miami, FL, 6 pp.

Gray, W. M., 1977c: Tropical disturbance to cyclone transformation. Paper prepared for the 11th Technical Conference on Hurricanes and Tropical Meteorology, Miami, FL, 8 pp.

Gray, W. M. and D. J. Shea, 1973: The hurricane's inner core region. II Thermal stability and dynamic characteristics. J. Atmos. Sci., 30, 1565-1576.

Gray, W. M. and D. J. Shea, 1976: Data summary of NOAA's hurricane inner-core radial leg flight penetrations 1957-1967, 1969. Colo. State Univ., Atmos. Sci. Paper No. 257, Ft. Collins, CO, 245 pp.

Gray, W. M., E. Ruprecht, and R. Phelps, 1975: Relative humidity in tropical weather systems. Mon. Wea. Rev., 103, 8, 685-690.

BIBLIOGRAPHY (cont'd)

Gray, W. M. and W. M. Frank, 1977: Tropical cyclone research by data compositing. Naval Environmental Prediction Research Facility, NEPRF Technical Report TR-77-01, Monterey, CA, 70 pp.

Guard, Charles P., 1977: Operational application of a tropical cyclone recurvature/non-recurvature study based on 200 mb wind fields. FLEWEACEN Tech. Note-JTWC 77-1. 40 pp. (Available from NEPRF, Monterey, CA).

Hawkins, H. F., and D. T. Rubsam, 1968: Hurricane Hilda, 1964: II. Structure and Budgets of the hurricane on October 1, 1964. Mon. Wea. Rev., 99, 427-434.

Hawkins, H. F. and S. M. Imbembo, 1976: The structure of a small, intense hurricane - Inez 1966. Mon. Wea. Rev. 104, 418-442.

Hubert, L., 1968: Personal Communication.

LaSeur, N. E. and H. F. Hawkins, 1963: An analysis of hurricane Cleo (1958) based on data from research reconnaissance aircraft. Mon. Wea. Rev., 91, 694-709.

Lilly, D. K., 1972: Wave momentum flux - A GARP problem. Bull Amer. Meteor. Soc., 20, 17-23.

Lopez, R. E., 1968: Investigation of the importance of cumulus convection and ventilation in early tropical storm development. Colo. State Univ., Atmos. Sci. Paper No. 124, Ft. Collins, CO, 86 pp.

McBride, J. L., 1977: Observational analysis of the differences between developing and non-developing tropical disturbances. Paper prepared for the 11th Technical Conference on Hurricanes and Tropical Meteorology, Miami, FL, 7 pp.

Miller, B. I., 1958: The three dimensional wind structure around a tropical cyclone. NHRP Rept. No. 15, 41 pp.

Miller, B. I., 1962: On the momentum and energy balance of hurricane Helene (1958). NHRP Rept. No. 53, 19 pp.

Núñez, E. and W. M. Gray, 1977: A comparison between West Indies hurricanes and Pacific typhoons. Proceedings of 11th AMS Conference on Hurricanes and Tropical Meteorology, Miami, FL, 13-16 December, 7 pp.

BIBLIOGRAPHY (cont'd)

Oliver, V. J. and R. K. Anderson, 1969: Circulation in the tropics as revealed by satellite data. Bull. Amer. Meteor. Soc., 50, 702-706.

Ooyama, K., 1969: Numerical simulation of the life cycle of tropical cyclones. J. Atmos. Sci., 26, 3-40.

Palmén, E., 1958: Vertical circulation and release of kinetic energy during the development of Hurricane Hazel into an extra-tropical storm. Tellus, 1, 1-23.

Palmén, E. and C. L. Jordan, 1955: Note on the release of kinetic energy in tropical cyclones. Tellus, 7, 186 pp.

Riehl, H., 1975: Further studies on the origin of hurricanes. Colo. State Univ., Atmos. Sci. Paper No. 235, Ft. Collins, CO, 24 pp.

Riehl, H. and J. S. Malkus, 1961: Some aspects of Hurricane Daisy, 1958. Tellus, 13, 181-213.

Rosenthal, S. L., 1970: A circularly symmetric primitive equation model of tropical cyclone development containing an explicit water vapor cycle. Mon. Wea. Rev., 98, 643-663.

Sadler, J. C., 1967a: On the origin of tropical vortices. Working Panel on Trop. Dynamical Meteor., Naval Postgraduate School, Monterey, CA, 39-75.

Sadler, J. C., 1967b: The tropical tropospheric trough as a secondary source of typhoons and a primary source of tradewind disturbances. Final report, Cont. AF19 (628)3860, AF Cambridge Res. Labs., Bedford, MA, Rept. 67-12, 44 pp.

Sadler, J. C., 1974: A role of the tropical upper tropospheric trough in early season typhoon development. Tech. Paper No. 9-74, US Navy Environmental Prediction Res. Facility Rept. 54 pp.

Sadler, J. C., 1976a: Tropical cyclone initiation by the tropical upper tropospheric trough. Tech. Paper No. 2-76, Naval Environmental Prediction Res. Facility, 103 pp.

Sadler, J. C., 1976b: A role of the tropical upper tropospheric trough in early season typhoon development. Mon. Wea. Rev., 104, 1266-1278.

Sarton, J., 1968: Monthly climatological wind fields associated with tropical storm genesis in the West Indies. Colorado State Univ., Ft. Collins, Atmospheric Science Research paper, 34 pp.

BIBLIOGRAPHY (cont'd)

Shea, D. and W.M. Gray, 1973: The hurricane's inner core region, I: Symmetric and asymmetric structure. J. Atmos. Sci., 30, 1554-1564.

Sheets, R. C., 1967a: On the structure of Hurricane Janice (1958). National Hurricane Res. Lab. Rept. No. 76, 30 pp. (available from NOAA Weather Bureau, Miami office).

Sheets, R. C., 1967b: On the structure of Hurricane Ella (1962). National Hurricane Res. Lab. Rept. No. 77, 33 pp. (available from NOAA Weather Bureau, Miami office).

Sheets, R. C., 1968: On the structure of Hurricane Dora (1964). National Hurricane R es. Lab. Rept. No. 83, 64 pp. (available from NOAA Weather Burea, Miami office).

Trout, D. and H. A. Panofsky, 1969: Energy dissipation near the tropopause. Tellus, 21, 355-358.

Wachtmann, R. F., 1968: Role of angular momentum transport in tropical storm dissipation over tropical oceans. Colorado State University, Ft. Collins, Atmospheric Science Research Paper, 46 pp.

Wright, S., 1976: The comparable development of tropical storm Holly with a gulf tropical disturbance. Mon. Wea. Rev., 104, 1451-1454.

Yanai, M., 1961: A detailed analysis of typhoon formation. J. Meteor. Soc. Japan, 39, 187-214.

Zehr, R., 1976: Tropical disturbance intensification. Colo. State Univ., Dept. of Atmos. Sci., Ft. Collins, CO, 91 pp.